Electrochemical Society

101, No. 2 November 19[illegible]

UNIV. OF MICHIGAN
EAST ENGINEERING
LIBRARY

Chlorine...

for the Petrochemical Industry

Chlorine is of swiftly growing importance in the production of many new and revolutionary petrochemicals.

Swiftly growing, too, is the use of uniformly high quality GLC GRAPHITE ANODES—in helping the electrolytic industry meet the increasing civilian and defense needs for chlorine and caustic soda.

ELECTRODE DIVISION

Great Lakes Carbon Corporation

Niagara Falls, N.Y. GLC Morganton, N. C.

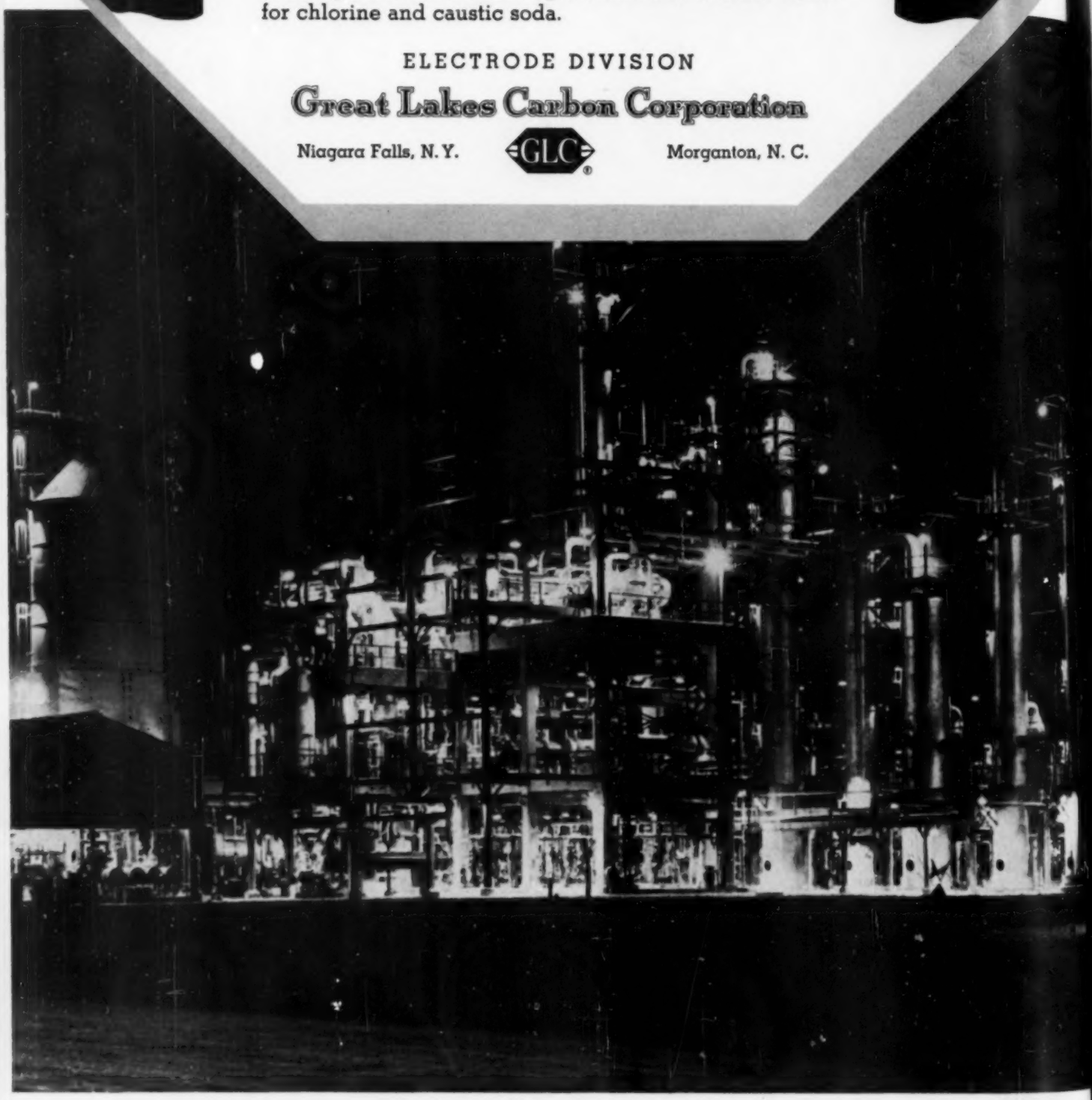

Courtesy Jefferson Chemical Company Inc.

Graphite Electrodes, Anodes, Molds and Specialties

Sales office: Niagara Falls, N.Y. **Other offices:** New York, N.Y., Oak Park, Ill., Pittsburgh, Pa.

Sales Agents: J. B. Hayes, Birmingham, Ala.; George O'Hara, Long Beach, Cal.; Great Northern Carbon & Chemical Co., Ltd., Montreal, Canada

Overseas Carbon & Coke Company, Inc., Geneva, Switzerland; Great Eastern Carbon & Chemical Co., Inc., Chiyoda-Ku, Tokyo

Lead-Acid Storage Batteries

Barium Sulfate as a Positive Plate Contaminant[1]

J. F. Dittmann and H. R. Harner

Eagle-Picher Company, Joplin, Missouri

Barium sulfate in fractional percentages is regularly used in the active material of negative plates in lead-acid storage batteries. At times, in preparing plates, some negative paste is accidentally mixed into positive paste, thus contaminating the positive paste with traces of barium sulfate. Rapid failure due to shedding has been traced to this barium sulfate contamination. Systematic tests show that as little as 0.0005% precipitated barium sulfate in positive paste markedly increases shedding on deep-cycling bench life tests. On the other hand, as much as 0.1% had no evident effect in overcharge bench tests, or in actual car service.

Introduction

The most widely used laboratory tests for storage battery durability, or life, involve successive cycles of fairly complete, or "deep", discharges followed by complete recharge. The test specified by the S.A.E. is of this type. It is widely used both as a laboratory tool for studying experimental batteries and as a a procurement specification. In the latter case, batteries must yield at least a specified minimum number of cycles on the test to be considered acceptable.

Occasionally, a battery or group of batteries that should easily meet the test requirements fails prematurely due to excessive positive plate shedding. In many instances, the active material from the positive plates of these failing batteries has been subjected to spectrographic analysis. Usually, barium has been found as a contaminant in these positive plates. Since barium sulfate as precipitated *blanc fixe* is a usual constituent of paste for negative plates, finding barium in the positive active material is evidence of contamination of the positive paste with negative paste at some step in plate preparation. Since the same equipment is used alternately in many plants for manufacturing both positive and negative plates, it is surprising that such contamination is not more common.

In view of the fact that there is always this danger of contamination, it was considered most desirable to define more clearly the effect of barium sulfate as an impurity in positive paste, not only in deep cycling tests where the effect was first noted, but also in actual car service and in overcharge type tests.

[1] Manuscript received May 7, 1954. This paper was prepared for delivery before the Boston Meeting, October 3 to 7, 1954.

Experimental

Nine lots of positive plates were prepared from nine carefully compounded batches of positive paste. The only known variable in the nine batches was the amount of barium sulfate as precipitated *blanc fixe* that was added, and which varied from none in the control mix to 0.10% as a maximum. The positive plates used 9% antimonial lead grids 1.72 mm thick. They were assembled into 15 plate elements with stock negative plates pasted in the same type grids. This assembly is rated at 85 amp-hr at the 20-hr rate and is intentionally deficient in positive active material. Forty-five batteries were prepared, nine for each of the three bench tests and eighteen for automobile service testing. In assembling the latter eighteen, positive plate groups from three different paste batches were assembled in each battery, i.e., formulas 1, 4, 7 in one battery, formulas 2, 5, 8 in the next, etc. By this means each positive formula was tested in six cars instead of only two, exposing it to a wider range of conditions of use.

Life Tests Used

S.A.E. cycling test.—This test (1) was developed shortly after 1930 and was later adopted as standard by the Society of Automotive Engineers. It is of the deep cycling type, subjecting the batteries to 4 cycles/day, each cycle comprising 40 amp-hr of discharge and 50 amp-hr of recharge with the batteries held at 110 ± 5°F. Each week a capacity test determines battery condition.

Emark life test.—This test (2) was developed to simulate one type of automobile service—that of a taxi or delivery car. It is of the "shallow-cycling" type in that a discharge of 300 amp for 5 sec is given, followed by 6 min 30 sec of recharge at 10 amp, then a rest of 3 min 25 sec, after which the cycle is re-

TABLE I. *Effect of barium sulfate in positive plates on battery performance under various conditions of test*

$BaSO_4$ content, %	0.0000	0.0005	0.001	0.003	0.005	0.0075	0.010	0.050	0.100
Battery Initial Capacity									
Cycle 1, Rate 5, 80°F, amp hr	84	84	84	86	86	87	86	86	87
Cycle 2, Rate 300, 0°F, min	4.6	4.4	4.4	4.7	4.3	4.4	4.4	4.4	4.3
Cycle 3, Rate 5, 80°F, amp hr	85	85	85	87	87	89	87	88	87
Battery Self-Discharge on 28 Day Stand at 80° F									
Initial acid gravity	1.279	1.280	1.282	1.274	1.278	1.277	1.278	1.282	1.283
Final acid gravity	1.241	1.237	1.237	1.239	1.238	1.237	1.240	1.242	1.242
decrease	0.038	0.043	0.045	0.035	0.040	0.040	0.038	0.040	0.041
Life on "Deep-Cycling" S.A.E. Life Test									
Yield cycle 32, amp hr	67	67	67	67	65	66	65	63	49
Yield cycle 84, amp hr	67	64	64	57	56	54	50	42	25
Yield cycle 188, amp hr	58	49	38	32	35	32	20	20	10
Estimated life, cycles	250	210	175	150	145	140	110	90	50
% Relative life	100	84	70	60	58	56	44	36	20
% Pos. shed cycle 188	5	20	30	35	40	45	55	60	75
Life on "Shallow-Cycling" Emark Life Test									
Yield cycle 860, amp hr	78	78	78	79	79	79	80	80	78
Yield cycle 6951, amp hr	41	40	40	43	42	40	40	43	39
Yield cycle 8468, amp hr	8	9	8	7	6	6	6	14	5
Estimated life, cycles	6960	6950	6950	7000	6975	6950	6950	7000	6900
% Pos. shed cycle 8468	Maximum estimated shedding 5%—No systematic differences.								
Life on S.A.E. Overcharge Test									
Yield after 1 week, min	8.0	8.2	8.2	7.5	8.4	8.3	8.5	8.1	8.0
Yield after 3 weeks, min	3.9	3.3	3.2	4.1	3.3	3.5	3.2	3.1	2.8
Yield after 4 weeks, min	0.65	0.40	0.60	0.70	0.30	0.25	0.40	0.25	0.45
% Pos. shed, 5 weeks	Maximum estimated shedding 5%—No systematic differences.								
Life in Automobile Starting and Lighting Service									
Yield after 18 months, amp hr	65	74	52	65	75	40	64	75	42
% Pos. shed, 18 months	6	5	14	7	5	14	8	5	13

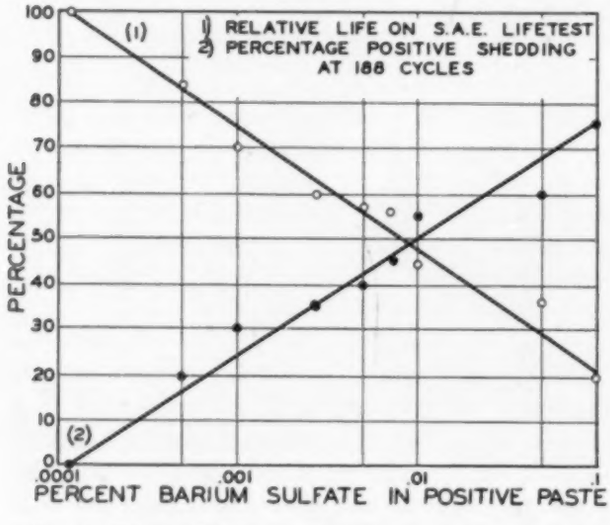

FIG. 1. Effect of barium sulfate content of positive plate active material on battery performance on S.A.E. life test.

peated. During the week the batteries are held in a water bath at 100 ± 5°F. As in the cycling test, the capacity test is imposed once a week to determine battery condition.

Overcharge test.—This test (1) is to provide data as to the life of positive grids and of separators. Since these are major causes of failure in automobile use, this test is a useful one. The batteries on test are charged continuously for 110 hr at 9 amp, then allowed to stand for 48 hr on open circuit before receiving the weekly capacity test cycle. During the test, the batteries are held in a water-bath at 100 ± 5°F.

Automobile service test.— Because of the great variation in the conditions of use, many thousands of batteries must be tested for definitive results. Except in a limited way it is, therefore, of little use for laboratory battery series. In the present case, many

possible auto test conditions were excluded by selecting the group of 18 test cars from among those owned by laboratory personnel. All were being used in the same kind of service and receiving similar mileage in the order of 10,000 miles/yr.

In addition to the above life tests, one set of the batteries was examined for self-discharge differences by being allowed to stand on open circuit for 28 days at 80°F.

Pertinent data have been summarized and are presented in Table I.

Discussion

Barium sulfate had no detrimental effect on the initial capacity of the batteries. In fact, there is a trend to slightly higher 20-hr-rate yields with increasing barium sulfate content. Unless verified by additional testing, this cannot be considered significant since the variation is within possible experimental error.

There was no effect on self-discharge. The decrease in electrolyte specific gravity was of the same order for all cells and displays no trend.

No trend was shown on the Emark type life test, on the S.A.E. overcharge test, or in actual car service. Differences found in the batteries after car service were due to operating conditions of the car and not to formulation. The significant finding was that all batteries were still operative after 18 months in cars.

Quite a different story developed from the S.A.E. life test. The significant data are plotted in Fig. 1. The life in cycles is an inverse function and the positive plate shedding a regular function of the logarithm of the percentage of barium sulfate in the positive plate active material.

From the above findings, the following conclusions may be drawn:

1. Barium sulfate contamination up to 0.1% of positive plate active material does not detract from the performance of batteries on noncycling tests or in average automobile use.

2. Barium sulfate contamination of positive plate active material is seriously detrimental to the life of batteries tested by a "deep-cycling" procedure and may be expected to be equally detrimental to the life of batteries used in "deep-cycling" service such as in battery propelled vehicles.

The only explanation for this harmful effect of barium sulfate is based on the theory that on "deep-cycling" the barium sulfate crystallites serve as nuclei for large lead sulfate crystals. Large lead sulfate crystals could then disrupt the bonding structure of the positive plate causing disintegration and shedding of active material.

Any discussion of this paper will appear in a Discussion Section to be published in the June 1955 issue of the Journal.

REFERENCES

1. Society of Automotive Engineers, Handbook, 715–716, Business Press Inc., Lancaster, Pa. (1952).
2. J. E. Hatfield and H. R. Harner, *Trans. Electrochem. Soc.*, **71**, 593 (1937).

The Role of Inverse Segregation and Redistribution of Solute Atoms in the Freezing of Hypoeutectic Lead-Antimony Alloys[1]

A. C. Simon and E. L. Jones

Naval Research Laboratory, Washington, D.C.

ABSTRACT

Inverse segregation has been found to occur in the lead-antimony alloys of the range of concentration used for battery grids. Because of the possible harmful effects of such large concentrations of antimony at the surface of the battery grid a study has been made as to the cause of this phenomenon. The extent of the antimony dispersion in the surface layer has been found to be larger than can be explained by any one of the existing theories of inverse segregation. The effect appears to be caused by an interdendritic flow of still molten alloy of near eutectic composition into the gap left between the semisolid crust and the mold face during the solidification contraction. The difficulty of inducing the nucleation of antimony produces a condition of supersaturation for the β phase in this layer while the lead continues to crystallize out at temperatures below the normal eutectic. The continually increasing concentration of antimony added to the decrease in temperature eventually brings a limit to supersaturation, whether or not nucleation is promoted by the mold face. The antimony present in excess of the eutectic concentration then forms primary dendritic crystals which grow until the eutectic composition is again reached, at which point eutectic crystallization occurs. The result is a surface film of antimony far in excess of the distribution found within the ingot.

Introduction

When a hypoeutectic lead-antimony alloy casting is examined a great deal more antimony is found in the surface layer than would be expected from the alloy composition. As the composition of the alloy approaches that of the eutectic the surface layer becomes almost entirely antimony instead of the expected eutectic. This effect is a factor of importance in the casting process and in the subsequent use of the alloy material. In the use of lead-antimony as a battery grid material this unequal distribution of antimony at and near the surface may be a factor in the adherence of the active material, as well as an influence on the rates of corrosion and growth. The presence of large amounts of antimony in the surface layer definitely influences the structure of the initial corrosion product that is formed and contributes to the deposition of antimony at the negative plate.

The present paper deals only with the investigation of inverse segregation itself. The effect of inverse segregation on battery grid performance will be reported at a later date.

The phenomenon of inverse segregation (decreased concentration of the solute constituent toward the center of the casting, with abnormally high concentration at, or near, the surface) is well known and has been reported in many alloy systems. Excellent reviews (1–3) include most of the literature on this subject prior to 1950. These analyze the existing theories of inverse segregation in a critical manner and contain excellent bibliographies of prior papers on inverse segregation.

Two forms of inverse segregation have been reported: (*a*) a gradual decrease in the low melting point constituent toward the center of the casting, detectable only by chemical analysis; and (*b*) exudations at the surface of high concentration of eutectoid, rich in the low melting point constituent, which may or may not be accompanied by a gradual internal change of composition. The inverse segregation observed in the lead-antimony alloys conforms to type (*b*), except that the surface is covered with primary crystals of antimony rather than an antimony-rich eutectic.

None of the theories of inverse segregation adequately explain the extent of antimony segregation found at the surface of the lead-antimony alloy castings nor do any of them explain the primary crystallization of the β phase in the surface layer. Further investigation of this phenomenon therefore seemed advisable.

Experimental Procedure

Both chill and slowly cooled castings were prepared from a series of lead-antimony alloys containing 1, 3, 5, 7, 9, 11, and 13% antimony, respectively. A microscopic examination was made of the surfaces and cross sections of the ingots. Since inverse segregation appeared principally as a surface exudation of the antimony-rich material there was little of value obtained from cross-sectional examina-

[1] Manuscript received June 10, 1954. This paper was prepared for delivery before the Boston Meeting, October 3 to 7, 1954.

tion and the principal reliance was laid upon surface examination. Surfaces were examined in the as-cast condition; the castings were then etched with acetic acid-hydrogen peroxide solution (2 ml of 30% Superoxol to 48 ml of glacial acetic acid) and again inspected. This etch dissolves the lead and the lead-rich solid solution but does not appreciably attack antimony or the β phase. The antimony present in solid solution is precipitated as a very finely divided black soot-like film only upon the surface of the lead against which larger particles of antimony stand out brilliantly. There is, therefore, no difficulty experienced in differentiating between lead and antimony in the surface layer. The black film which obscures the surface of the lead-rich areas can be readily rubbed off, although it cannot be removed by washing. Rubbing, however, distorts the surface structure of the soft lead matrix. Scotch tape applied to this surface and gently pressed (but not rubbed) into contact with the surface by means of a very soft pencil eraser or other soft rubber pad was found to be very effective in removing this black deposit. If the etch is prolonged slightly, the thin surface layer of antimony is undermined and can be transferred intact to the Scotch tape. Thus, both sides of the antimony film can be examined as well as the new surface of the ingot revealed by the removal of the antimony. In one case this stripped film was subjected to x-ray analysis and identified as antimony as a check on other observations. Repeated etching and stripping in this manner revealed the structure to a considerable depth below the original surface.

On another series of castings, heavily plated with copper, taper sectioning (4) was employed to observe the structure of the very thin surface layer. Taper sectioning caused an apparent increase in the sectional thickness of the surface layers while the copper preserved the original surface contours.

Still another series of castings were made in a special mold, the two opposite sides and bottom of which were composed of aluminum while the other two sides were of transite. The top was left open to the air. Such a mold design insured very rapid chill casting at the cold aluminum faces and a progressive growth of the dendrites into the much more slowly cooled interior and provided a means of studying the effects of unequal freezing. All castings were approximately 1¼ in. high, 1 in. wide, and ½ in. thick.

Observed Surface Structure

Examination revealed that antimony appeared at the surface in excessive amounts under all the conditions that were investigated. The excess antimony that appeared on the surface increased as the antimony concentration in the alloy increased but to a greater proportional extent. Thus, an alloy that had contained 10% antimony in the liquid state showed a surface after freezing that appeared to be almost entirely antimony.

For equal amounts of antimony, the alloys chill cast very suddenly showed the least amount of exudation of antimony on the surface and the surface structure agreed with the internal structure. Alloys cooled very slowly (less than 1°C/min) appeared to show no exudations but closer inspection revealed a high concentration of antimony at the bottom of the ingot (which was also the last portion to cool). The dendritic structure of the ingot was clearly revealed elsewhere on the surface by a withdrawal of the low freezing constituent, but at the bottom surface and a short distance up the sides the surface was smooth as if all the low freezing constituent had drained to this area. Alloys that were cast in a mold with unequal cooling of the mold faces gave the greatest evidence of exudations at the surface. Here also the greatest amount of exudation appeared at the more slowly cooled face and the surface structure was quite different from that found in the interior of the ingot.

For the alloys of low antimony content the surface antimony was concentrated at interdendritic and grain boundaries in a continuous layer that had no similarity to eutectic crystallization (Fig. 1).

As the amount of antimony in the alloy was increased the antimony-rich layer was found to cover the whole surface. This film, apparently continuous

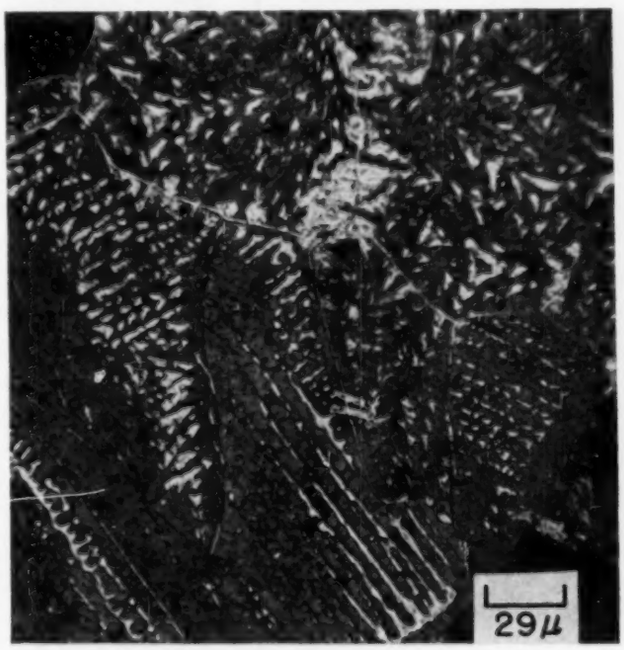

Fig. 1. Appearance of the vertical surface of chill cast lead-antimony ingot containing 2% antimony after an etch with acetic acid-hydrogen peroxide solution. Inverse segregation is indicated by excessive antimony (lightest areas) at interdendritic and intergranular extrusions. 300×.

FIG. 2. Appearance at vertical surface of chill cast lead-antimony ingot after etch with acetic acid-hydrogen peroxide solution. Antimony (light areas) covers almost the entire surface and shows primary crystallization although representing only 5% of the total alloy. 500×.

FIG. 3. Surface area from vertical wall of unequally cooled lead-antimony ingot containing 2% antimony. Original surface containing a few interdendritic and intergranular extrusions of antimony has been overrun by a molten stream of antimony-rich material originating at a mold face of lesser chill. Last formed film can be distinguished by its disregard for grain boundaries and other crystal structure. (Acetic acid-hydrogen peroxide etch.) 300×.

before etching, was found after etching to present a dendritic structure in which the antimony appeared as the primary crystallization and in amounts far in excess of the lead (Fig. 2). When this surface film was removed, a second layer was revealed which had the appearance of a true eutectic crystallization and in which the proportions of lead and antimony appeared to be normal. Beneath this second layer the true dendritic structure of the alloy was found.

For castings in which unequal cooling had occurred the still molten metal from the warmer regions was found to have flowed into the space between the frozen crust and the chill wall of the colder portion, forming a second antimony-rich film on top of that which had been formed by flow through the interdendritic channels (Fig. 3). The path of this flow was often plainly marked by the difference in crystal appearance and the fact that the frozen wave was actually visible, arrested by the freezing process before completely covering the original surface (Fig. 4).

Where the surface layer was thick, as in the case where flow had occurred from one area to another along the mold face, the surface was characteristically covered with tetrahedral crystals originating in the primary crystallization of antimony. Examination showed that while these crystals showed primary dendritic crystallization of antimony and a surface layer that was essentially antimony there appeared beneath the surface a layer of eutectic crystallization

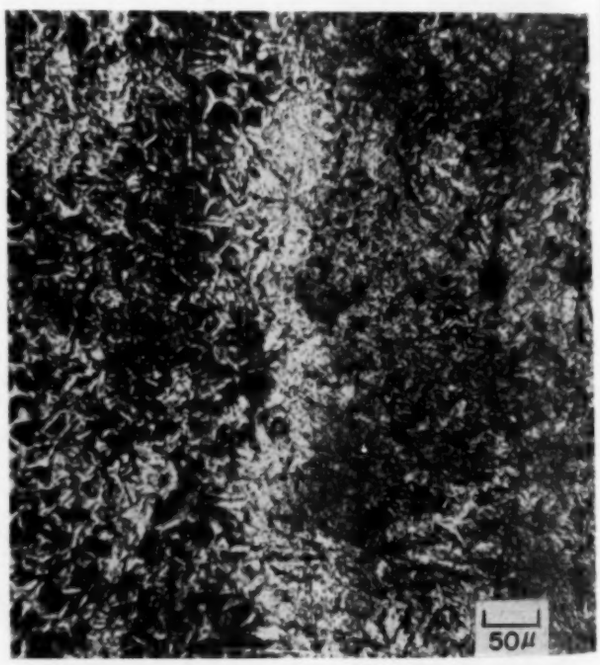

FIG. 4. Surface area from unequally cooled lead-antimony ingot containing 4% antimony showing crest of secondary wave of antimony-rich alloy (left) frozen in the process of covering the original surface film (right) of antimony-rich alloy. (Unetched specimen.) 150×.

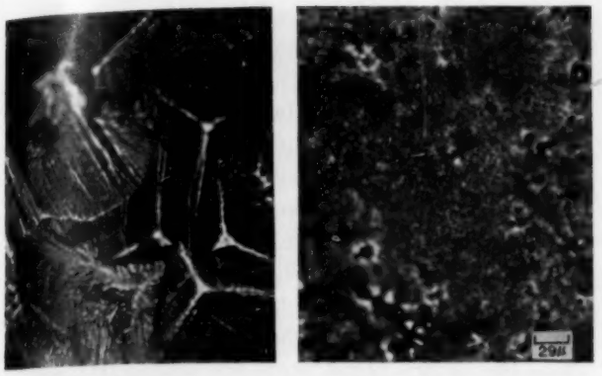

FIG. 5. Surface appearance of chill cast lead-antimony alloy with 9% antimony. (a) Before etching; (b) after etching with acetic acid-hydrogen peroxide solution and subsequent stripping of the surface film of antimony with Scotch tape. The subsurface layer here shown consists of an eutectic mixture of lead and antimony. 150×.

which nevertheless conformed to the general shape of the crystal (Fig. 5).

Taper sectioning confirmed the observations made at the ingot surface. A columnar dendritic growth was revealed a short distance inward from the ingot surface, separated from the surface by a layer of eutectic structure, while at the surface there appeared a very thin layer of antimony.

The appearance of the surface as viewed under the microscope left no doubt that the original frozen surface had withdrawn from the mold face through shrinkage of the ingot surface layer, expansion of the mold, or both. This space then appeared to have been filled by still molten material that flowed to the surface through interdendritic channels or flowed along the mold wall from regions still molten. The surprising feature is that the liquid metal flowing to the surface did not appear to have frozen instantly. Equally surprising is the fact that, when freezing did begin, primary crystallization of antimony should first occur, and to such an extent.

Discussion

The type of inverse segregation that causes exudations of a low-melting point constituent at the surface is common in binary tin bronzes, phosphorus-tin bronzes, zinc-tin bronzes, leaded bronzes, leaded gun metals, and aluminum-copper alloys. For all of these alloys there are certain factors in common from which the following significant observations have been made (1, 3).

(*A*) Inverse segregation occurs only in alloys with a considerable freezing range.

(*B*) The exudation type of segregation is observed with alloys in which there separates a low-melting point constituent during solidification.

(*C*) Inverse segregation occurs only in alloys that contract during solidification.

(*D*) The presence of gas absorption tends to increase the effect.

(*E*) Inverse segregation increases with increasing rate of solidification with the exception that very rapidly chilled thin sections fail to exhibit this effect.

(*F*) Inverse segregation is favored by the formation of coarse columnar grains.

On the basis of these observations a comparatively simple explanation of inverse segregation is possible.

Redistribution of Solute Atoms during Freezing

At the instant a melt is poured into a mold at lower temperature there is formed a surface of intense supercooling and heat begins to flow from the interior of the liquid, through the interface, and into the mold. Immediately after contact is made, the region of supercooling or chill is confined to a very thin section of the melt, parallel to the chill wall, and the balance of the melt is essentially without a thermal gradient (5). After a brief interval a thermal gradient is set up that extends into the interior. When a thermal gradient is established, dendritic growth will proceed simultaneously from a great many points along the dendritic arms that first developed in the undercooled layer (Fig. 6). This secondary dendritic growth will extend along the thermal gradient toward the interior of the melt and the growth rate will depend upon the steepness of the thermal gradient. The steepness of the thermal gradient depends upon the thermal properties of the mold wall, the liquidus to solidus range of the alloy, conductivity of the solidifying metal, and the temperature level of solidification (6).

This growth produces a series of parallel dendritic arms extending from the surface layer well into the interior of the ingot. The spacing of these parallel dendritic arms has been shown (7) to increase with increasing concentration of the solute atoms and with deceleration of growth, and also to vary in the same manner as the ratio of the heat of fusion to the thermal diffusivity. These interrelating factors indicate that each growing dendritic arm of the crystal is surrounded by thermal and concentration gradi-

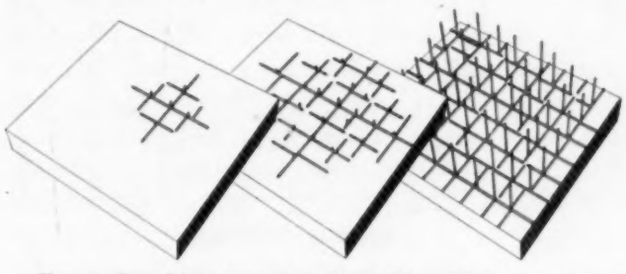

FIG. 6. Dendritic growth from mold wall into interior of melt. (a) Initial nucleation in the supercooled layer of melt next to the mold wall; (b) rapid dendritic growth parallel to mold wall to remove initial condition of supercooling in this layer; (c) dendritic growth toward the interior of the melt following the establishment of a temperature gradient.

ents that extend for considerable distances into the surrounding melt.

For the purpose of illustration the space occupied by the growing crystal may be considered as made up of an assemblage of cells (parallelograms) of practically uniform size with a growing dendritic arm occupying the longitudinal axis of each. Dimensions of the cells (spacing of the dendritic arms) are determined by the concentration and thermal gradients set up at the time that the dendritic arms were embryonic. Subsequent radial growth of each dendritic arm is restricted to the confines of the original cell because of the presence of surrounding cells. Conditions existing at successive stages of growth are therefore not exactly as depicted in Fig. 6 because the dendritic arms would not have a uniform thickness throughout their length, as shown, but would also grow in diameter as solidification proceeds.

Normally, in the case of diffusion to an expanding surface, the area of the diffusion field would increase continuously, but under the conditions outlined above the area of the diffusion field cannot increase. The concentration gradient will change continuously, however, affected by the concentration changes at the boundaries of the other cells.

The extent of dendritic growth for any instant can be calculated, if it is assumed that equilibrium conditions exist, by reference to the equilibrium phase diagram and application of the lever rule. The calculation can also be made for nonequilibrium conditions, if the assumption is made that diffusion into the solid is negligible while diffusion throughout the liquid is complete (8). Conditions applying for equilibrium and extreme nonequilibrium can then be compared graphically. All actual freezing conditions will occur somewhere between these extremes.

How this would affect dendritic growth is shown graphically in Fig. 7 for an alloy of 1% antimony in lead. The figure represents three stages in the growth

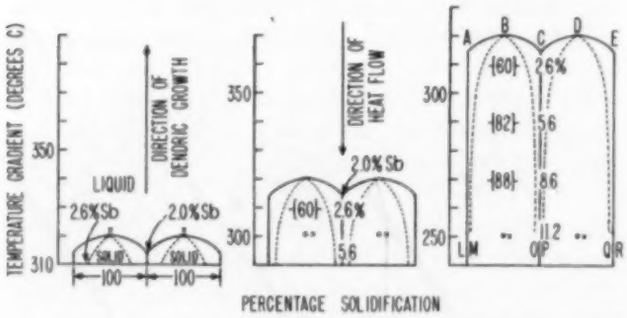

FIG. 7. Graphic representation of growth of parallel dendritic arms toward the interior of a melt under the influence of a temperature gradient. ——— Solidification under equilibrium conditions; - - - - solidification under nonequilibrium conditions; -[ ]- percentage solidified at given temperature.

of two dendritic arms, parallel to a thermal gradient, as the temperature of point x varies from 320.5° to 250.5°C (608.9° to 482.9°F). As the temperature of point x drops there will be a progressive solidification of the remaining liquid portion upon the dendritic arm that includes point x, and the latter will progressively become thicker. At the same time there will be a progressive increase in the antimony concentration of the still liquid portion surrounding point x. The numbers in brackets indicate the percentage solidification at the indicated temperatures, while the unbracketed numbers represent the concentration of the melt at the solid-liquid interface. The dendritic arms are assumed to have equal growth rates and to be surrounded by others with similar conditions of growth.

For equilibrium conditions (solid line), with a temperature gradient as shown, the advancing boundary of solidification would assume in cross section the form indicated by the line ABCDE, and the boundaries AL and ER would be in contact with neighboring dendritic arms. The entire solidification of the dendritic arms would take place in the temperature interval between 320.5° and 314°C (608.9° and 597.2°F), with the composition of the melt at the beginning being 1% and increasing to 2% just prior to final solidification. The composition of the solid would approach 1.0% as a limit and at the moment of final solidification would have a uniform composition of 1.0%. At 314°C (597.2°F) there would be no gap remaining between the dendritic arms.

The boundary condition between solid and liquid metal for conditions of extreme nonequilibrium (broken line) are represented by the line LMBOP-DQR. Solidification in this case begins at the same temperature but extends over a much larger interval, reaching the eutectic temperature of 252°C (485.6° F). The melt also varies in composition along the interface, approaching the eutectic composition of 11.2% antimony just prior to final solidification. With a considerable gap still remaining between

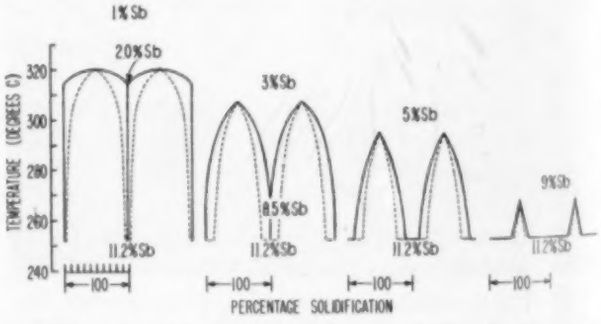

FIG. 8. Graphic representation of change in interdendritic channels for increase in antimony concentration. ——— Solidification under equilibrium conditions; - - - solidification under nonequilibrium conditions.

the dendritic arms even at the eutectic temperature, there is a definite possibility of interdendritic flow through the porous surface crust.

The space remaining between solidifying dendritic arms at the eutectic temperature increases as the amount of antimony in the alloy is increased (Fig. 8). This is true not only because of the decreased solidification taking place but also because the spacing increases with increasing concentration of the solute atoms (7). The length of the dendritic arms as compared with their thickness is dependent upon the steepness of the temperature gradient so that in chill casting quite long dendrites are possible before the surface layer is completely frozen. Fig. 7 and 8 are two-dimensional graphic representations of a three-dimensional effect. For any actual cross section the total solidification would therefore appear greater and the liquid layer surrounding each dendrite would actually appear thinner than represented here.

The assumption that diffusion in the liquid layer is complete, used here in the calculation of nonequilibrium conditions and previously by others (9–12), has been attacked (13) on the grounds that a diffusion coefficient of 1–10 cm^2/day for liquid metals (14, 15) would be entirely inadequate to insure uniform composition of the melt during freezing. That the entire melt is not of a uniform composition is undoubtedly true, as witness the concentration gradient that exists between the tip and base of a growing dendritic arm. If the diffusion coefficient was sufficiently high, there would be diffusion from regions of higher concentration to lower with uniform solidification and elimination of dendritic growth. For actual dendritic growth, however, where the mass of liquid metal is, figuratively speaking, divided into many small cells in which diffusion distances are small, the assumption can be made without serious error that complete diffusion has occurred in the liquid cross section under consideration. Spacing between dendritic arms has been measured to be about 0.001 mm for cubic metals (7) and a large portion of this pace is filled with solidified metal in the first part of the freezing interval when there is but slight change in the liquid concentration. In the final part of the freezing interval when concentration gradients are large, the diffusion would be operating through such short distances that the diffusion coefficient of 1 to 10 cm^2/day would seem adequate.

However, if the above rate of diffusion is not sufficient to produce uniform concentration in the remaining molten layer, the argument is not basically altered. The effect of an inadequate diffusion rate would be to pile up an excess of solute atoms at the solidifying interface. This, in turn, would result in a lower percentage of solidification at a given temperature and result in a larger space between dendritic arms when the eutectic temperature was reached. The net effect would be to push nonequilibrium conditions to a greater extreme than discussed above and thus increase the possibility of interdendritic channels in the outer crust.

Interdendritic Flow

While the interdendritic flow theory now seems to be generally accepted, the exact reason for an outward flow of metal between the solidifying dendrites has been the subject of some dispute. It has been suggested (16) that, as solidification proceeds, dissolved gases become increasingly concentrated in the residual liquid until the saturation point is exceeded, whereupon the gas is liberated and forces the liquid metal along the interdendritic passages toward the ingot exterior. Exudation in an 11% tin bronze does not occur when melting is performed in an oxidizing atmosphere, but becomes very noticeable in a reducing atmosphere (17, 18). Inverse segregation is greatest under atmospheres of hydrogen, water vapor, hydrogen sulfide, or methane (19). Similar results have been found for aluminum alloys (20). This evidence suggests that dissolved hydrogen causes severe segregation.

However, gas is not the sole factor or even a necessary one as demonstrated by experiments which show that inverse segregation can occur in alloys melted in a vacuum (21–25).

Lead reportedly dissolves less than 0.1 ml of hydrogen per 100 g of lead when near the melting point of the liquid metal (26). For oxygen a solubility of 0.2 ml per 100 g of lead has been reported (27), with a marked decrease in solubility for increasing additions of antimony. This volume of gas, while small, nevertheless constitutes better than 1% of the alloy by volume so that its liberation in the later stages of freezing could have an appreciable effect. However, it has been shown (25) that inverse segregation occurs in lead-antimony even when vacuum cast. One alloying constituent has been experimentally substituted for another in the interdendritic channels of a semisolid metal (28) thus proving that interdendritic flow is possible when motivated by purely gravitational forces. In the present investigation no internal porosity was found. Such porosity would be expected if gas was the motivator of interdendritic flow to the surface. The behavior of very slowly cooled ingots in which the low melting constituent withdrew from between the primary lead dendrites at the side surfaces and concentrated at the bottom surface of the ingot indicated an interdendritic flow caused by hydro-

static pressure of the still molten metal and the simple effort of a liquid to seek the lowest level.

In the case of steels cast in chill molds an air gap has been found to form between the mold wall and the frozen crust of the alloy (5). Microscopic examination of the surface of the lead-antimony alloys indicates that a gap is formed in this case also. Whether the gap was formed due to shrinkage of the original dendritic crust or expansion of the mold was not determined. Both factors probably occur to some extent and reinforce each other. Existence of an actual air gap such as occurs in steel appears to be unlikely. Instead the gap is probably filled continuously as it is produced by an inflow of molten metal. Whether or not the supercooled conditions survive long enough to cause complete filling will depend upon the conditions at the mold surface.

From the foregoing discussion it may be seen that no special force is necessary to cause interdendritic flow of metal after a gap is formed. The melt remaining between the solidifying dendrites will be near the eutectic composition. As this metal is forced into the gap by the hydrostatic pressure of the liquid interior, that portion of the liquid moving toward the surface from more remote regions will be brought to the eutectic composition. The metal flowing to fill the gap would therefore be expected to have essentially eutectic composition, whatever the composition of the original hypoeutectic melt.

Primary Crystallization of Antimony

Presence of a surface layer of antimony-rich phase in which lead appears as only a minor constituent is surprising. From the foregoing discussion a eutectic composition would be expected at the surface, but the interdendritic flow theory is inadequate to explain a structure in which antimony is plainly far in excess of the eutectic amount. In addition, antimony shows unmistakable evidence of primary dendritic crystallization and has the same crystal structure as it exhibits in the hypereutectic alloys where primary crystallization of antimony is to be expected.

Primary crystallization of antimony could occur in either of two possible ways. Either primary crystallization of antimony has occurred at the mold surface at the moment of initial chill or antimony has formed primary crystals from the eutectoid solution that flows into the air gap subsequent to the initial freezing at the mold face.

Primary crystallization of antimony at the surface in the initial chill could only occur by some process of phase inversion whereby the antimony crystals were momentarily precipitated before the expected and usual crystallization of lead crystals. Such a condition might be brought about by the extreme condition of chill and resultant supercooling produced at the moment of first contact of molten metal with mold surface. This would imply a change in the liquid prior to solidification. Theories of this type have been advanced and were considered as a possible cause of the primary crystallization of antimony.

Re-examination of Smith's theory of mobile equilibrium (29), Benedick's theory of the Ludwig-Soret effect (30), Hanson's (31) and Johnson's (32) theory of undercooling, and Ubblohde's (33) theory of minimum volume change do not suggest any mechanism that would so completely invert the normal order of precipitation as to allow primary crystallization of antimony prior to the solidification of the α phase crystals. In addition, the above theories have been more or less discredited either because of lack of favorable evidence or actual conflict with observed phenomena. Recent demonstrations (34–36) that metals can undergo extensive supercooling in the absence of nucleating agents, however, suggest a possible mechanism of phase inversion. If the molten metal were to be heated to a temperature sufficient to destroy all nuclei for lead nucleation but insufficient to destroy those effective for antimony, then the liquidus curve for the hypereutectic alloys could conceivably be extended into the hypoeutectic region, provided the lead remained supercooled and did not precipitate. Primary crystallization of antimony could then occur in regions where lead would normally be expected to appear.

Careful investigation, however, leads to the conclusion that antimony crystals were formed subsequent to the formation of the metal crust of primary lead crystallization and not at the instant that the molten metal first contacted the mold face. This conclusion is based upon the following considerations.

(*A*) In alloys of low antimony concentration, primary crystals of antimony (surface film) did not completely cover the surface but were concentrated at grain boundaries and interdendritic boundaries. If initial precipitation of antimony (inverse chill) occurred at the mold face, the distribution of the primary crystals would be expected to be random. Concentration at grain and dendritic boundaries indicates prior formation of a primary lead dendritic structure.

(*B*) The greater the differential between mold temperature and alloy freezing point the less the amount of antimony film present at the surface. Extremely rapid chill produced practically no exudations in alloys with low concentration of antimony. This is the opposite effect to that expected from an initial freezing of antimony due to surface chill.

(*C*) In the ingots that were adjusted for conditions

of unequal cooling, the greatest exudation of antimony and the appearance of well-formed tetrahedral crystals of antimony occurred at the face of lesser chill which is likewise contrary to a concept of surface chill.

(*D*) In very slowly cooled ingots, exudations occurred as a result of drainage, and primary antimony crystals were present only at the bottom of the mold which was also the last surface to cool (mold heated from below). In such slowly cooled ingots (mold and melt both originally above the freezing point of the melt) surface chill should be absent and the presence of primary crystallization of antimony at the warmest point of the mold suggests the alternate mechanism.

(*E*) In those cases where visible flow of metal could be traced across the original surface, the number, size, and perfection of the antimony crystals was greater on the secondary surface than on the primary.

(*F*) If primary crystallization of antimony is due to supercooling of lead at the initial chill surface, then the presence of nuclei for the crystallization of lead should prevent this supercooling and lead should precipitate first, in the normal manner. The ability of solid metal or metal powder to promote homogeneous nucleation of its own melt has been demonstrated (37). Castings made in a lead mold, however, continued to show primary crystallization of antimony at the surface.

(*G*) It has been demonstrated (36) that the more complex type of crystal structures show a greater tendency to supercool and that antimony shows a greater tendency to supercool than lead. Considering also that at the moment of initial chill large masses of metal are involved, it does not seem likely that lead could be supercooled to any such extent that antimony would first precipitate. More logically, antimony could be expected to supercool in the solution of eutectic composition that is extruded at the surface. In such a solution most of the heterogeneous nucleating agents would have been filtered out by passage through the narrow channel between solidifying dendrites. The mass of metal would also be separated into small droplets, a necessary condition for extreme supercooling (36). Due to a difference in crystal structure and lattice spacing the lead could not act as a nucleating agent for the antimony (37). Primary crystallization of lead could continue upon existing lead surfaces until the antimony became sufficiently supercooled to precipitate or until the molten solution was brought into contact with the mold face where nucleating agents might be present.

The primary crystallization of antimony is therefore considered to take place as a consequence of interdendritic flow of a melt of practically eutectic composition into the gap left by the cooling of the metal. Lack of nucleating agents produces supercooling of the antimony while the lead continues to precipitate with consequent enrichment of the remaining metal in antimony. The primary dendritic crystallization of antimony apparently occurs at the colder mold surface, and dendritic arms extend through the still liquid melt filling the gap to the original metal crust. The observed appearance of small tetrahedra in the new surface with the dendritic arms extending along the tetrahedra edges in the [100] directions (Fig. 9) agrees with the report that surface crystals of castings of rhombohedral metals usually have a preferred orientation with the [111] direction normal to the cold surface (38). Solidification of the antimony in the layer brings the remaining melt to the eutectic composition and eutectic crystallization occurs within the primary antimony dendritic structure. Continued solidification of the liquid eutectic causes a volume decrease and the metal recedes from the mold face and the sides of the tetrahedra so that they become exposed in relief at the surface.

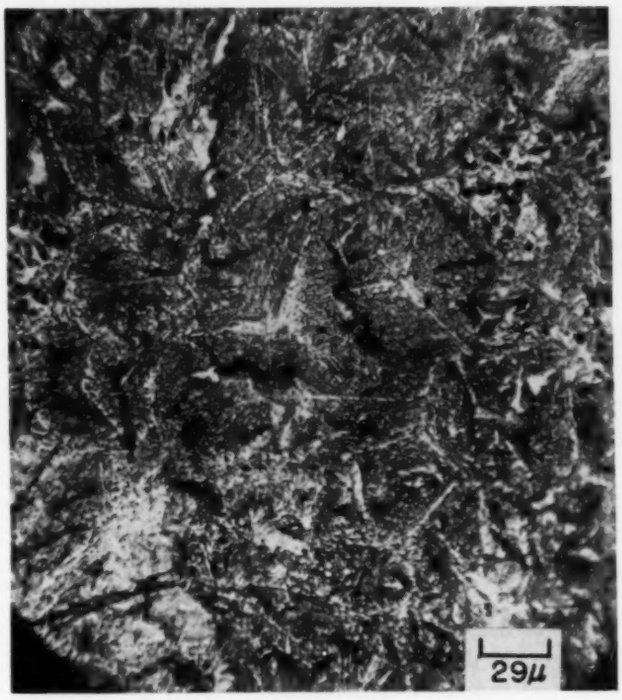

FIG. 9. A portion of the field of view to the left of the center of Fig. 4, considerably magnified. The tetrahedral shape of the individual crystals and the nature of the dendritic structure indicate oriented primary growth of antimony in the surface layer. 300×.

SUMMARY AND CONCLUSIONS

Inspection of commercially cast lead-antimony battery grids revealed the same phenomenon of excessive antimony at the surface as was found in all laboratory experiments. Laboratory experiments show that the excess amount of antimony in the sur-

face layer increases with increasing antimony content of the alloy and decreases with increasing chill. The observation that exudations decrease with increasing chill does not appear to check with previous reports. However, the terms slow chill and fast chill are relative. Castings referred to herein were made in small molds, of which at least two sides were aluminum, while some of the previous work is based on very large ingots cast in sand molds. Exudations observed on the very slowly cooled ingots (in metal molds) although highly localized in one portion of the casting probably represented as great a degree of segregation as did the more uniformly distributed (and much more noticeable) exudations of the more rapidly cooled specimens. Unequal cooling at various mold faces appeared to be as important a factor on inverse segregation behavior as was rate of chill.

Whether considered to be beneficial or harmful, inverse segregation in the lead-antimony alloys is a factor of importance. For some applications, inverse segregation may have advantages. Improved brightness and tarnish resistance result from the presence of a surface layer of antimony, and the effect of the phenomenon is to seal off and prevent any surface appearance of shrinkage cavities (except on the last surface to cool, which acts as a feeder). Whether such a layer would contribute to the physical properties of the alloy is problematical. The antimony layer is very thin and would not be expected to contribute materially to hardness or wear resistance, but the layer of eutectic material beneath it may reach a considerable thickness. Interdendritic flow of still molten alloy into the cavity left by shrinkage of the original frozen crust makes possible close casting tolerances and undoubtedly is in part responsible for the onetime belief that lead-antimony alloys expanded during freezing.

Inverse segregation may prove detrimental in applications involving corrosion resistance, such as storage battery grids. Preferential leaching out of antimony from the surface of lead-antimony alloys when subjected to anodic corrosion in sulfuric acid has been previously reported (39). Such action will have a twofold effect: (*A*) the surface antimony and eutectic structure extend from the surface into the interior of the casting along the interdendritic channels so that a penetrating type of corrosion may occur; (*B*) if the battery paste is applied to the as-cast surface, subsequent forming will remove the thin antimony layer and the exposed antimony in the surface eutectic so that poor electrical conductance and poor adherence of the active material would seem likely. Since the resulting surface will be much rougher, however, the active material may tend to adhere more firmly. Which effect predominates remains to be determined from future investigation.

The effect of inverse segregation on casting should also be pointed out. As already stated, formation of a second surface film tends to cover over any defects in the original frozen surface so that sound, pore-free castings of close dimensional tolerance are possible when the temperatures at the various mold faces are properly regulated and a proper feeding head of molten metal is provided. If all mold faces are equally chilled, however, then internal porosity should result.

The phenomenon of inverse segregation appears to be intimately associated with dendritic growth. Factors that tend to prevent dendritic growth should also tend to eliminate inverse segregation. While there is a possibility that supercooling of the eutectic and primary crystallization of the antimony could be prevented by the use of proper nucleating agents incorporated in the mold facing (37) or in the melt, there would still be a layer of eutectic structure and composition formed at the surface.

In some cases where excess antimony at the surface may be detrimental, as possibly for battery grids, the simplest solution would appear to be the removal of the surface film by chemical or electrochemical means before subsequent operations are undertaken.

Any discussion of this paper will appear in a Discussion Section to be published in the June 1955 issue of the JOURNAL.

REFERENCES

1. N. B. VAUGHAN, *J. Inst. Metals*, **61**, 35 (1937).
2. W. T. PELL-WALPOLE, *Metal Treatment*, **16**, 103, 171 (1949).
3. D. HANSON AND W. T. PELL-WALPOLE, "Chill Cast Tin Bronzes," Chapter IX, Arnold and Co., London (1951).
4. A. J. MOORE, *Metallurgia*, **38**, 71 (1948).
5. H. F. BISHOP, F. A. BRANDT, AND W. S. PELLINI, *Trans. Am. Foundrymen's Soc.*, **59**, 435 (1951).
6. H. F. BISHOP AND W. S. PELLINI, *Foundry*, **80**, 86 (1952).
7. B. H. ALEXANDER AND F. N. RHINES, *J. Metals*, **188**, 1267 (1950).
8. A. C. SIMON AND E. L. JONES, *This Journal*, **100**, 1 (1953).
9. W. G. PFANN, *J. Metals*, **4**, 747 (1952).
10. G. H. GULLIVER, "Metallic Alloys," Appendix, C. Griffin and Co., London (1922).
11. E. SCHEUER, *Z. Metallkunde*, **23**, 237 (1931).
12. A. HAYES AND J. CHIPMAN, *Trans. Am. Inst. Mining Met. Engrs.*, **135**, 85 (1939).
13. W. A. TILLER, K. A. JACKSON, J. W. RUTTER, AND B. CHALMERS, *Acta Metallurgica*, **1**, 428 (1953).
14. J. FRENKEL, "Kinetic Theory of Liquids," p. 201, Oxford University Press, Oxford (1946).
15. W. JOST, "Diffusion," p. 479, Academy Press, New York (1952).
16. R. GENDERS, *J. Inst. Metals*, **37**, 241 (1927).

17. C. H. Bierbaum, *ibid.* **37,** 281 (1927).
18. F. Höhne, *Giesserei*, **20,** 523 (1953).
19. W. Claus and F. W. Bauer, *Metallwirtschaft*, **15,** 587 (1936).
20. G. Masing and O. Dahl, *Z. anorg. Chem.*, **154,** 189 (1926).
21. W. Fraenkel and W. Gödecke, *Z. Metallkunde*, **21,** 322 (1929).
22. M. V. L. Gayler, *J. Inst. Metals*, **44,** 97 (1930).
23. H. Bohner, *Metallwirtschaft*, **11,** 437 (1932).
24. K. Iokibe, *Science Repts. Tôhoku Univ.*, **20,** 608 (1931).
25. L. Jacoby and A. Vëro, *Roy. Hung. Palatine-Joseph Univ. Tech. Econ. Sci. Soprom Publs. Dept. Mining Met.*, **14,** 347 (1942).
26. W. R. Opie and N. J. Grant, *J. Metals*, **3,** 244 (1951).
27. H. W. Worner, *J. Inst. Metals*, **66,** 131 (1940).
28. M. L. Samuels, A. R. Elsea, and K. Grube, *Trans. Am. Soc. Metals*, **31,** 459 (1943).
29. S. W. Smith, *Bull. Inst. Mining Met.*, **35,** 248 (1926).
30. C. Benedicks, *Trans. Am. Inst. Mining Met. Engrs.*, **71,** 597 (1925).
31. D. Hanson, Communication on paper by S. Smith, *J. Inst. Metals*, **17,** 112 (1917).
32. F. Johnson, Communication on paper by R. T. Rolfe, *J. Inst. Metals*, **20,** 274 (1918); **21,** 413 (1919).
33. Ubbelohde, Discussion on paper by N. B. Vaughan, Ref. (1).
34. M. D. Eberall, *J. Inst. Metals*, **76,** 295 (1949).
35. A. Cibula, *ibid.*, **76,** 321 (1949).
36. D. Turnbull and R. E. Cech, *J. Appl. Phys.*, **21,** 804 (1950).
37. J. A. Reynolds and C. R. Tottle, *J. Inst. Metals*, **80,** 93 (1951).
38. F. C. Nix and E. Schmid, *Z. Metallkunde*, **21,** 286 (1929).
39. J. B. Burbank and A. C. Simon, *This Journal*, **100,** 11 (1953).

Electroluminescence with Nonsinusoidal Fields[1]

SOL NUDELMAN[2] AND FRANK MATOSSI

U. S. Naval Ordnance Laboratory, White Oak, Maryland

ABSTRACT

Electric fields in the form of square or rectangular waves, saw-tooth waves, and exponential waves were applied to an electroluminescent phosphor. The light output contained green and blue luminescence bands, which were examined separately by means of filters, a photomultiplier, and an oscilloscope. Square wave fields produce luminescence peaks whenever the field is changing, followed by a decline in luminescence when the field is steady. Peak heights increase proportionally to about the fourth power of the field strength. They decrease with increasing frequency for the green band, while for the blue band they first increase up to about 2000 cps and then decrease. The decay obeys power laws with different exponents before and after a critical time of about 0.7 msec. A rectangular field pulse of greater duration than the critical time produces, in the green band, peaks of equal total intensity at the field reversals; in the blue band, the same excitation produces peaks with equal changes in intensity. Other field shapes produce peaks of luminescence whose heights and shapes depend on field shape and duration of the steady field before it is changed. Additional peaks in the green band appear whenever the field begins to decrease.

Observations are interpreted by using the following assumptions: excitation is due to collision processes of accelerated electrons; green luminescence involves transitions to the conduction band and to traps; blue luminescence is caused by transitions within a luminescence center; the effective field changes in time because of the development of polarization charges. Additional peaks in the green band are due to recombination processes of the polarization charges.

INTRODUCTION

In general, experiments on electroluminescent phosphors have been conducted with d-c or sinusoidally varying electric fields. These investigations have already offered valuable information and have led to conjectures on the mechanisms involved in electroluminescence (1). Additional information on the fundamental processes can be expected from application of nonsinusoidal field changes, particularly in the form of square waves, since in these cases all effects related to duration of the field show up more clearly, and the influence of the field as such can be better separated from the influence of the manner of its application. Here, therefore, fields have been applied in the form of square pulses, saw-tooth waves, rectangular pulses variable in width and repetition rate, and exponential waves to an electroluminescent ZnS:Cu, Pb-phosphor.[3] It was necessary to make the observations separately for the green and the blue luminescence bands (2) of this phosphor since characteristic differences in the electroluminescence properties of these two regions were found.

Quantitative measurements with respect to field dependence, frequency dependence, and decay laws were made on the electroluminescence patterns [brightness waves (3)] obtained by using square wave electric fields. For other field shapes only qualitative observations are reported.

Work related to this has recently been published on the influence of step functions on the time-average light output (4), on oscillograms obtained with trapezoidal waves (5) and other field shapes (6).

Although a complete and quantitative interpretation of every experimental detail is as yet impossible, sufficient information seems to be available to justify a discussion of some mechanisms contributing to electroluminescence in the light of the present observations. Other workers have suggested basic mechanisms that are relevant to some of the results of this study (1–3, 7–11). These proposals, either in their original or in a modified form, are incorporated with those given here in order to obtain an integrated picture.

EQUIPMENT AND PROCEDURE

The fields were produced by using generators giving a variety of signal wave shapes. The genera-

[1] Manuscript received March 8, 1954. This paper was presented at the meetings of the Swiss and German Physical Societies in Lugano, Switzerland, September 5, 1953, and Innsbruck, Austria, September 20, 1953, respectively; and at the Chicago Meeting of The Electrochemical Society May 2 to 6, 1954.

[2] Also at the University of Maryland, College Park, Maryland.

[3] Sylvania Electric Products Inc., Bayside, N. Y.

tors for square waves and saw-tooth waves were variable from 10 to 10,000 cps, while a pulse generator variable in pulse width and repetition rate had a range of 100–1000 cps. A direct coupled amplifier with a rise time under load of less than 10 μsec supplied an output peak to peak voltage of 0–320 volts. Exponential wave shapes were obtained by feeding a square wave into a square wave amplifier with a large RC time constant in its output circuit. This unit had a rise time under load of 250 μsec, which could be increased still more by appropriate condensers. It supplied a continuously variable peak to peak voltage of 0–4000 volts.

Light output from the phosphor was observed by a 1P21 photomultiplier tube followed by a direct coupled oscilloscope. In general, data were obtained by taking pictures of the signal trace on the oscilloscope, then reading these films with an optical comparator.

The electroluminescent phosphor investigated was in the form of a cell containing a ZnS:Cu, Pb-phosphor[3] exhibiting predominantly green light at excitation (12). Different samples of these green cells gave essentially equal results. In order to separate observations for the blue and the green luminescence band of this phosphor, a Wratten filter No. 21, which transmits wave lengths above 5300 Å, or No. 36, which transmits between 3700 and 4600 Å, was used.

Experimental Results

Square waves.—When a square pulse of about 10 μsec rise time is applied to the electroluminescent phosphor, the light output exhibits sharply rising peaks at the time of every field change. The peaks are followed by decreasing light output or "decay", which generally does not have time to reach zero light output before the appearance of the next peak. The resultant luminescence pattern contains, therefore, a varying component or "ripple" superimposed on a steady background. All measurements of luminescence intensity, as peak heights or decay curves, are taken from the level of zero light output ("reference level"), which corresponds to the oscilloscope trace obtained without field.

For the same potential difference, the luminescence pattern is generally the same, whether the field is reversed in direction or simply applied and then removed.

Fig. 1 is a reproduction of an oscillogram made with three exposures for different field strengths. Besides illustrating the general peak pattern obtained with square wave fields, this figure also shows that with increasing field it takes less time for the luminescence to reach the maximum of the peak.

Dependence of height of luminescence peaks on the repetition rate of square pulses is shown in Fig. 2. As the frequency increases, green peaks decrease in height, while blue peaks increase to a maximum value, then decrease. Experiments with manually switched D. C. indicate, however, that green peaks also decrease at extremely low frequencies, i.e., below about 2 cps. Voltage at the cell was maintained constant for these measurements.

The frequency dependence of the peak heights can be described empirically by a formula like

$$I_p = A + B \log f$$

over the frequency range 10–10,000 cps for the green peaks, and up to about 2000 cps for the blue peaks. I_p is peak height, f, frequency; A and B are constants.

Dependence of the steady background on repetition rate is also shown in Fig. 2. These curves appear to have some of the characteristics of the curves shown by Waymouth (2), obtained for the time-average light output with sinusoidal fields. There, too, the green electroluminescence increases with frequency from zero to a steady maximum value in the vicinity of 1000 cps, while the blue intensity is still growing in a nearly linear manner at about 2000 cps; but, in addition, a decrease is found in the mag-

Fig. 1. Triply exposed oscillogram for blue electroluminescence, square wave fields, 90 cps, 250 μsec rise time.

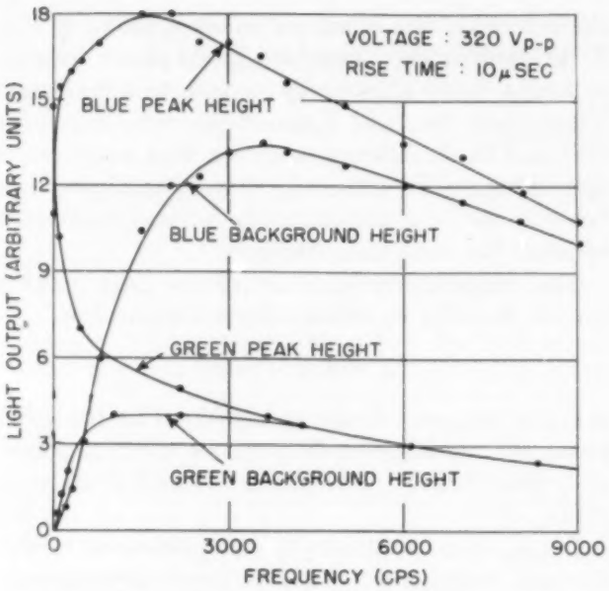

FIG. 2. Peak and steady background heights vs. repetition rate. Curves for green luminescence not drawn to same scale as for blue luminescence. Ordinates are measured from the reference ordinate for zero light output.

nitude of the steady background for both blue and green luminescence at sufficiently high frequencies. The analogy to Waymouth's results is understandable since the time-average light output is determined, to an appreciable extent, by the steady background.

Dependence of the height of the luminescence peaks on the field strength is shown in Fig. 3. Green and blue peaks grow with increasing field strength, although the green peaks do so at a more rapid rate. The curves of Fig. 3 may be described by power laws in the form $I_p = AE^n$, except for the low field region

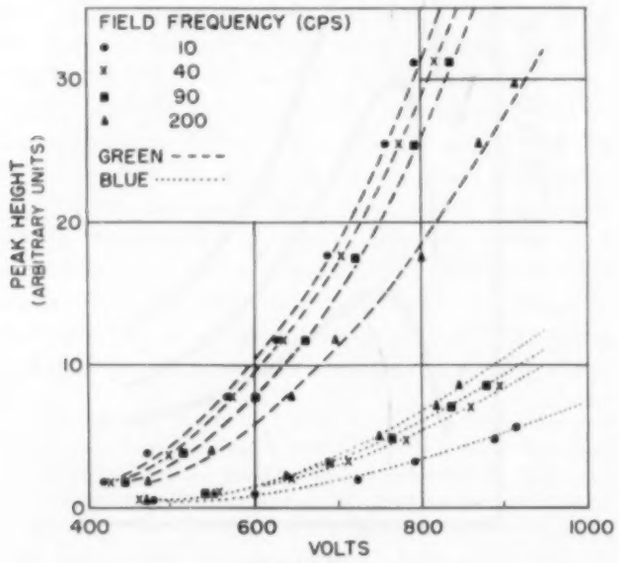

FIG. 3. Peak height vs. applied voltage. Curves for green luminescence not drawn to same scale as for blue luminescence.

of the curves for the blue peaks. The values of n obtained are 4.3 and 3.8 for the green and blue peak heights, respectively. It is also possible to represent the curves by a law of the form $I_p = aE^2 \exp(-b/E)$ as is found also by Destriau (3), with the exception that at frequencies higher than about 100 cps experimental curves of the blue luminescence depart from this relationship.

Fig. 4 shows decay curves in semi-log or log-log representation. Since the longest linear region appears in the log-log representation, it is preferable to describe the electroluminescent decay by power laws of the form $I = At^{-m}$. Furthermore, the early "linear" region of the semi-log plots is still more complex when observed with an enlarged time scale.

"Natural decay" was obtained after exposing the phosphor to weak radiation from an Argon lamp.

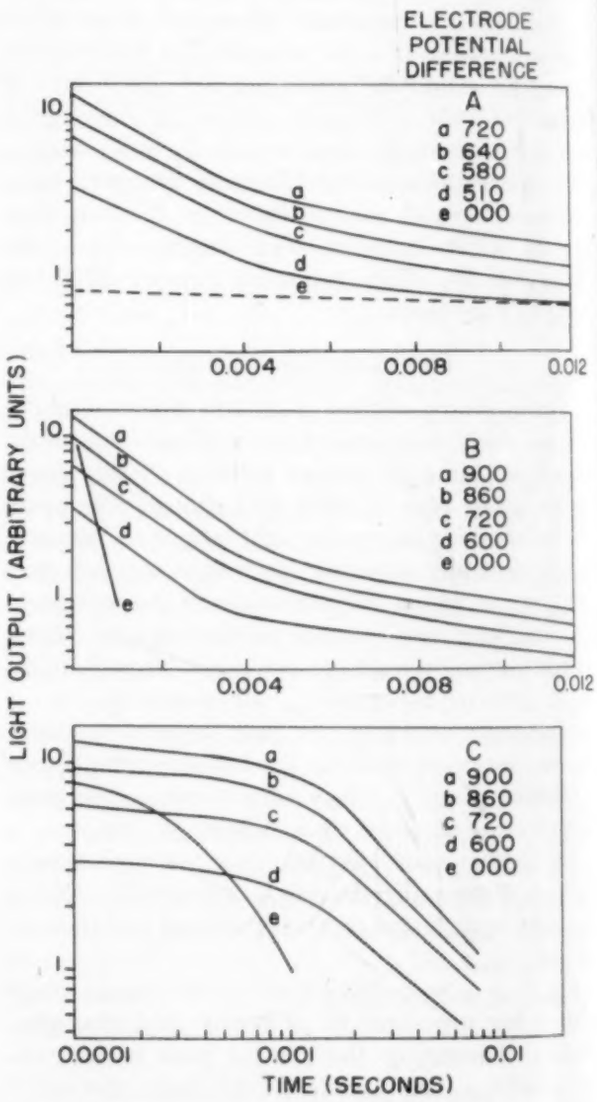

FIG. 4. Decay curves, 10 cps, 250μ sec rise time. (A) Green luminescence, semi-log; (B) blue luminescence, semi-log; (C) blue luminescence, log-log.

The natural decay curve for the blue luminescence appears to be strictly exponential, while that for the green band is more complex. The blue natural decay is much faster than decay of the blue electroluminescence, while the natural decay curve for the green band declines at a slower rate than the corresponding electroluminescence decay.

Slopes of the decay curves vary somewhat with the field. This is particularly noticeable in Fig. 4*c* for the late decay of the blue band. However, for higher frequencies and for decay curves of the green luminescence in general, there is much less change, if any, of the slopes. There is also a variation of the slopes with frequency for constant field strength, particularly for the late decay of the blue luminescence where, for example, values of m vary from about 0.72 at 10 cps to 0.95 at 90 cps (at about 800 volts) (13). If the rise time of the field was changed, there was again a distinct change of m. Similar remarks would apply to the constants of an exponential decay law.

Rectangular pulses.—When fields of rectangular pulses like those indicated in Fig. 5 are applied to the phosphor, with different times t_1 and t_2, observations reveal a marked qualitative difference between the green and the blue luminescence.

The significant features are: if t_1 is larger than about 0.7 msec, the blue electroluminescence peak increments, P_1 and P_2 in Fig. 5, are about equal, while for the green luminescence the heights H_1 and H_2 are of about the same magnitude. If t_1 is decreased to less than about 0.7 msec, the increment P_2 of the blue peaks becomes smaller. This critical time is of the same order of magnitude as the transition time observed between the two linear decay regions in Fig. 4*c*.

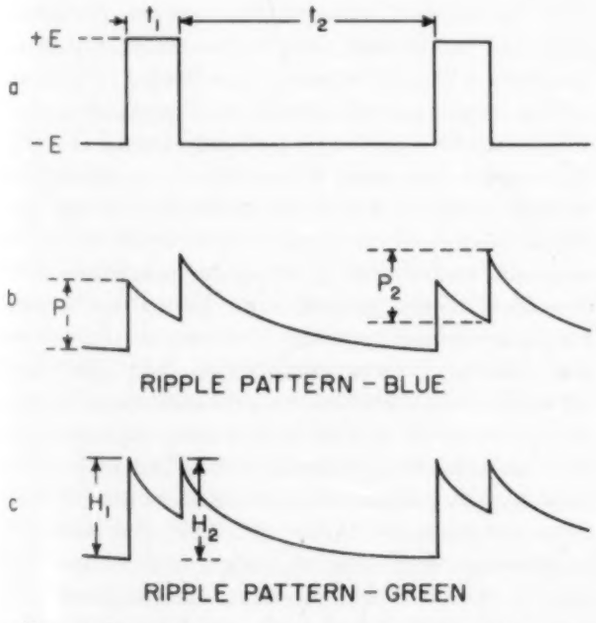

FIG. 5. Luminescence patterns for rectangular wave shapes.

Also, H_2 of the green luminescence begins to change its value if t_1 becomes smaller than the critical time. The complex quantitative details of the electroluminescence observed at small pulse time are the subject of a separate investigation and are not relevant to the discussions of this paper.

The patterns illustrated in Fig. 5 were produced by electric fields of 10 μsec rise time. Fields with longer rise times give similar results although they are not as well defined.

Exponential and saw-tooth fields.—Fig. 6, 7, and 8 are examples of oscillograms taken with a dual beam d-c oscilloscope showing a variety of electric field wave shapes and corresponding electroluminescent patterns. These oscillograms have peaks labeled by different letters. General observations pertaining to these peaks are as follows.

The A and B peaks begin to grow whenever the applied field starts to grow from zero. The A peaks, observed at sudden field reversals, have the same appearance as peaks for square wave fields. D peaks are essentially identical with A peaks, except that they occur on sudden field removals.

The C and C' peaks appear when the applied field starts to change from some steady value. They exist in the green band only and are observable only on relatively slow field changes since, for rapid field changes, A peaks would hide the C peaks. C peaks

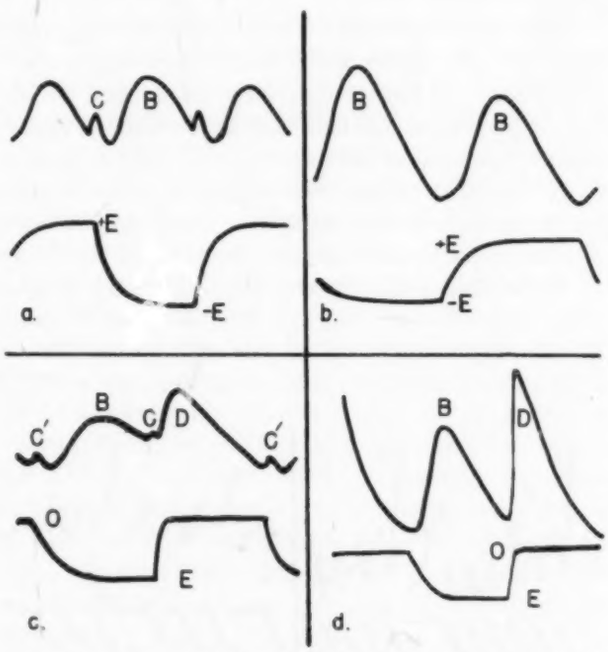

FIG. 6. Exponential fields, 500 cps, reversed and unidirectionally pulsed. (In the oscillograms in Fig. 6, 7, and 8, pictures a and c refer to green luminescence; b and d to blue luminescence. In each picture, the upper curve shows the ripple pattern; the lower curves, the corresponding applied fields.)

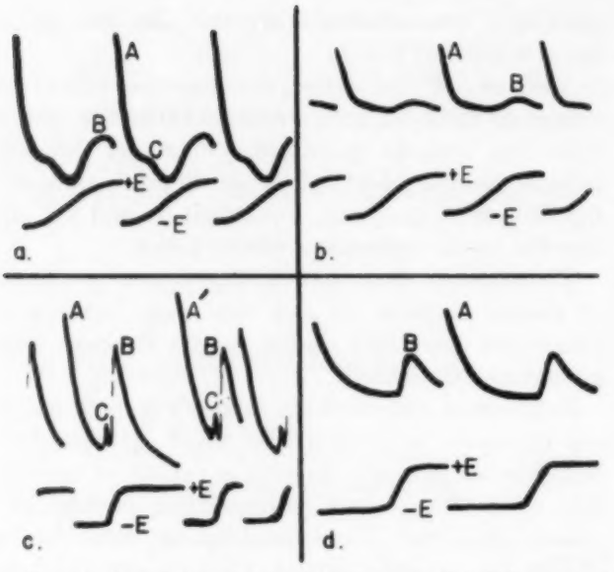

FIG. 7. Saw-tooth fields. (a) 100 cps; (b) 250 cps; (c) modified saw-tooth, rise time, 2.8 msec; (d) rise time, 2 msec.

occur when the field starts to decrease, while C' peaks appear when the field starts to rise in the case of unidirectional pulsing.

C and C' peaks decay rapidly compared with the corresponding B peaks. The C' peaks become smaller relative to the B peaks at lower frequencies. If the field strength is raised, the B peaks grow faster than the C peaks, indicating that B peaks are sensitive to the rate of growth of the applied field while C peaks are not.

Zalm and coworkers (5, 6) also report the appearance of C-like peaks under similar circumstances.

Intensity of the peaks seems to depend on the rate of growth of the field and on the time of steady field before or after field reversals (A' and B' peaks).

At very high frequencies (higher than the reciprocal of the critical time) still more complicated details appear, in particular a general decrease of the height of succeeding peaks in the green band as long as field reversals are going on (Fig. 8). This is much more conspicuous at still higher frequencies.

Finally, it should be pointed out that the patterns

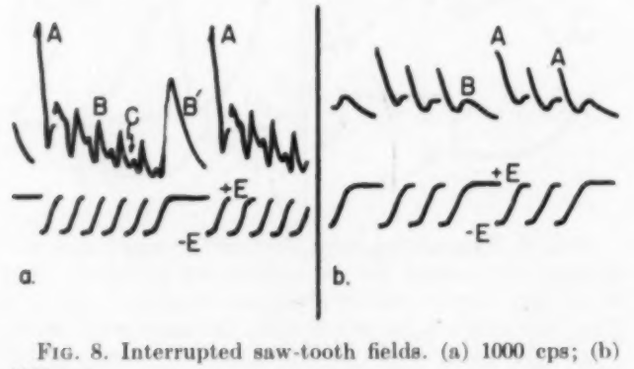

FIG. 8. Interrupted saw-tooth fields. (a) 1000 cps; (b) 1100 cps.

obtained for square pulses may be considered as simplifications of those described here inasmuch as only A-type peaks would be present.

Extinguishing effect.—If the cell is first exposed to near ultraviolet radiation and then, in addition, is placed under the influence of an electric field that is too weak to produce electroluminescence, the luminescence excited by ultraviolet radiation is diminished (14). The behavior resembles that observed for a long decay nonelectroluminescent ZnS: Cu-phosphor (15). This extinguishing effect seems to exist only in the green band. It appears with fields produced by potential differences as low as 2 volts.

INTERPRETATION

Basic assumptions.—A satisfactory basis for an interpretation must include, even if only in general terms, a description of the excitation mechanism, the luminescence processes for green and blue emission bands, and the properties of the effective internal field as distinguished from the applied external field.

Although there is no general agreement on a definite solution of the problem of the excitation mechanism, it is reasonable to assume some collision process between electrons accelerated by the field and luminescence centers. The details of such collision excitation are irrelevant as far as these considerations are concerned. The picture proposed by Curie (7) and Piper and Williams (11) (field excitation of donors, creating conduction electrons being accelerated to impact ionize or excite activators) may be accepted readily. In any case, the assumption of collision processes certainly implies that excitation must depend on the field strength, the number of electrons available for acceleration in the conduction band, and the number of centers available for excitation.

The rapid natural decay of blue luminescence, which can be described by an exponential law (Fig. 4), suggests the assumption that the blue luminescence is probably due to excitation of electrons from the ground level to some excited level within the same center, followed by an almost immediate direct transition to the ground level. Decay of the phosphor's green luminescence, however, is much slower and follows a more complicated law. The green luminescence, therefore, is probably due to some phosphorescence process with a delaying mechanism such as traps or metastable states and with transitions involving the conduction band. Similar assumptions are made by Burns (8). Also, the strong extinguishing effect observed for green luminescence only is evidence that electrons excited from green centers reach the conduction band where they can be removed by the field and made ineffective by

nonradiative transitions as considered in another case (16).

It is further assumed that green centers are excited with high efficiency, so that the number of excitable green centers strongly depends on the rate at which they are refilled. The efficiency of exciting blue centers may or may not be high. In any case, the number of excitable blue centers will remain practically unchanged because of the fast rate of refilling indicated by fast natural decay. The term "excitable center" shall indicate that the total number of centers may be much larger, but that for every field strength there may be a certain limit as to how many centers can be excited out of the total. This limit may be related to the energy level of the center.

The effective field strength in a semiconducting particle embedded in a dielectric material between metal electrodes may be expected to be different from the field applied to the electrodes. At any one instant, the effective field may be different in various regions of the phosphor particle, since strong fields are probably concentrated near the surface. One should also expect that the effective field changes in time as space charges or polarization charges build up. Thus, the field in the interior of the particle will diminish because of the polarization charges drawn to the surface by the field. If the applied field is suddenly removed after the polarization charges have accumulated, these charges themselves should create a field whose strength would decrease as the charges flow back to a neutral distribution. Therefore, if the applied field is removed or reversed faster than the polarization charges would disperse, one would expect an effective field with a maximum value shortly after application of the field reversal or removal. For slower changes of the external field, this maximum would shift to longer times. The rates of change of field and accumulation and dispersal of space charges, therefore, determine the growth and decay of the internal field.

This picture is essentially identical with ideas proposed by Kallmann (10) to explain photoconductivity experiments. He infers from his observations that at least some part of the polarization charge is trapped so that a quasi-persistent polarization of the phosphor particle is produced, which builds up and decays very slowly. Waymouth and Bitter (4) arrived at similar conclusions from electroluminescence experiments.

If the field is only removed or diminished and not reversed, the polarization charges not only provide the effective field at the removal time, but also act as an additional supply of electrons released for recombination with holes.

There is evidence that electroluminescence is restricted to small regions of the phosphor particle (6, 17). The discussion applies to this sensitive region only. However the variation of luminescence in time is of more concern than its location.

General discussion.—The basic assumptions enumerated above appear sufficient to account for most of the observations, at least qualitatively. The general mechanism responsible for the production of peaks like those in Fig. 1 may be described as follows. At the time the field is suddenly applied or reversed, electrons in the conduction band are accelerated by the field and excite luminescence centers by some collision process. In due time, conduction electrons pile up near one surface, weakening the effective field in the interior of the particle (or its sensitive region) with a corresponding decrease of the phosphor light output. The break in decay curves at the critical time of about 0.7 msec indicates two polarization processes, a fast one and a slow one which may be identified with the piling up of electrons held either in the conduction band by the field alone or in traps producing the "persistent" polarization.

At removal of the field, the polarization charges for some time provide the field necessary for occurrence of the peaks. Similarly, at field reversals the effective field is, for the first moment, the sum of the applied field and the field of the polarization charges, after which the effective field decays again.

It is easily understood that the shape of the luminescence peaks depends on the manner of growth and decay of the internal field which itself is determined by the wave shape of the applied field. Therefore, the *B* peaks and *D* peaks in Fig. 6 to 8 are considered generally to be of the same origin as the *A* peaks, the difference in shape being due only to the difference in field shapes.

Results obtained with rectangular field pulses (Fig. 5) furnish further information that shall be used to specify the model presented here in some respect and to test its applicability.

Events leading to the blue curve of Fig. 5 may be described as follows. At some field reversal, blue centers are excited, but the excited electrons return almost immediately to their ground levels so that there is always a sufficient number of excitable centers. Decay of the blue liminescence must, therefore, be considered as being due to decay of the effective field, although the intensity may not be a direct measure of the field strength. If the field is reversed again, the situation is the same as before: a sufficient number of excitable centers and an effective field that decays from a maximum value at the time of reversal. Therefore, an intensity increase equal to that observed before is found.

For intervals shorter than the critical time, polarization charges apparently do not have sufficient time to accumulate so that the effective field con-

tributed by these charges at the time of reversal is smaller than it would have been for longer time intervals, with a corresponding decrease of the light output so that P_2 decreases as it is observed.

The typical green curve of Fig. 5 can also be understood on the basis of these general assumptions. The centers excited at some field reversal are refilled relatively slowly since the green luminescence involves trapping. A subsequent field reversal, therefore, does not find the same number of excitable centers as before, but, because one assumed the field excitation of green centers to be very efficient, all the refilled centers will be excited again. This brings the number of empty centers, the number of excited electrons, and the luminescence intensity to the same absolute value as at the previous field reversal.

While the effective field lasts, i.e., within the critical time, green decay is much faster than natural decay. This indicates an additional loss of electrons from the conduction band caused by the field. This may be due to the same kind of "field-induced nonradiative transitions" that had to be introduced (16) for the interpretation of the quenching effect of the field on a phosphor during ultraviolet excitation, but there may be still another mechanism involved. During the short time of excitation by the field pulse, the traps, which are essential for the slow natural decay, may not fill as completely as in the case of the continuous ultraviolet excitation; but, in any case, the quenching effect, for whose existence there is independent evidence, should be a contributing factor.

The critical time, interpreted here as the time necessary to pile up polarization charges, is of the same order of magnitude as the lifetime of an electron in the conduction band as determined by Curie (18). This is plausible since, on the one hand, a much shorter lifetime would make it impossible to collect a sufficient number of electrons in the cloud of drifting polarization charges; and since, on the other hand, a much longer lifetime would leave so many electrons in the conduction band that polarization charges could not be restricted to a relatively small region near the surface. In order that phenomena as described above can be observed, the indicated relation between lifetime and piling-up time should, therefore, be obeyed in the particular phosphor.

As pointed out further above, the dependence of C and C' peaks on field strength is different from that observed for B peaks. The mechanism for C and C' peaks should, therefore, be of a different kind. It is assumed that recombination of excess electrons released whenever the external field is diminished after polarization charges had time to pile up is responsible for the appearance of C peaks. Polarization charges flowing back during a time of "field off" will be stopped suddenly when the field is applied again before they have been neutralized. They will then have an additional change of transitions, which may produce the C' peaks. At low frequencies, these peaks should disappear, as is observed, since the flow of the polarization charges has ceased before renewed field application. Both C and C' peaks should be absent for the blue band since the blue luminescence does not involve transitions from the conduction band.

The foregoing discussion provides an adequate description of the more important qualitative features of the electroluminescence patterns. Further details are considered below.

Details.—The difference between A and A' peaks in the green band is assumed to be due to the difference in numbers of excitable centers at the respective times of field reversal. For the A' peaks there is much more time for centers to be filled before the field is reversed than for the A peaks. Consequently, A' peaks are larger. There is no corresponding phenomenon for the blue peaks since the blue centers are filled much faster.

The pattern of Fig. 8 can be understood as being due to a combination of the effects previously considered, but already, without any reference to a mechanism, one should expect a decrease of the heights of subsequent B peaks in the green band since the green B peaks, according to experience, need a relatively long time to develop up to their maximum. This time is cut short while the high frequency field reversals are going on. The height of the B' peak, however, is normal again since there is sufficient time available.

The frequency dependence of the peak heights shown in Fig. 2 may also be understood on the basis of the picture developed here. Since, with increasing frequency, fewer electrons get back to the green centers before the beginning of the next half period, the number of electrons available for acceleration at this moment increases. Therefore, peaks of the blue luminescence should grow initially with frequency because of the increase in the number of accelerated electrons, but eventually the influence of the decrease of the effective field at field reversal because of the decrease of the number of polarization charges piled up during one half period must prevail. For the heights of the green peaks, it is necessary to take into account the fact that the number of filled green centers decreases with increasing frequency. This effect becomes unimportant only at extremely low frequencies. The fact that the frequency dependence follows empirically a logarithmic law is not yet understood. It may be purely fortuitous.

Finally, the general features of the electroluminescence patterns obtained with sinusoidal fields should also be governed by the processes consid-

ered here. In particular, one would expect C-like and B-like peaks, which may be distorted and shifted because of the different time characteristics of the fields. Indeed, the usually observed two peaks per half period may be identified with such peaks. The "in-phase" peaks correspond to B peaks, the "out-of-phase" peaks are equivalent to C peaks. A similar interpretation has recently been given by Curie (18).

The discussion above corroborates and supplements the general picture outlined in the previous sections, although not every detail has been treated. Thus, general aspects of the observed electroluminescence phenomena can be understood in terms of a few plausible assumptions on excitation, luminescence processes, and internal field.

Acknowledgments

The authors would like to thank Dr. R. M. Talley for helpful discussions, and Mr. W. W. Talbert and Mr. P. N. Buford for their assistance in matters dealing with experimental design. They also thank the Sylvania Electric Company for supplying them with electroluminescent lamps, and Dr. J. F. Waymouth for information about the phosphors.

Any discussion of this paper will appear in a Discussion Section to be published in the June 1955 Journal.

References

1. W. W. Piper and F. E. Williams, *Phys. Rev.*, **87**, 151 (1952); C. W. Jerome and W. C. Gungle, *This Journal*, **100**, 34 (1953).
2. J. F. Waymouth, *ibid.*, **100**, 81 (1953).
3. G. Destriau, *Phil. Mag.*, **38**, 700 (1947).
4. J. F. Waymouth and F. Bitter, Electrochem. Soc., Enlarged Abstracts of Papers Presented by the Electronics Division, April 1953, Abstract No. 27.
5. P. Zalm, H. A. Klasens, and G. Diemer, *ibid.*, Abstract No. 28.
6. P. Zalm, G. Diemer, and H. A. Klasens, *Philips Research Repts.*, **9**, 81 (1954).
7. D. Curie, *J. phys. radium*, **13**, 317 (1952); **14**, 135, 510, 672 (1953).
8. L. Burns, *This Journal*, **100**, 572 (1953).
9. G. Déchêne, *J. phys. radium*, **9**, 109 (1938).
10. H. Kallman, Progress Reports, Contract No. DA 36-039sc-15297, U. S. Signal Corps, SCEL, Little Silver, N. J., September, 1952 and May, 1953.
11. W. W. Piper and F. E. Williams, *Bull. Am. Phys. Soc.*, **29**, 40 (1954).
12. H. H. Homer, R. H. Rulon, and K. H. Butler, *This Journal*, **100**, 566 (1953).
13. E. Krautz, *Z. Naturforschg.*, **4a**, 284 (1949). (Krautz has found similar values of m for the decay of Gudden–Pohl flashes.)
14. G. Destriau, Private communication; T. Miller, *J. Appl. Phys.*, **23**, 1289 (1952); M. Ueta, *J. Phys. Soc. Japan*, **8**, 429 (1953).
15. G. Destriau and J. Mattler, *J. phys. radium*, **11**, 529 (1950); F. Matossi and S. Nudelman, *Phys. Rev.*, **89**, 660 (1953).
16. F. Matossi, *Naturwiss.*, **40**, 239 (1953); *ibid.*, **94**, 1151 (1954).
17. J. F. Waymouth and F. Bitter, Private communication.
18. D. Curie, *J. phys. radium*, **14**, 672 (1953).

Measuring Problems and Techniques at A-C Furnace Arcs[1]

W. E. Schwabe

National Carbon Research Laboratories, Cleveland, Ohio

ABSTRACT

A quantitative investigation of an a-c electric furnace arc is dependent upon measurement of the true arc voltage. The electrical resistance of an a-c arc is a function of many variables including current, arc length, electrode composition, furnace atmosphere, and temperature. Experimental procedures specially adapted to arc voltage measurement have been evolved and are described, together with a unique circuit which automatically compensates an inherent measurement error.

Introduction

The electric arc furnace and its power supply circuit form a costly tool of production and must be constructed with the rugged simplicity necessary to continuous trouble-free operation. Such construction does not provide for the wide variation of circuit parameters desirable from a research viewpoint. In a three-phase furnace, electrophysical investigations of the arc are further complicated by the interaction of the three phases.

To facilitate a practical small-scale approach to fundamental investigations of the electric furnace arc, a laboratory size, single-phase experimental arc furnace was constructed. The furnace is rated at 100 kva and was built for operation with two graphite electrodes permitting a steel capacity of 250 lb. However, to permit a more accurate control of arc length, the furnace has been adapted to single electrode operation for electrodes up to three inches in diameter. The electrical circuit is completed to the furnace shell by means of a bottom electrode. An independent electrode-positioning mechanism permits push-button control of the arc length. Power is supplied from a 440-v a-c line through a 100-kva power transformer tapped and regulated to provide a continuous variation of secondary voltage up to 280 v. Current limitation is accomplished with a number of variable resistance and inductance elements, which may be connected individually or in combination to provide the ballast desired. Fig. 1 is a schematic diagram of the experimental arc furnace circuit.

In addition to a variety of conventional electrical meters, special photographic and high-speed recording equipment is used in studies of the arc.

An extremely important parameter in an a-c electric arc furnace circuit is the arc voltage, i.e., the voltage drop between the electrode tip and the melt surface.

Measuring the arc voltage is a problem from both a technical and physical viewpoint. It is the objective of this paper to describe problems associated with the measurement of arc voltage, to discuss measuring techniques together with experimental results, and to propose a standard terminology for certain electrical quantities heretofore classified as arc voltage.

Measurement of A-C Arc Voltage

Measurement errors may be roughly divided into two groups as follows:

(*a*) external errors—introduced by the inclusion in the measurement of arc voltage, unwanted voltage drops across circuit elements adjacent to the arc; such elements include the electrode, the melt, and the furnace shell;

(*b*) internal errors—due to the electrophysical characteristics of arc conduction.

External errors.—An ideal measurement of arc voltage would be accomplished by connecting the leads of a suitable measuring device to the terminal points of the arc, the so-called anode and cathode spots. From a practical viewpoint such direct measurements are impossible, due to the high temperature existing inside the furnance, particularly in the arc zone. Even probe measurements, normally restricted to a short time interval, may not be applied because of the erratic travel of anode and cathode spots, characteristic of an open arc. Fig. 2 is a sequence of three photographs taken at an open arc and shows the successive half cycle locations of the arc stream occurring during each film exposure of approximately 1/30 sec (four electrical half cycles based on 60-cycle supply frequency).

In order to permit practical arc voltage measurements, meter connections have been established at the electrode clamp and on the arc furnace shell. Such measurements include the unwanted series voltage drops previously described.

[1] Manuscript received March 1, 1954. This paper was prepared for delivery before the Chicago Meeting, May 2 to 6, 1954.

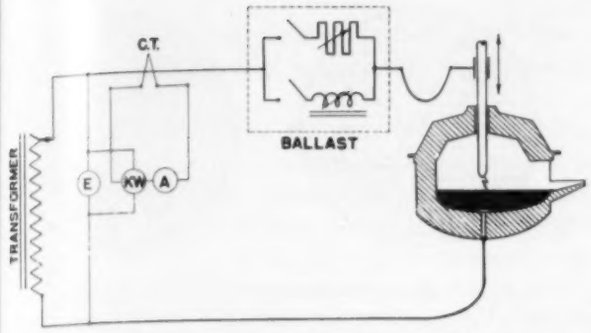

FIG. 1. Schematic diagram of experimental circuit

It is well to point out that in submerged arc furnaces the problem of measuring the arc voltage is further complicated by the contact between charge and electrode which forms parallel current paths shunting the arc, and so increasing the current through the series elements. The author's investigations have dealt primarily with the open arc, excluding detailed studies of the parallel resistance effect.

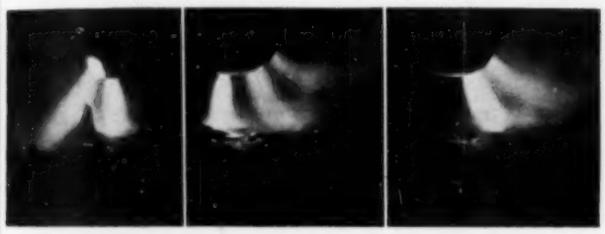

FIG. 2. Arc in a melting furnace. Three consecutive frames of a movie taken at a speed of 16 frames/sec.

The magnitude of the inherent series error has been determined for the author's circuit by lowering the electrode into the melt and measuring the short-circuit current as well as the voltage drop across the included circuit elements.

Fig. 3 is an oscillogram taken from such a test. One cycle of short-circuit current and the associated

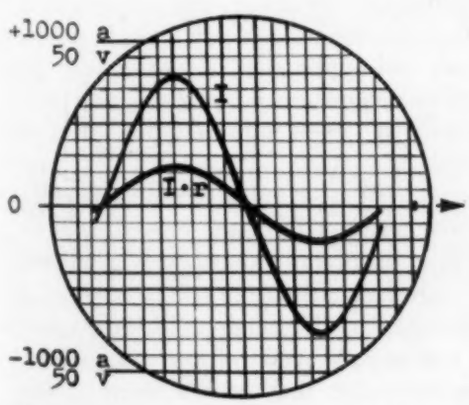

FIG. 3. Oscillogram showing the current I and the associated voltage drop $I \cdot r$ of an electrode being short circuited with the melt.

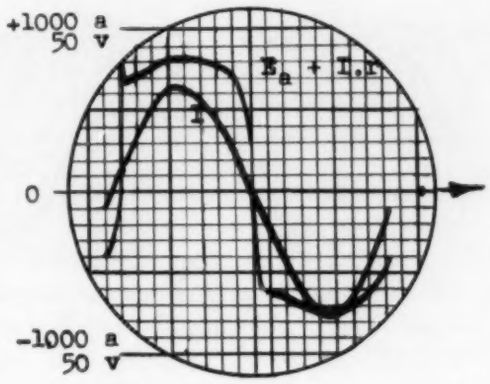

FIG. 4. Oscillogram of arc current I and arc voltage E_a including $I \cdot r$ drop.

voltage drop are plotted vs. time on the screen of a cathode-ray oscilloscope. One scale division represents 100 amp and 5 v. Peak values are 780 amp and 12 v, respectively.

An arc is established by raising the electrode from the short-circuit position, this operation being characterized by a decrease in current from its short-circuit magnitude to a value governed by the arc length and the parameters of the external circuit. Fig. 4 illustrates one cycle of current with the uncorrected arc voltage, which includes the drop previously discussed. The voltage trace is a combination of a square and a sinusoidal wave.

The error made by including the series $I \cdot r$ drop may be eliminated through a tedious point-by-point subtraction based on a knowledge of the instantaneous values of I and R. To overcome the necessity of such an operation, however, a relatively simple circuit arrangement has been developed which automatically eliminates the unwanted $I \cdot r$ drop from the recorded values of arc voltage. Both the arc and the electrode-melt-shell combination are considered to be purely noninductive resistance elements, and each in simple series circuit with the arc. Therefore, if a voltage equivalent to that across these elements, but of opposite polarity, be impressed in the metering circuit, the error is automatically canceled at every instant. The necessary voltage

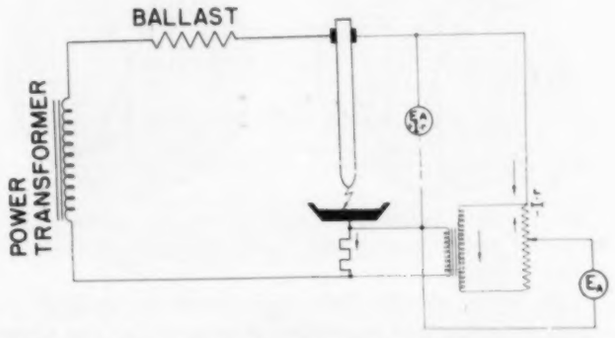

FIG. 5. Negative feedback circuit applied to measurement of arc voltage.

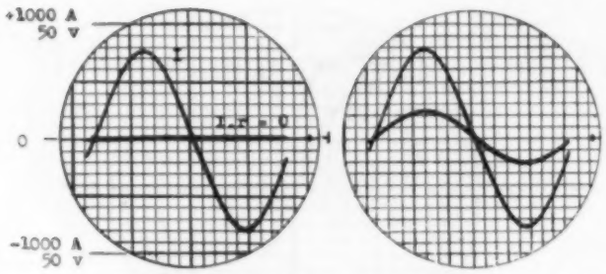

FIG. 6. Oscillograms of short circuit current and $I \cdot r$ voltage drop. *Left*, $I \cdot r$ drop cancelled; *right*, $I \cdot r$ drop present as shown in Fig. 3.

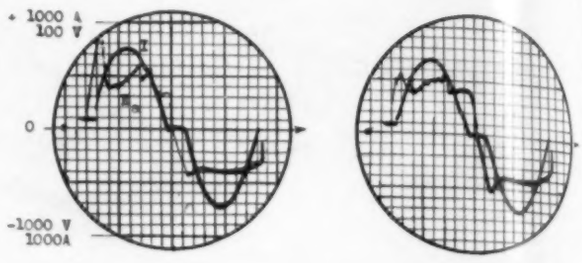

FIG. 8. Disturbance of the arc voltage during melt-down of steel. Upper half-cycles: melt = cathode; lower half-cycles: graphite-electrode = cathode.

drop is readily obtained from a noninductive shunt in series with the arc, and the reversal of polarity is accomplished with a transformer. Fig. 5 illustrates the essential features of such a negative feedback circuit.[2]

The negative feedback circuit is very easily calibrated by establishing a short circuit between electrode and melt, and adjusting the potentiometer to precisely compensate the inherent $I \cdot r$ drop. Fig. 6 illustrates one cycle of short-circuit current and the compensated $I \cdot r$ drop. For purpose of comparison, the short circuit current and uncorrected $I \cdot r$ traces of Fig. 3 are also shown.

Fig. 7 is an arc voltage and current trace in which the $I \cdot r$ drop has been compensated by the negative feedback circuit. The uncorrected trace of Fig. 4 has been inserted for comparison. Note that the sinusoidal cap on the voltage trace of Fig. 4 has been eliminated with the negative feedback circuit, and that the voltage trace of Fig. 6 now approaches a square wave. Other changes in the voltage and current wave forms of the two oscillograms are attributed to changes in the arc during the time elapsed between the two photographs.

It is of interest at this point to call attention to the fact that in Fig. 7 peak values of both voltage and current differ in each half cycle, the voltage reaching peak values of 33 and 25 v, respectively, with current peaks of 660 and 630 amp, respectively.

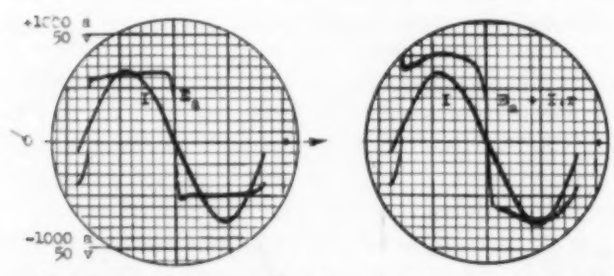

FIG. 7. Oscillograms of current I and arc voltage. *Left*, corrected arc voltage; *right*, uncorrected arc voltage as shown in Fig. 4.

[2] It is conceivable that this circuit be modified to compensate the true impedance drop given by $I \cdot z$, where $z = \sqrt{r^2 + x_L^2}$, in cases where the inductive component assumes significant proportions.

This effect is primarily due to differences between the cathode behavior of graphite and iron, as the polarity reverses with the alternating current. During the first half cycle when the graphite is cathode, a better arc conductivity is shown by the higher current and lower arc voltage. During the succeeding half cycle the converse is true.

The arc studied in Fig. 4 and 7 was struck between a graphite electrode and a slag-covered melt. Presence of a slag on the surface of the melt has a smoothing effect on the arc voltage wave form. In the case of an arc between a graphite electrode and liquid metal in the absence of slag, the arc voltage wave form is distorted by an erratic high-frequency disturbance in the half cycle during which the melt is cathode. This disturbance also deforms the current trace. The oscillograms of Fig. 8*a* and *b* were taken at an arc struck directly to liquid steel and illustrate the effect of this disturbance on the arc voltage wave forms.

Finally, it should be mentioned that, as an alternate source, the opposing voltage for the negative feedback circuit may be obtained from the secondary circuit of a current transformer connected in the furnace circuit, and that a calculation of the required opposing voltage may be made if the circuit parameters are known. Such a calculation eliminates the necessity of conducting a short-circuit test.

This negative feedback principle is readily adaptable to measurements of arc power and resistance and may find application in the precise determination of maximum arc power occurring at optimum current as well as in automatic electrode regulating systems.

Internal errors.—Having eliminated external errors with the negative feedback circuit, calculations of arc power based on independent measurements of arc voltage and current are still in error by a varying positive quantity. Through an oscillographic analysis of individual half cycles of arc voltage and current, it was concluded that conventional voltmeters indicating either rms or average values receive a positive influence from a portion of each half cycle of voltage which does not contribute to arc power,

so that arc power computations based on independent voltage and current measurements are necessarily in error.

Each half cycle of arc voltage is characterized by an initial period during which the open-circuit voltage rises to the value necessary to re-ignite the arc. As soon as the arc strikes, the voltage drops suddenly to a relatively constant value for the remainder of the half cycle. Compared with submerged arc, the open arc of an electric steel furnace is subject to a more rapid heat dissipation accompanied by a more rapid cooling of both anode and cathode spots, and so necessitating a relatively higher ignition voltage in each half cycle. The time delay until this ignition voltage is reached varies with the nature of the circuit. In a circuit containing little reactance, the time delay between zero voltage and ignition voltage is increased, whereas the phase displacement between current and voltage due to the inductance in a conventional arc furnace circuit promotes arc re-ignition by delivering an additional voltage of self-induction, $L\ di/dt$, which reaches its maximum when the current is near zero.

The oscillograms of Fig. 9 were taken at an arc circuit containing very little inherent reactance and demonstrate two extremes of ignition peak and correlated time delay. Fig. 9*a* shows the arc voltage and current at the beginning of a half cycle. The arc was struck between a graphite electrode and a slag-covered melt. Some time elapses before the current increases; this represents the ignition delay and, in this case, may be expressed as approximately five electrical degrees. Fig. 9*a* was taken at a short arc, the graphite electrode having been cathode in this particular half cycle. When the input voltage, governed by its sinusoidal variation, reaches the arc ignition value of approximately 15 v, a current flows.

In this case of short arc, there is no clearly defined ignition peak, and the arc voltage actually rises from its ignition value to remain almost constant at twenty volts. This phenomenon is attributed to the superior conductivity of the short arc. In Fig. 9*b* the arc length has been increased, the other circuit parameters having been unchanged. In this case, the ignition delay is almost 45 electrical degrees, and the current flows only when an ignition voltage of about 90 v is reached. When the current flow is established, the voltage drops from its ignition value to 60 v and remains almost constant.

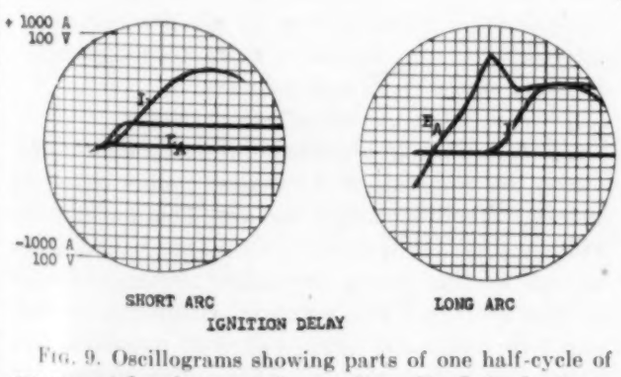

FIG. 9. Oscillograms showing parts of one half-cycle of arc current I and corrected arc voltage E_a. *Left*, short arc, current flow starts immediately; *right*, long arc, current flow delayed.

The time portion of the arc voltage from its intersection with the zero axis to the ignition peak is essentially the open-circuit voltage, and does not contribute significantly to the power of the arc. For this reason, it is referred to as the *passive* arc voltage. The time portion of the arc voltage during which a current flows has been designated the *active* arc voltage.

It is apparent that a conventional voltmeter responds to the passive as well as to the active arc voltage and that its over-all indication is higher than it should be. Arc power computations based on independent measurements of arc voltage and current are, therefore, in error by this varying positive value.

It should also be noted that in the case of prolonged ignition delay, the current does not reach its maximum at 90 electrical degrees as with a sine wave, but somewhat later. Although Fig. 9*a* and *b* illustrate the usual extremes of ignition delay, occasional delays of 55–60 electrical degrees have been observed.

Fig. 10 is a simplified reconstruction of another arc voltage trace. The input voltage in this case is 50 v rms (70.7 v peak). The ignition delay is 30 electrical degrees, and the ignition voltage is 35 v. The active arc voltage is 23.3 v and remains constant from 30 electrical degrees to 160 electrical degrees

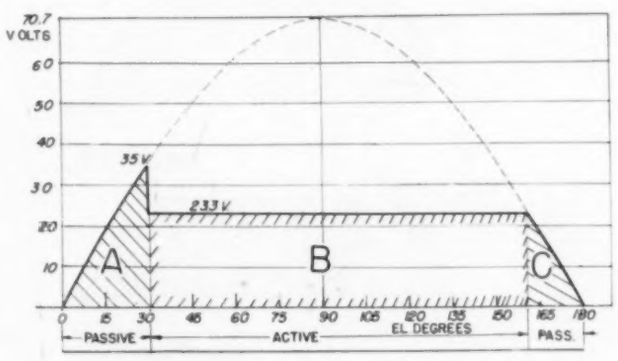

FIG. 10. Reconstruction of a typical arc voltage half-cycle. Areas A and C are passive; area B is active. Calculated meter readings of rms and average values:

Meter type	Indication	Active arc voltage (B)	Apparent arc voltage (A + B + C)	Error %
Dynamometer or thermo.	RMS	19.3	21.8	+13
Rectifier	Avg	16.4	19.3	+18

at which point it breaks down to zero. Areas A and C are passive, only area B being active in contributing to arc power.

The average and rms values for the entire voltage curve as well as for the active portion have been calculated. Both sets of calculations are based on a full half cycle (180 electrical degrees). The results of the calculations are listed in the table of Fig. 10 and indicate errors of +13 and +18% in the conventional meter readings of rms and average arc voltage, respectively. The error values calculated in this particular case are only indicative, since they apply only to the particular half cycle in question, although they do demonstrate the existence of a very considerable error.

Measurement of Active A-C Arc Voltage

It is apparent from the foregoing discussions that the active arc voltage for any short period may be measured by oscillographic means, provided that the negative feedback principle is applied. A much more desirable arrangement would provide a continuous rms meter reading of the active arc voltage. An intermediate solution may be based upon the ratio of watts to rms amperes to give the effective rms voltage. It can be assumed that the arc is a pure resistance, so that the power factor is unity. A major disadvantage of this wattmeter-ammeter method lies in the fact that two simultaneous readings are necessary. These readings are difficult to obtain, especially at melting furnaces during the melt down period, when current and arc power fluctuate rapidly.

To overcome the necessity of making two simultaneous readings, it is conceivable that the wattmeter and ammeter indications might be combined in a single instrument so calibrated that its resultant continuous indication is watt/amp, or active rms arc voltage. Such a circuit has not been developed. A relatively simple electronic circuit is also conceivable, by means of which the voltmeter circuit is only closed when current is flowing.

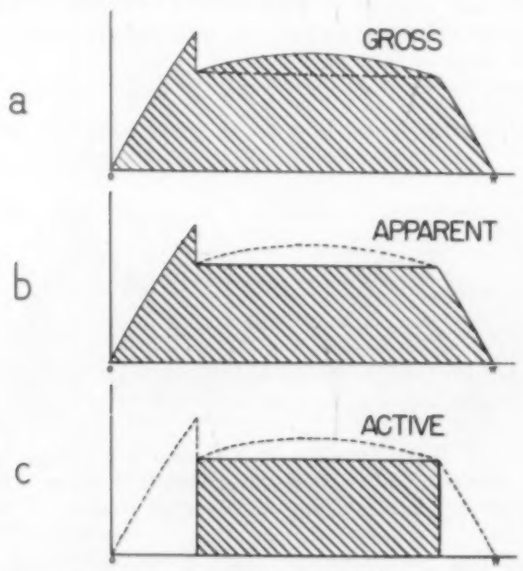

Fig. 11. Schematic definition of gross, apparent, and active a-c voltage.

The ratio of the active part of the arc voltage to the apparent arc voltage expressed as a percentage may be designated an *arc form factor*. Having measured the active and apparent arc voltage by means of the previously described wattmeter-ammeter method and an electrodynamometer voltmeter, respectively, arc form factors of 80–90% at an open arc between a graphite electrode and steel have been determined.

Lower values between 60 and 70% were found at arcs with a more pronounced rectifying effect.

It is essential to keep in mind that such meter readings average the conditions of both half waves.

Discussion

As previously stated, electrophysical investigations of the electric furnace arc conducted at producing installations have many practical limitations. Therefore, small-scale investigations utilizing an experimental furnace have been undertaken in preliminary studies of this important arc.

In the past, a considerable obstacle to the efficient collection of comparison data has been a certain ambiguity of terms commonly used in reference to the electrical operating characteristics of industrial arc furnaces. Clarification and standardization of these terms is considered to be of importance with respect to continued investigations of the complex physics of the electric furnace arc.

It is pointed out that the indications or reactions of many conventional electrical or electromechanical devices depend to some degree on the arc voltage as an activating impulse, and are positively influenced by both external and internal errors as described in the foregoing sections. The following definitions of terms related to a-c arc voltage are offered as a step toward a more thorough understanding of the electric furnace arc.

1. *Gross A-C Arc Voltage*

The alternating potential difference existing between the two nearest convenient points of the arc furnace circuit including the arc. This includes the voltage drop between the anode and cathode spots as well as that across resistance elements external to the arc, e.g., the potential difference between electrode clamp and furnace shell as measured by a voltmeter indicating rms or average values (see Fig. 11*a*).

2. *Apparent A-C Arc Voltage*

The alternating potential difference existing between the anode and cathode spots of an a-c arc. This can be measured either by connecting adequate probe contacts directly to the anode and cathode spots or, more practically, by making connections at external points and correcting the indication by means of a feedback circuit (see Fig. 11*b*).

3. *Active A-C Arc Voltage*

That portion of each individual half cycle of apparent arc voltage contributing to arc power. The rms value of active arc voltage can be calculated from simultaneous wattmeter and ammeter readings (see Fig. 11*c*).

4. *Arc Form Factor*

The per cent ratio between the active and the apparent arc voltage.

Any discussion of this paper will appear in a Discussion Section to be published in the June 1955 issue of the JOURNAL.

Diffusion of Hydrogen and Deuterium in High Purity Zirconium[1]

EARL A. GULBRANSEN AND KENNETH F. ANDREW

Westinghouse Research Laboratories, East Pittsburgh, Pennsylvania

ABSTRACT

Kinetics of the reaction of zirconium with pure hydrogen and deuterium was studied for 60°–250°C, H_2 pressures of 1.1–5.0 cm Hg, and composition range Zr–$ZrH_{1.70}$, using a vacuum microbalance method. The reaction was shown to be diffusion-controlled with diffusion occurring from a surface of constant concentration into a heterogeneous system.

The diffusion equation was solved for these conditions using the method originally developed by Neuman and recently applied by Wagner to this type of problem. Average concentration according to this view is given by

$$\bar{C} = 2.845 \frac{D^{1/2} t^{1/2}}{h}$$

where D is diffusion coefficient in cm²/sec, t is time in seconds,and h is specimen thickness in centimeters.

Plots of $\bar{C}$ vs. $t^{1/2}$ show this relationship to hold over wide variations in time, temperature, pressure, and specimen thickness. Diffusion coefficients were calculated and when plotted against $1/T$ on a logarithmic plot gave a heat of activation of 11,400 cal/mole. The corresponding entropy of activation was 2.7cal/mole/°C.

The following equation expresses data for diffusion of hydrogen in zirconium:

$$D = 1.09 \times 10^{-3}\, e^{-11,400/RT} \text{ cm}^2/\text{sec}$$

For the composition range of Zr to $ZrH_{1.6}$, experimental data fit the proposed explanation for the reaction. At higher compositions, deviations were observed.

Diffusion of deuterium in zirconium was also studied and data found to fit the equation:

$$D_{D_2} = 0.73 \times 10^{-3}\, e^{-11,400/RT} \text{ cm}^2/\text{sec}$$

The relationship between the diffusion coefficient of hydrogen and deuterium was found to be 1.5. The theoretical value should be $\sqrt{2}$.

The diffusion mechanism proposed was verified by experimental results.

INTRODUCTION

Much of the work on the reaction of zirconium with hydrogen was reviewed by Smith in 1948 (1) and by Gulbransen in 1954 (2). Two studies have been made of the kinetics of the reaction with hydrogen. Gulbransen and Andrew (3) studied the rate of hydriding between 200° and 300°C using high purity metal and a source of highly purified hydrogen. Although some kinetic data were obtained, the rate of reaction was difficult to reproduce and appeared to be sensitive to pretreatment and to surface films. Since the initial surface oxide film was not removed and its importance was not recognized at that time, these kinetic results must be interpreted in terms of an oxide-contaminated surface.

Bernstein and Cubicciotti (4) studied the permeation of zirconium by hydrogen at 545°–920°C. Again, results were difficult to reproduce, and evidence for a contaminating film was observed in all experiments.

Recent studies by Gulbransen and Andrew (5) showed that the room temperature surface oxide film has a remarkable inhibiting effect on rate of hydriding. Unless great care was taken to remove the initial oxide film and to purify the hydrogen, the rate of hydriding was limited by a surface reaction.

Since the mechanism of hydriding of zirconium may involve one or more diffusion processes, precise information on the phase diagram of zirconium-hydrogen alloys is required. Although Hägg (6)

[1] Manuscript received March 29, 1954. This paper was prepared for delivery before the Chicago Meeting, May 2-6, 1954.

studied the system earlier and showed the existence of several hydride phases, the ranges of homogeneity of these phases were not established.

To supplement this work, Gulbransen and Andrew (7) determined ranges of homogeneity of several phases from thermodynamic studies and from x-ray diffraction studies. In brief, for temperatures below 500°C, the ϵ-phase of Hägg was shown to have a composition range of $ZrH_{1.965}$ to $ZrH_{1.64}$, while the δ-phase has a range from $ZrH_{1.56}$ to $ZrH_{1.40}$. A two-phase region of α- and δ-phases exists for all compositions between zirconium saturated with hydrogen in solid solution and $ZrH_{1.40}$. At 250°C, the maximum temperature used in this work, the solubility of hydrogen in zirconium corresponds to the composition $ZrH_{0.001}$ (8).

With this new information on the phase diagram, and with techniques available for removing the initial surface oxide film and for purifying hydrogen, it was possible to study the mechanism of the reaction of pure hydrogen with a clean zirconium surface.

Analysis of Diffusion Problems

Wagner (9) has discussed the general problem of diffusion in binary systems of more than one phase. From a mathematical point of view this problem was similar to that of melting or solidification in which one substance changes into another with emission or absorption of heat. The common feature of these problems was the existence of a moving surface of separation between two phases, at which material or heat was being transferred. The original solution of the heat problem was due to Neuman and was presented in a book by Carslaw and Jaeger (10).

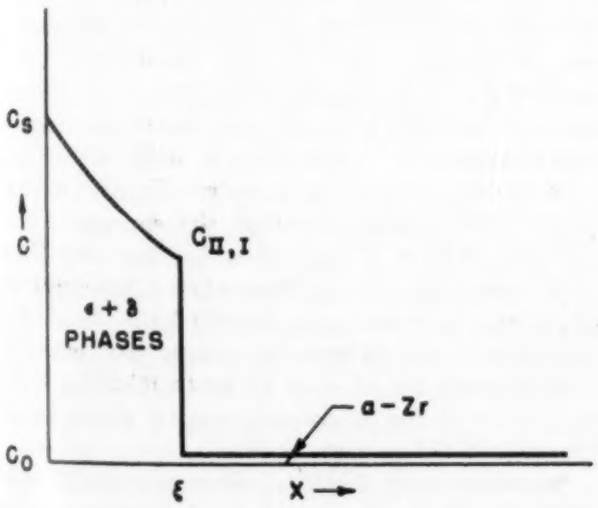

Fig. 1. Diffusion picture, hydrogen in zirconium (after Wagner). $t > 0$; $c_s = ZrH_{1.965}$; $c_{II,I} = ZrH_{1.60}$; $c_o = ZrH_{0.001}$ at 250°C.

General picture.—Fig. 1 shows the analysis given by Wagner (9) for diffusion from a surface into a heterogeneous system for a flat plate. c_s is the surface concentration at $x = o$, c_o is the concentration at time $t = o$, and $c_{II,I}$ is the concentration in phase II at the interface ξ with phase I. Diffusion proceeds from the surface in the homogeneous phase II. At time t the region of phase II extends from $x = o$ to $x = \xi$.

Since hydrogen reacts with zirconium to form two hydride phases in addition to dissolving in α-zirconium, the validity of the diffusion picture shown in Fig. 1 may be questioned. However, the ϵ and δ hydride phases for most purposes can be considered as one phase, since their ranges of homogeneity are nearly continuous (7) and since their crystal structures are similar. The effect of solution of hydrogen in the metal is negligible since the solubility at 250°C is of the order of $ZrH_{0.001}$ (8).

General solution.—The following equation governs the diffusion process:

$$\frac{\partial c}{\partial t} = D\frac{\partial^2 c}{\partial x^2} \qquad \text{(I)}$$

Here the diffusion coefficient, D, is assumed to be independent of concentration. The boundary condition is

$$c = c_s \text{ at } x = o \text{ and } t > 0 \qquad \text{(II)}$$

At the interface $x = \xi$ the concentration of diffusing species in phase II is that relating to the equilibrium value between phases I and II.

$$c = c_{II,I} \text{ at } x = \xi \qquad \text{(III)}$$

When the interface is displaced by $d\xi$ for a time dt, the quantity $[c_{II,I} - c_o]\, d\xi$ of hydrogen must be supplied from the region $x < \xi$. Thus,

$$[c_{II,I} - c_o]\, d\xi = Ddt\left(\frac{\partial c}{\partial x}\right)_{\xi - o} \qquad \text{(IV)}$$

A particular solution of equation (I) for boundary condition (II) is

$$c = c_s - B\, erf\left(\frac{x}{2\sqrt{Dt}}\right), \quad \text{for} \quad o < x < \xi \qquad \text{(V)}$$

Here B is a constant and *erf* is the error function. Wagner (9) assumes as does Neuman (10) that the plane of discontinuity is shifted proportional to $t^{1/2}$. Thus,

$$\xi = \gamma\, 2\sqrt{Dt} \qquad \text{(VI)}$$

Here, γ is a dimensionless parameter.

Substituting, one obtains

$$c_s - c_{II,I} = B\, erf\,(\gamma) \qquad \text{(VII)}$$

$$c_{II,I} - c_o = \frac{B}{\sqrt{\pi}} \exp(-\gamma^2) \qquad \text{(VIII)}$$

Eliminating B, one has

$$\frac{c_s - c_{II,I}}{c_{II,I} - c_o} = \sqrt{\pi}\,\gamma e^{\gamma^2}\, erf\,\gamma \qquad \text{(IX)}$$

γ can be found from equation (IX) and B from equations (VII) and (VIII).

D is usually found by observing the displacement ξ and by the use of equation (VI). However, if the reaction is followed by a weight gain method, D must be obtained from the average concentration in the sample as a function of time.

Solution for weight gain method.—Let $\bar{c}$ be the average concentration in phase II, $o < x < \xi$. Then,

$$\bar{c} = \frac{1}{\xi}\int_o^\xi c(x,t)\,dx$$

$$= \frac{1}{\xi}\int_o^\xi \left[c_s - B\,erf\frac{x}{2\sqrt{Dt}}\right]dx \qquad \text{(X)}$$

$$= \frac{1}{\xi}\left[c_s\xi - B\int_o^\xi erf\frac{\gamma x}{\xi}\right]dx \qquad \text{(XI)}$$

Integrating,

$$\bar{c} = c_s - B\,erf\,\gamma + \frac{B}{\gamma\sqrt{\pi}}(1 - e^{-\gamma^2}) \qquad \text{(XII)}$$

This shows that $\bar{c}$ is independent of t.

Substituting (VII) and rearranging,

$$\frac{\bar{c} - c_{II,I}}{c_s - c_{II,I}} = \frac{1 - e^{\gamma^2}}{\gamma\sqrt{\pi}\,erf\,\gamma^2} \qquad \text{(XIII)}$$

Using this analysis, equations (IX) and (XIII) are plotted as a function of γ. From the plot of equation (IX) a value for γ is obtained and from a plot of equation (XIII) and this value of γ, a value for

$$\frac{(\bar{c} - c_{II,I})}{(c_s - c_{II,I})}$$

can be obtained.

From these plots $\gamma = 0.425$ and

$$\frac{\bar{c} - c_{II,I}}{c_s - c_{II,I}} = 0.485$$

Now an expression can be written for the average concentration $\bar{C}$ over the whole specimen:

$$\bar{C}\frac{h}{2} = \bar{c}\xi + c_o\left(\frac{h}{2} - \xi\right) \qquad \text{(XIV)}$$

Here, $h/2$ is the half thickness and c_o the solubility of hydrogen in α-Zr. For temperatures of 250°C and lower, c_o has a value of 0.001 or less in terms of the ratio H/Zr and is, therefore, negligible.

Substituting equation (VI) and (XIV) and the values for γ and $\bar{c}$,

$$\bar{C} = 2.845\frac{D^{1/2}t^{1/2}}{h} \qquad \text{(XV)}$$

For the 0.0127 cm specimens, this equation becomes

$$\bar{C} = 224\,D^{1/2}t^{1/2} \qquad \text{(XVI)}$$

and for the 0.0508 cm specimens,

$$\bar{C} = 56\,D^{1/2}t^{1/2} \qquad \text{(XVII)}$$

In deriving equation (XV) from (XIV) it is assumed that c_s is constant and independent of pressure. Phase diagram studies by Gulbransen and Andrew (7) show that c_o has a value of 1.965 in terms of the ratio H/Zr, and for temperatures of 250°C and lower, c_s is independent of pressures of the order of 1 cm Hg and higher.

Testing of the mechanism of the reaction.—The reaction mechanism upon which equation (XV) is based can be tested experimentally. First, plots of $\bar{C}$ vs. $t^{1/2}$ can be used to test the square root of time relationship. Second, use of different thicknesses of samples tests the validity of equation (XV). Third, use of both hydrogen and deuterium having different diffusion coefficients gives an additional way of testing equation (XV). Fourth, the analysis assumes a constant value for c_o. The effect of pressure, therefore, should be negligible. Fifth, a plot of log D vs. $1/T$ should give a straight line and a reasonable heat of activation. Sixth, the entropy of activation of the diffusion process should have a value near zero or slightly positive.

Experimental

A vacuum microbalance was used to determine the rate of reaction of hydrogen with the metal. Its construction and use has been described in previous publications (11, 12). The sensitivity of the balance was 1.25 divisions (0.00125 cm) per microgram for the 0.05 g sample, and the weight change was estimated to ¼ of a division (0.20×10^{-6} g).

A mullite furnace tube sealed directly to the Pyrex glass system contained the specimen. The vacuum behavior of this system has been described (13). Special precautions necessary for the study of zirconium have also been described (5). In all experiments described here, the system and specimen were pumped for at least 15 hr to minimize contamination of the gas atmosphere by degassing of the walls of the vacuum system.

Specimens were sheets of zirconium 0.0127 and 0.050 cm thick. Two weights of specimen were used, 0.0486 g or 0.4995 g. The larger specimens were used for experiments at 60°–100°C where the

TABLE I. *Analysis of zirconium samples*

	Foote Zr typical wt %
Si	0.01
Fe	0.04
Al	0.01
Cu	<0.01
Ti	0.03
Mn	<0.001
Ca	0.01
Mg	<0.003
Pb	<0.001
Mo	<0.001
Ni	0.01
Cr	0.001
Sn	0.001
W	<0.001
N	<0.01
O	<0.01
H	<0.02
C	<0.001
Hf	2.40

amount of reaction was small, while the smaller specimens were used where a large reaction with hydrogen was expected.

Pure hydrogen or deuterium was prepared by diffusing the purified electrolytic hydrogen or high purity grade of deuterium (99.66% D_2) through a palladium tube (11). To minimize contamination the gas was prepared immediately before use.

High purity iodide zirconium was obtained from Foote Mineral Company. The analysis is given in Table I. All specimens were given an abrading and cleaning treatment as previously described (5). They were placed in turn on the balance, and the tube sealed off. The specimen and vacuum system was pumped for 15 hr or longer. Before reacting with hydrogen, each sample was heated to 700°C in high vacuum for 1–2 hr.

Results and Discussion

General

Fig. 2 shows a series of weight gain vs. time curves for the hydriding of zirconium at 150°–250°C and for a hydrogen pressure of 5 cm Hg. A new specimen was used for each experiment. For the area and weight of the specimens, a weight gain of about 715 $\mu g/cm^2$ corresponds to a concentration of $ZrH_{1.965}$. In several of the experiments shown in Fig. 2, this concentration was achieved. No visual evidence was found for the presence of an oxide film after concluding the experiment.

Fig. 3 shows a similar series of curves for 60°–125°C. The curves were of similar shape to those of Fig. 2. However, the maximum concentration attained in these experiments for one hour of reaction was $ZrH_{0.2}$.

There is no evidence of an induction period which suggests that the surface was free of oxide film and that the reaction is diffusion-controlled. Previous studies (5) have shown that very thin oxide films (*a*) exert a strong inhibiting influence on the hydrogen reaction, (*b*) were responsible for the observed induction period of the reaction, and (*c*) explain many of the supposedly inert characteristics of the metal to reaction with hydrogen.

Rate law correlation.—To test the mechanism of reaction, the average concentration $\bar{C}$ was plotted against the square root of time according to equation (XV). Fig. 4 shows this type of plot for the 250° and 175°C experiments. The 250°C data follow a straight line relationship up to a concentration corresponding to an H/Zr ratio of 1.60 or the limit of the two-phase region. The 175°C data show a straight line relationship to the concentration limit of the experiment, namely, a value of H/Zr of 0.86.

Fig. 5 shows similar plots for the 60° and 100°C experiments. Although only the initial stage of the reaction was studied, straight line relationships were

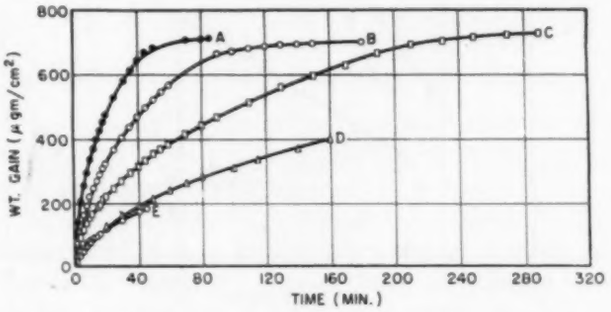

Fig. 2. Effect of temperature on hydriding zirconium. Curve A, 250°C, 5 cm of Hg of H_2; curve B, 225°C, 5 cm of Hg of H_2; curve C, 200°C, 5 cm of Hg of H_2; curve D, 175°C, 5 cm of Hg of H_2; curve E, 150°C, 5 cm of Hg of H_2.

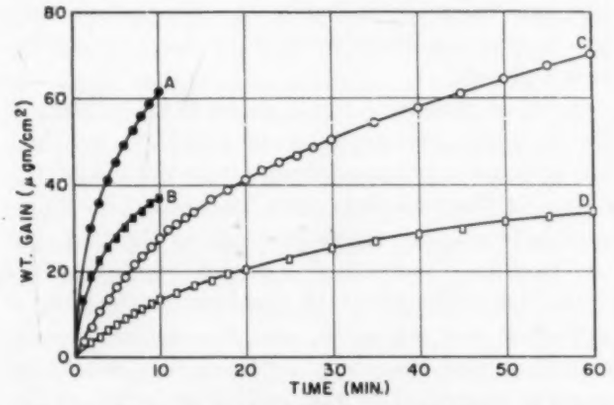

Fig. 3. Effect of temperature on hydriding zirconium. Curve A, 125°C, 2.3 cm of Hg of H_2; curve B, 100°C, 2.4 cm of Hg of H_2; curve C, 80°C, 2.4 cm of Hg of H_2; curve D, 60°C, 2.4 cm of Hg of H_2.

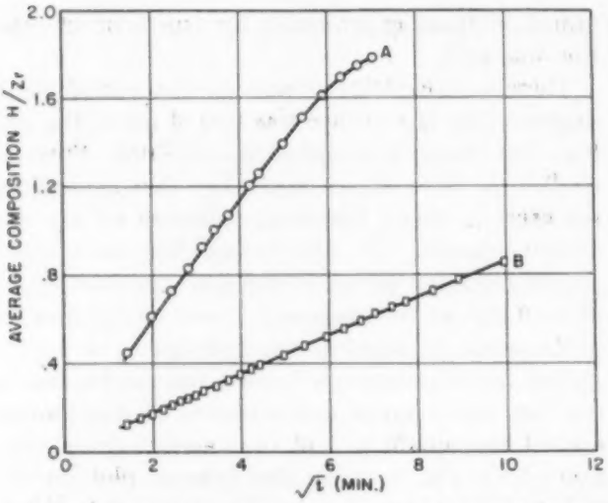

FIG. 4. Effect of temperature on hydriding zirconium. Curve A, 250°C, 5.0 cm of Hg of H_2; curve B, 175°C, 5.0 cm of Hg of H_2.

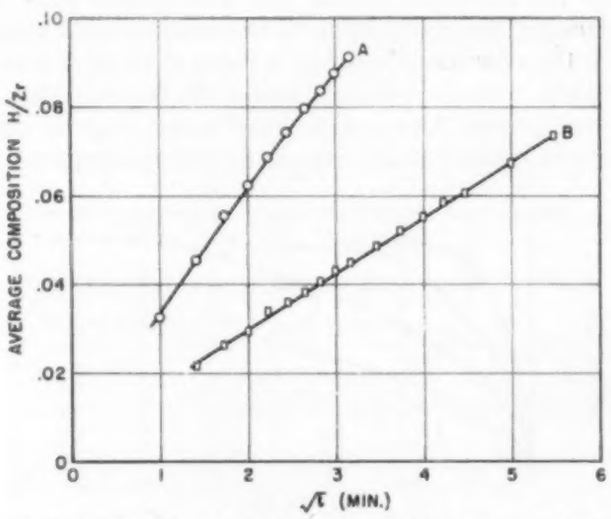

FIG. 5. Effect of temperature on hydriding zirconium. Curve A, 100°C, 2.4 cm of Hg of H_2; curve B, 60°C, 1.4 cm of Hg of H_2.

found. Thus equation (XV) adequately describes the time behavior, including the assumption made by Wagner on the movement of the interface between phases.

Effect of pressure.—Fig. 6 shows $\bar{C}$ vs. $t^{1/2}$ plots of the data for two experiments at 225°C in which the pressure was varied from 1.1 to 5.0 cm of Hg. Slopes of the two plots were identical. The difference between the curves was due to the fact that the buoyancy correction[2] was not applied to the data. Hence the effect of pressure on the rate of hydriding was negligible, and the surface concentration c_s was essentially $ZrH_{1.965}$. This conclusion was also supported by thermodynamic evidence (7).

Effect of sample shape.—According to equation (XV) the sample thickness, h, affects the slope of the $\bar{C}$ vs. $t^{1/2}$ plot by the factor $1/h$. Fig. 7 shows a comparison of this type of plot for two thicknesses of metal, 0.0127 and 0.0508 cm. The effect of h on the plots was that predicted by equation (XV).

[2] This correction was a result of thermal convection currents set up in the furnace tube. It could be evaluated from the final vacuum reading.

Calculation of Diffusion Coefficients

Equation (XV) was used to calculate diffusion coefficients from the $\bar{C}$ vs. $t^{1/2}$ plots. These are summarized in Table II. Fig. 8 shows these data on a log D vs. $1/T$ plot, and from the slope a heat of activation of 11,400 cal/mole was calculated. Data for samples of different thicknesses were included.

D_o was calculated from the equation

$$D = D_o e^{-\Delta H^*/RT} \qquad \text{(XVIII)}$$

Here, D_o was the value of D at infinite temperature, and ΔH^* was the heat of activation of diffusion. The values of D_o were tabulated and an average value of 1.09×10^{-3} was calculated. The data could be represented by

$$D = 1.09 \times 10^{-3} \times e^{-11,400/RT} \text{ cm}^2/\text{sec} \qquad \text{(XIX)}$$

The value of 11,400 cal/mole for the heat of activation of diffusion for hydrogen in zirconium

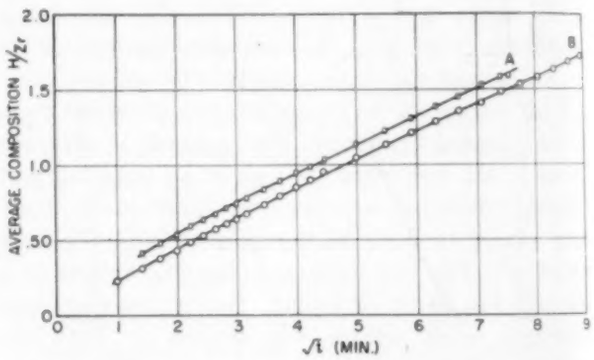

FIG. 6. Effect of pressure on hydriding zirconium. Curve A, 225°C, 5 cm of Hg of H_2; curve B, 225°C, 1.1 cm of Hg of H_2.

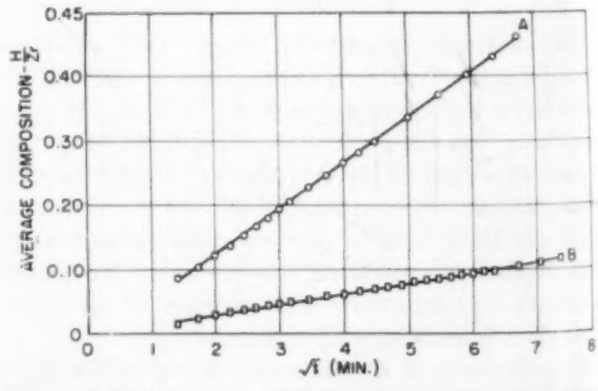

FIG. 7. Effect of sample thickness on hydriding zirconium. Curve A, 0.0127 cm thick, 150°C, 2.4 cm of Hg of H_2; curve B, 0.0508 cm thick, 150°C, 5.0 cm of Hg of H_2.

TABLE II. *Diffusion data hydrogen in zirconium*

t°C	$1/T \times 10^3$	D_{avg} cm²/sec	D_o cm²/sec
60	3.0021	4.60×10^{-11}	1.341×10^{-3}
80	2.832	7.09×10^{-11}	0.784×10^{-3}
100	2.680	2.54×10^{-10}	1.178×10^{-3}
120	2.544	3.25×10^{-10}	0.705×10^{-3}
125	2.512	6.43×10^{-10}	1.144×10^{-3}
150	2.360	1.625×10^{-9}	1.26×10^{-3}
175	2.232	2.470×10^{-9}	0.876×10^{-3}
200	2.114	6.02×10^{-9}	1.099×10^{-3}
225	2.008	1.33×10^{-8}	1.33×10^{-3}
250	1.912	2.215×10^{-8}	1.217×10^{-3}
			avg 1.09×10^{-3}

appears to be reasonable since value heats of activation of 5,740–10,100 cal/mole have been observed (14) for the diffusion of hydrogen in palladium. The most reliable work on diffusion of hydrogen in palladium gave a value of 5,740 cal/mole (15, 16).

Calculation of Entropy of Activation

One of the best ways to check on diffusion results is to make an approximate calculation of the entropy of activation using the classical theory of diffusion as restated by Zener (17). According to this theory, D_o is given by the expression

$$D_o = ga^2\nu e^{\Delta S^*/R} \qquad \text{(XX)}$$

Here, a is the distance between sites for diffusion, ν is the frequency of vibration along the path of the diffusion, ΔS^* is the entropy of activation of diffusion, and g is a constant determined by the geometry of the particular processes of diffusion.

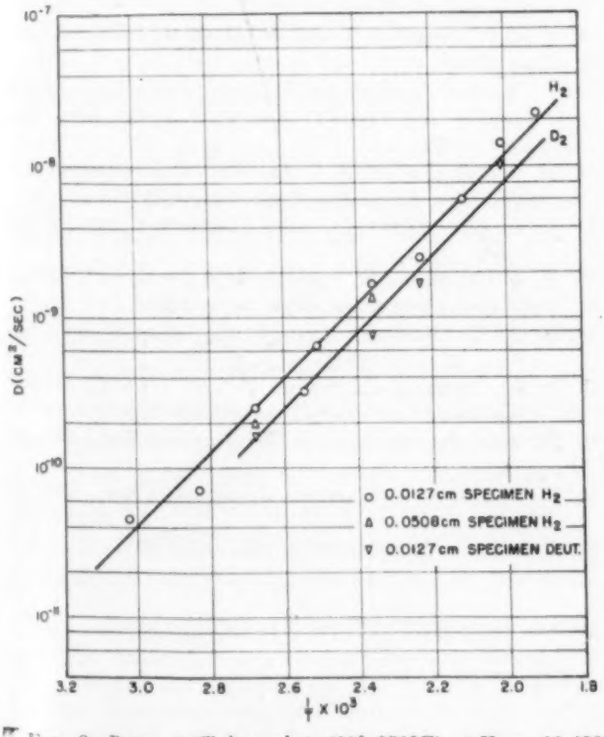

FIG. 8. D vs. $1/T$ log plot (60°–250°C). ΔH = 11,400 cal/mole; P = 1.1–5.0 cm of Hg of gas.

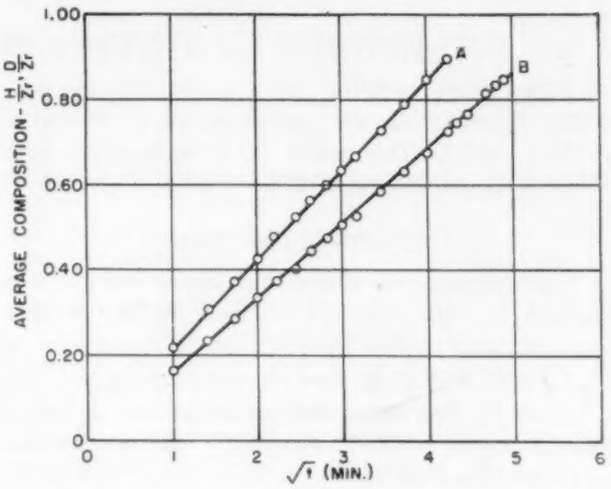

FIG. 9. Comparison of reaction of hydrogen and deuterium with zirconium. Curve A, H_2, 225°C, 1.1 cm of Hg; curve B, D_2, 225°C, 1.8 cm of Hg.

TABLE III. *Diffusion data deuterium in zirconium*

t°C	$1/T \times 10^3$	D, cm²/sec	D_o, cm²/sec
100	2.680	1.62×10^{-10}	7.5×10^{-4}
150	2.360	7.70×10^{-10}	6.0×10^{-4}
175	2.232	1.64×10^{-9}	5.8×10^{-4}
225	2.008	1.023×10^{-8}	10.0×10^{-4}
		D_o avg =	7.3×10^{-4}

In many diffusion problems the experimentally determined values include entropy and heat of activation terms for the process of forming the defects by which diffusion occurs. For the case of hydrogen in metals, such as zirconium, the tetrahedral sites in the hydride structures are already available for diffusion. Therefore, diffusion of hydrogen in the hydride structures should involve only the entropy and heat of activation terms for diffusion. According to theory, the entropy of activation should have slightly positive values.

The frequency of vibration of hydrogen atoms in the equation has been evaluated from entropy of solution data which will be discussed in a future paper. A value for ν of 4×10^{13} vibrations/sec was found. The distance a between tetrahedral sites in the δ-phase was 2.39 Å.

To evaluate the constant g, the diffusion of hydrogen atoms or ions is assumed to occur through the movement of unoccupied tetrahedral sites. g is evaluated by calculating the probability P_i of an unoccupied site occurring next to a particular hydrogen atom or ion. The probability varies from a value of $\frac{2 - 1.965}{2}$ at the surface to a value of

$\frac{2 - 1.4}{2}$ at the interface $c_{II.I}$. The geometrical mean of these values is 0.072. Since $g = \frac{1}{6} \Sigma P_i$, $g = 0.012$. Substituting the values of D_o, g, a^2 and ν, $\Delta S^* = +2.7$. This value is in agreement with theoretical predictions of Zener (17).

Diffusion of Deuterium

The diffusion of deuterium in zirconium was studied at 100°, 150°, 175°, and 225°C. Weight gain vs. time curves were similar to those seen in Fig. 2 and 3. Fig. 9 shows a comparison of $\bar{C}$ vs. $t^{1/2}$ plots for hydrogen and for deuterium diffusing into the metal at 225°C. A straight line relationship was found for both gases.

Diffusion coefficients are summarized in Table III and plotted in Fig. 8. Although the data were somewhat scattered, the temperature dependence was the same as that found for the case of hydrogen, so the heat of activation for the diffusion process was the same for both gases. Calculated D_o values for hydrogen and for deuterium were 1.09×10^{-3} and 7.3×10^{-4}, respectively. Therefore, the ratio of D_{H_2}/D_{D_2} was independent of temperature and approximately equal to 1.5.

Jost and Widman (15, 16) observed a ratio of 1.3 for $D_{H_2}D_{D_2}$. Using the transition state theory of diffusion, they show that the effect of the mass of the diffusing specie was in the frequency term in the expression for the diffusion coefficient, the frequency of vibration being proportional to $1/\sqrt{m}$ or $1/\sqrt{2}$. Thus, the simple theory gives a ratio of D_{H_2}/D_{D_2} of 1.41. This compares with the experimental value of about 1.5.

A similar analysis could be made using the classical theory of diffusion as expressed in equation (XIX). The major effect appears to be that of mass on frequency of vibration along the path for reaction. Considering the scattering of experimental results, the diffusion of deuterium in zirconium is adequately explained by equation (XV) with the effect of mass on the frequency of vibration of the particular diffusing specie explaining the ratio of D_{H_2}/D_{D_2}.

Limit of Application of Diffusion Equation

Equation (XV) was derived on the basis of the diffusion of hydrogen from the surface through the ϵ and δ hydride phases to form new δ-phase. It was assumed in the derivation that the plane of discontinuity was shifted proportional to $t^{1/2}$. At some value of the average concentration $\bar{C}$, the planes of discontinuity meet at the distance $h/2$. Equation (XIV) was used to calculate $\bar{C}$ for this condition, and a value of 1.67 was obtained. Fig. 4 shows a plot of $\bar{C}$ vs. $t^{1/2}$ for the hydrogen reaction at a temperature of 250°C. A straight line was found for concentrations up to 1.6–1.7. This agrees with the prediction of the equation.

ACKNOWLEDGMENT

The authors wish to express their appreciation to Dr. C. Zener and Dr. G. Comenetz for their helpful suggestions on the solution of the diffusion equation.

Any discussion of this paper will appear in a Discussion Section to be published in the June 1955 issue of the JOURNAL.

REFERENCES

1. D. P. SMITH, "Hydrogen in Metals", The University of Chicago Press, Chicago (1948).
2. E. A. GULBRANSEN, Chapter in book, "Zirconium and Its Alloys", to be published.
3. E. A. GULBRANSEN AND K. F. ANDREW, *J. Metals*, **1**, 515 (1949).
4. R. B. BERNSTEIN AND D. CUBICCIOTTI, *J. Phys. and Colloid Chem.*, **55**, 238 (1951).
5. E. A. GULBRANSEN AND K. F. ANDREW, *J. Electrochem. Soc.*, **101**, 348 (1954).
6. G. HÄGG, *Z. physik. Chem.*, **11**, 439 (1930).
7. E. A. GULBRANSEN AND K. F. ANDREW, *J. Electrochem. Soc.*, **101**, 474 (1954).
8. E. A. GULBRANSEN AND K. F. ANDREW, To be published by AIME.
9. C. WAGNER, quoted by W. Jost, "Diffusion in Solids, Liquids and Gases", Academic Press, Inc., New York (1952).
10. H. S. CARSLAW AND J. C. JAEGER, "Conduction of Heat in Solids", Clarendon Press, Oxford (1947).
11. E. A. GULBRANSEN, *Trans. Electrochem. Soc.*, **81**, 327 (1942).
12. E. A. GULBRANSEN, "Advances in Catalysis", 120–174, Academic Press, Inc., New York (1953).
13. E. A. GULBRANSEN AND K. F. ANDREW, *Ind. Eng. Chem.*, **41**, 2762 (1949).
14. R. M. BARRER, "Diffusion in and Through Solids", Cambridge University Press, Cambridge (1951).
15. W. JOST AND A. WIDMAN, *Z. physik. Chem.*, **B29**, 247 (1935).
16. W. JOST AND A. WIDMAN, *Z. physik. Chem.*, **B45**, 285 (1940).
17. C. ZENER, *J. Applied Phys.*, **22**, 372 (1951).

High Temperature Crystal Structure of Thorium[1]

PREMO CHIOTTI

Ames Laboratory, Atomic Energy Commission, Iowa State College, Ames, Iowa

ABSTRACT

High temperature x-ray diffraction patterns and electrical resistivity measurements show that thorium of 99.8% purity transforms from face-centered cubic to body-centered cubic on heating to 1400 ± 25° C. At 1450° C the lattice constant of body-centered cubic thorium is 4.11 ± 0.01 Å. The extrapolated lattice constant of face-centered cubic thorium at the same temperature is 5.180 ± 0.005 Å. The lattice constant of the metal used is 5.089 ± 0.001 Å at room temperature. The transformation temperature is rapidly increased as the amount of carbon in the metal is increased. Zirconium has the opposite effect in that small amounts of it are very effective in lowering the temperature at which the transformation begins.

INTRODUCTION

Thorium at ordinary temperatures has a close-packed face-centered cubic structure. In an earlier investigation (1) some resistance measurements on thorium in the temperature range between 750° and 1700°C gave evidence of a possible allotropic transformation. At about the same time, an investigation of the thorium-zirconium system by Carlson (2) indicated that a complete series of solid solutions is formed between these two elements at elevated temperatures. Since zirconium is body-centered cubic at temperatures above 865°C, the results obtained by Carlson can be explained more satisfactorily on the supposition of the existence of a body-centered cubic form for thorium. In order to resolve this question, further resistance measurements were made and x-ray diffraction patterns were taken in the temperature range in question.

EXPERIMENTAL METHODS

The change in electrical resistance with temperature of thorium was measured over a temperature range of 750°C to its melting point. The method employed and apparatus used have been described in detail elsewhere (3). In this method, a specimen approximately a quarter-inch in diameter and four inches long is clamped between two water-cooled copper electrodes and is heated under vacuum or in an inert atmosphere to various temperatures by passing a 60-cycle alternating current through it. Two thin thorium wires are spot welded one centimeter apart near the middle of the bar where the temperature is reasonably uniform. The potential developed between these two leads is balanced against the output of a current transformer whose primary is connected in series with the specimen. Since the output of the current transformer is proportional to the current through the primary, and the potential developed across the one-centimeter length of the specimen is the product of the same current and specimen resistance, the change in resistance with temperature is measured directly. Essentially, this is an alternating-current potentiometric null-point method. In order to balance one alternating voltage against another, it is necessary that the two voltages be of identical wave form and 180° out of phase. These conditions can be met quite closely in the method described. However, Corbino (4) has shown that, on heating a metal filament by means of an alternating current, a second harmonic is introduced due to small variations in resistance with temperature in the course of current reversal. This effect could not be readily detected with an oscilloscope in the present investigation and was considered negligible as far as the qualitative course of the resistance vs. temperature curve of thorium is concerned. Temperature measurements were obtained by focusing a disappearing-filament type optical pyrometer onto a small hole drilled into the middle of the specimen.

X-ray diffraction data were obtained with a North American Philips Company high angle goniometer diffractometer which was adapted for high temperature investigations (5). A sketch of the goniometer specimen holder and furnace developed for this purpose is shown in Fig. 1. Both the base and furnace cover are water-cooled. The incident and diffracted x-rays pass through a 2.5-mil aluminum window which extends over a 180°C arc on the furnace cover. The furnace is evacuated through a

[1] Manuscript received May 28, 1954. This paper was prepared for delivery at the Chicago Meeting, May 2 to 6, 1954. Contribution No. 330 from the Institute for Atomic Research and Department of Chemistry, Iowa State College, Ames, Iowa. Work was performed in the Ames Laboratory of the Atomic Energy Commission.

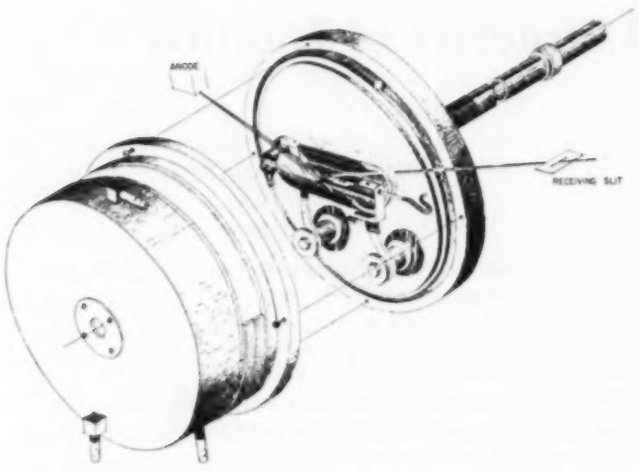

FIG. 1. Isometric projection of furnace and specimen holder attachment for x-ray diffraction goniometer.

hollow stainless steel shaft which extends through the goniometer.

Two types of specimens were used. One consisted of a thorium bar approximately $\frac{5}{16}$ x $\frac{3}{16}$ x $3\frac{1}{2}$ in., held in place by the clamp shown on the left side of the furnace base in Fig. 1. The other consisted of a smaller piece of thorium, $\frac{1}{4}$ x $\frac{1}{8}$ x $\frac{3}{4}$ in., supported in an appropriate slot on a tantalum bar, the bar being held in place by the same clamp mentioned above. No appreciable reaction between the tantalum and the thorium was observed at temperatures up to 1575°C. The latter arrangement proved more satisfactory since thorium bars were found to sag when heated to this temperature.

Samples are heated by means of a tantalum sheet resistance element. Radiation shields surround the heating element to reduce radiation losses. The specimen is heated by radiation from the heating element and does not make direct contact with it. Temperature measurements are made by sighting an optical pyrometer on a small hole (No. 65 drill) drilled into the side of the specimen. The hole in the specimen is so arranged that it can be viewed through a glass window sealed onto the furnace cover and through a $\frac{1}{8}$-in. hole drilled through the radiation shields.

Experimental Results

The first evidence for a transformation in thorium was obtained from electrical resistance measurements. Results of measurements on a thorium specimen taken from cast metal are shown in Fig. 2. The resistance is seen to rise rapidly in the temperature range of 1425° to about 1525°C. The average heating rate through this temperature range was 1.6°/min. There is evidence of a second break in the curve at 1700°C which is believed to be due to incipient fusion; however, the bar did not melt in two until heated to 1740°C. Similar runs on other bars cut from cast metal, bars made from pressed metal powder, and on Westinghouse metal all gave a sharp increase in resistance at 1400° ± 25°C. The range of temperature over which this increase takes place is evidently related to the impurities in the metal and to some extent to temperature gradients in the specimen. Carbon is very effective in increasing the temperature at which the transformation begins. Metal containing as little as 0.2 wt % carbon along with the usual impurities no longer gives any definite indication of a transformation.

X-ray diffraction data confirmed the existence of a transformation in thorium. The metal transforms from face-centered cubic to body-centered cubic on heating to above 1400°C. Copper radiation and a nickel foil filter placed in the receiving slit were used in studying the transformation. In some cases where the alpha peaks were particularly strong, the corresponding beta peak was not completely suppressed. The scanning speed in each case was two degrees 2θ per minute. Fig. 3 shows the diffraction peaks of a sample which initially contained approximately 345 ppm carbon, 195 ppm nitrogen, 1000 ppm oxygen, and 1200 ppm metallic impurities. At 1375°C the 111 face-centered cubic peak was very strong. The temperature was then increased to 1415°C. The range from 26° to 33° 2θ was immediately scanned. As may be seen from this figure, a new peak identified as the 110 body-centered cubic peak appeared. This region was then rescanned and the diffraction peaks up to 146° 2θ recorded. The possible identification of the peaks is shown on the figure. The pressure in the system during the run was maintained between

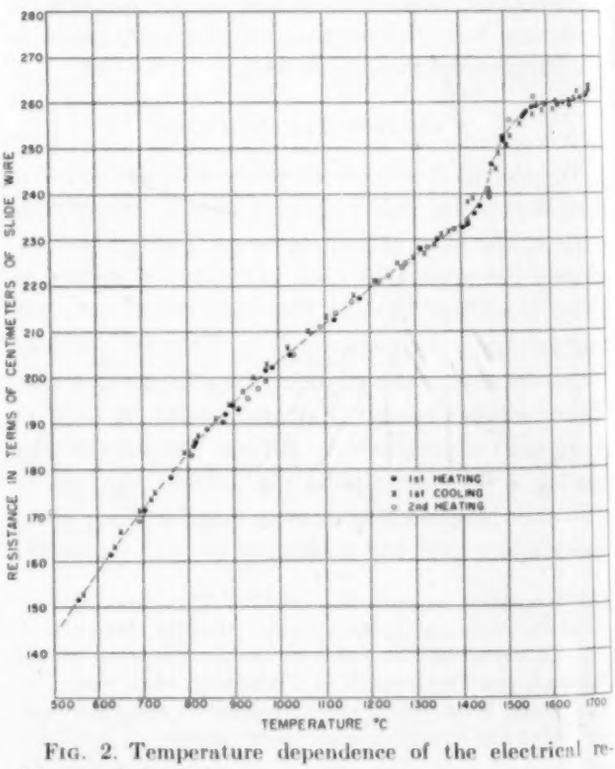

FIG. 2. Temperature dependence of the electrical resistance of thorium.

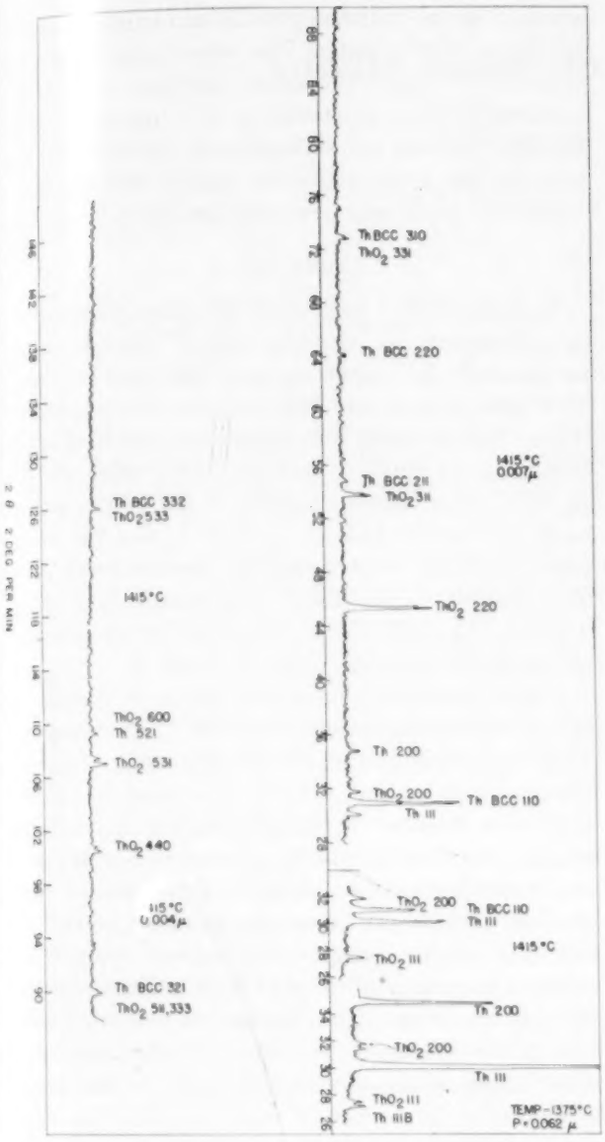

FIG. 3. Diffraction patterns of thorium contaminated with ThO_2.

2.0×10^{-6} to 7.0×10^{-5} mm of Hg. The missing body-centered cubic peaks and the peculiar relative intensities of the peaks observed is believed to be due to excessively large grains and grain orientation.

Fig. 4 shows the nature of a thorium specimen surface after being heated for about six hours at temperatures between 1200° and 1500°C during the course of x-ray diffraction studies. The large dark spots are believed to be oxide particles in the metal initially. The fine structure is probably due to contamination by oxygen or other gaseous impurities during the heating operation. Large recrystallized grains and the outlines of the old grains are evident.

Fig. 5 shows the front reflection peaks obtained with a sample of iodide crystal bar thorium of unknown purity. At 1440°C only one face-centered cubic peak and two body-centered cubic peaks are present. At 1505°C only two body-centered cubic peaks remain; however, these two peaks are not the

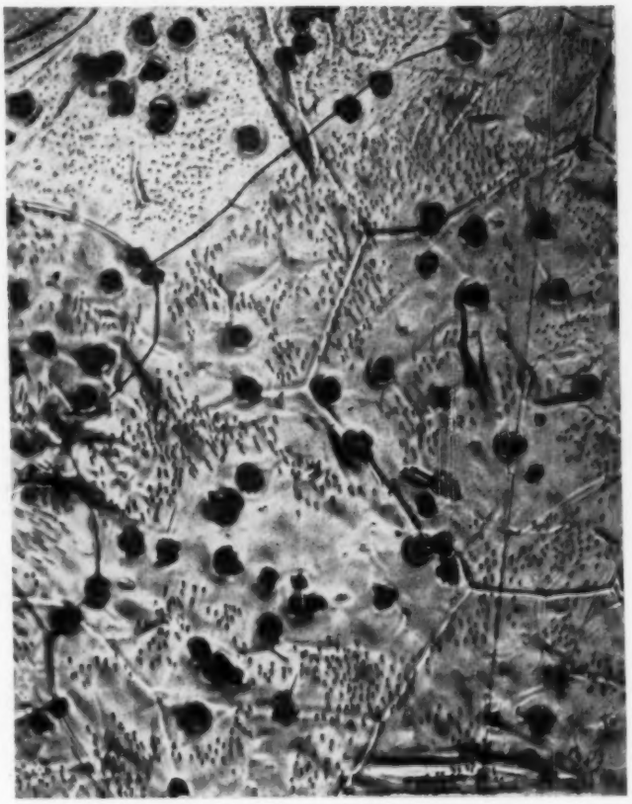

FIG. 4. Surface of thorium sample after about 6 hr at temperatures between 1200° and 1500°C, unetched. 100×.

same as the body-centered peaks present at 1440°C. A possible explanation for this observation is that a change in orientation of the grains results as the transformation goes to completion. Absence of thorium oxide peaks is noted.

Both tantalum and niobium lower the temperature at which the transformation begins to approximately 1375°C. The lowering of the transformation temperature may be due to solubility of these metals in body-centered thorium or due to removal of impurities which normally increase the stability of the face-centered modification. Tantalum, when added to thorium in small amounts, effectively removes carbon from solid solution to form insoluble Ta_2C. In this case the thorium matrix can be dissolved with nitric acid leaving the insoluble carbide as a residue. Niobium presumably does likewise. The extent of solid solubility of either niobium or tantalum in body-centered thorium is uncertain, but from atomic size considerations it is expected to be small. Zirconium, however, is very effective in lowering the temperature at which thorium transforms. Diffraction peaks obtained from a sample containing 1 wt % each of niobium and zirconium are shown in Fig. 6. It is evident from this figure that some of the body-centered phase is present at 1340°C and that the face-centered cubic phase has disappeared at 1375°C.

Small variations in alignment of the specimens along with the effects of orientation resulted in a

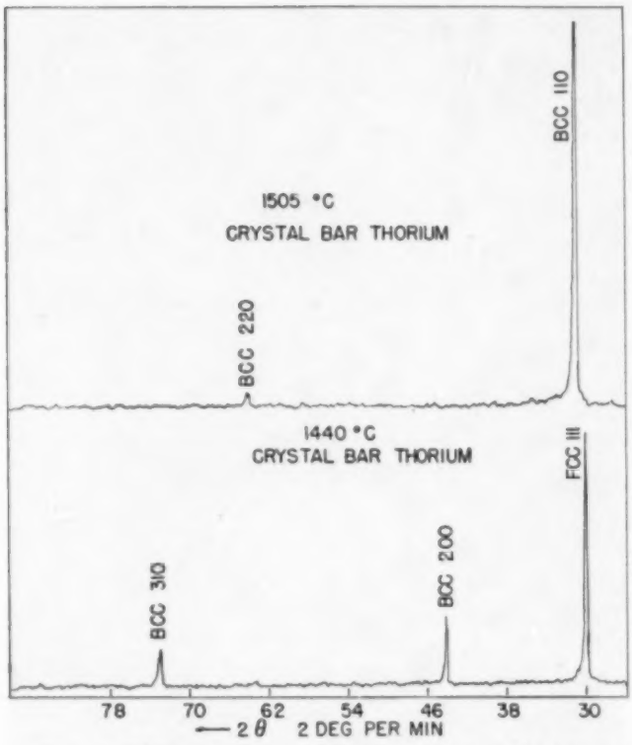

FIG. 5. Diffraction patterns of crystal bar thorium of unknown purity.

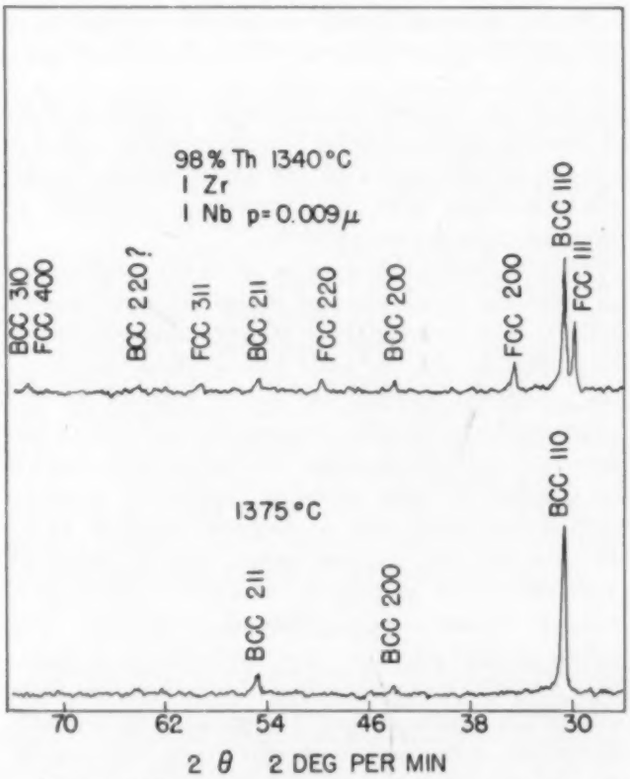

FIG. 6. Diffraction patterns of thorium containing 1 wt % each of niobium and zirconium taken at 1340° and 1375°C.

much greater variation in peak position than is normally obtained with well-aligned samples with small, randomly oriented grains. Nelson and Riley's (6) extrapolation method was used in determining the lattice constants. Individual peaks were also scanned at one-fourth degree 2θ/min to obtain better resolution of the peaks. The uncertainty in the extrapolated value of the lattice constant of the body-centered thorium was found to be rather large due to the fact that the well defined peaks usually occurred only in the front reflection region and the total number of peaks was generally limited to five or less.

CONCLUSIONS

As a result of a large number of x-ray diffraction measurements on thorium metal containing approximately 345 ppm carbon, 195 ppm nitrogen, 1000 ppm oxygen, and 1200 ppm metallic impurities, it may be concluded that this metal transforms from face-centered cubic to body-centered cubic at 1400 ± 25°C. The lattice constant of the body-centered metal at 1450°C is 4.11 ± 0.01 Å, and the extrapolated lattice constant of the face-centered cubic modification at the same temperature is 5.180 ± 0.005 Å. At room temperature the lattice constant of the metal used was 5.089 ± 0.001 Å.

Some contamination of the specimen surface by carbon on heating at 600° and 900°C was observed. This was probably because of outgassing of rubber vacuum seals or the Apiezon wax used to seal the aluminum window. Prolonged heating in this range usually resulted in the appearance of extraneous peaks which could be indexed as face-centered cubic thorium carbide. At temperatures above 1000°C, no difficulty in this respect was observed, possibly because of the rapid diffusion of carbon into the metal. Possible variation of the carbon content on the surface of the specimens due to these effects probably contributed to the observed variation in the lattice constants.

ACKNOWLEDGMENTS

The author wishes to acknowledge the cooperation and assistance of fellow members of the Ames Laboratory. The high temperature x-ray diffraction patterns were obtained with the assistance of Robert White.

Any discussion of this paper will appear in a Discussion Section to be published in the June 1955 JOURNAL.

REFERENCES

1. P. CHIOTTI, "Thorium-Carbon System," Atomic Energy Commission Report No. AECD-3072 (1950).
2. O. N. CARLSON, "Some Studies on Uranium-Thorium-Zirconium Ternary Alloy Systems," Atomic Energy Commission Report No. AECD-3206 (1950).
3. P. CHIOTTI, "Measurement of the Electrical Resistance of Metals and Alloys at High Temperatures," to appear in *Rev. Sci. Instr.*
4. O. M. CORBINO, *Atti recle accad. Lincei*, Ser. 5, **19**, 133 (1910); *ibid.*, **20**, 222 (1911).
5. P. CHIOTTI, "Adaptation of a Geiger-Counter X-ray Spectrometer for High Temperature Investigations," to appear in *Rev. Sci. Instr.*
6. J. B. NELSON AND D. P. RILEY, *Proc. Phys. Soc. London*, **57**, 160 (1945).

Anodic Behavior of Copper in HCl[1]

LEE STEPHENSON[2] AND J. H. BARTLETT

Department of Physics, University of Illinois, Urbana, Illinois

ABSTRACT

Anodic behavior of copper in 2*N* HCl has been studied by both electrical and optical methods. The temporal behavior of current and voltage have been found, as well as the current vs. voltage characteristics. The anode surface has been observed both visually and photographically with the aid of conventional microscopes, and the anolyte has been photographed cinematographically using a schlieren microscope.

When the current is turned on, a layer, probably CuCl, starts to form at random nucleation spots on the anode. This grows until the whole anode is covered, at which time the current drops abruptly. Up until this time the anolyte becomes less concentrated, but the concentration may increase again after the current has become low.

The anode-calomel voltage may be written as $V = \epsilon(i) + ir$, where $\epsilon(i)$ becomes constant at high current densities. The values of $\epsilon(i)$ have been found by both the interruption and the direct method, and there appear to be at least four of physical significance. These values are -0.35, -0.27, -0.05, and $+0.11$ v.

In general, the current drops twice before reaching its minimum value. If t_I is the time from the make to the first drop, and if $Q = \int_o^{t_I} i\,dt$, and if i_o is the "initial" current after the make, then empirically $Q = 24(i_o - 0.70)^{-0.53}$, where i_o is in ma.

The anode layer is about 3 μ thick in the steady state. When the circuit is broken, r and ϵ change rather rapidly (in about 0.1 sec), but the layer dissolves off slowly.

INTRODUCTION

In an endeavor to further the understanding of electrochemical phenomena, such as overshoot and oscillations, which occur in biological systems, Bartlett (1) studied the anodic behavior of iron in aqueous H_2SO_4 with special attention to various kinds of transient phenomena which may arise when the applied voltage is changed. The work was continued by Bartlett and Stephenson (2) with emphasis now on the steady-state behavior of passive and active iron, and on the transients resulting from brief interruptions of the active steady state. Microscopic observation of the anode *in situ* revealed that evolution of hydrogen caused disruption of the layer which tended to form, so that this introduced an uncontrollable variation with resulting lack of reproducibility. The conclusion was reached that the Fe | H_2SO_4 system is an undesirable one to use for the study of layer formation, which seems to be basic for any analysis of overshoot and oscillation.

Fortunately, other systems do exhibit these transient phenomena, and these are much more reproducible.[3] Bartlett and Stephenson decided to investigate the system consisting of a copper anode in aqueous HCl. This is admirably suited for the study of layer formation because of the following properties: (*a*) Cu is attacked only very slowly by 2*N* HCl; (*b*) the anode layer which is formed is readily detected by simple optical means; (*c*) rates of reaction are such that the transient phenomena can be followed easily; (*d*) compositions of the layer and the soluble anode product are known; and (*e*) no undesirable products are formed during electrolysis. The purpose of the present paper is to report on various physical changes which take place at the surface of a copper anode immersed in HCl, and on changes occurring in the diffusion layer next to this anode. The work may be regarded as a theoretical contribution to the behavior of metal electrodes covered with precipitated salt, as found in corrosion reactions.

Procedure

The experiments to be described fall into two main categories: electrical and optical. The electrical experiments involve studies of temporal behavior of current and voltage, and of the current vs. voltage characteristics. The optical experiments consist of both visual and cinematographic observation of the anode surface with conventional microscopes, and of cinematographic studies of the

[1] Manuscript received December 9, 1953. This paper sums up investigations which have been reported at the Philadelphia Meeting, May 4 to 8, 1952, the Montreal Meeting, October 26 to 30, 1952, and the New York Meeting, April 12 to 16, 1953.

[2] Present address: California Research Corporation, La Habra, California.

[3] The high degree of reproducibility in the system reported on here is evident from Fig. 5–8, 13, and 14, where each point represents one run only and is not an average of several runs.

anolyte using a schlieren microscope. The optical experiments are carried out in conjunction with the electrical experiments so that accurate correlation of all related phenomena is possible.

Apparatus

Cell.—The circuit employed in these experiments is shown semipictorially in Fig. 1. The electrolytic cell consisted of a rectangular box made of glass with an optical window of glass 0.1 mm thick in one face to permit microscopic observation of the anode *in situ*. The inside dimensions of the cell were 2.5 x 7.5 x 7.5 cm. The cell contained 110 ml of an aqueous solution of hydrochloric acid, into which were placed two working electrodes and a reference electrode. Unless otherwise noted, the acid concentration was 2 moles/l (2*N*) and the temperature was 25°C. Preliminary experiments were carried out in both air-saturated and oxygen-free solutions in order to determine the effects of dissolved oxygen on the phenomena to be observed. No differences in the transient behavior were apparent, and microscopic observations failed to show any changes in the anode film due to dissolved oxygen. Consequently, the more convenient air-saturated solutions were used. Because of physical limitations imposed upon the structure and the orientation of the anode by the microscopic experiments and the schlieren experiments, it was decided to conduct all experiments with a vertical anode and to permit free convection of the anolyte. The anode structure consisted of a vertical brass rod with a 1 cm length of # 14 (1.63 mm diameter) copper wire (Anaconda) soldered horizontally into its lower end. Picein 105[4] covered the entire assembly except for the end cross section, *A*, of the copper wire, which constituted the anode surface. Filed anodes were prepared using a Nicholson "Mill Smooth" file. Electropolished anodes were prepared by mechanical polishing down to 4/0 polishing paper (Norton) followed by electropolishing in 50% orthophosphoric acid. The cathode, *K*, was a 0.005 in. thick platinized platinum sheet, 3.0 x 3.3 cm, supported by a brass rod which was covered with Picein. A 0.1*N* calomel half-cell was used as the reference electrode. Provided the distance between the anode and the cell walls was at least 2 mm, the transient behavior was found to be independent of cell geometry (2).

The potential measurement, source of emf, recording of current and voltage, and interruption techniques were as described in a previous paper (2). In addition, a Brown recording potentiometer (0–10 mv) was used to record slow transients (i.e., those lasting longer than about 20 sec). The external

[4] Obtained from E. H. Sargent Company, Chicago, Illinois.

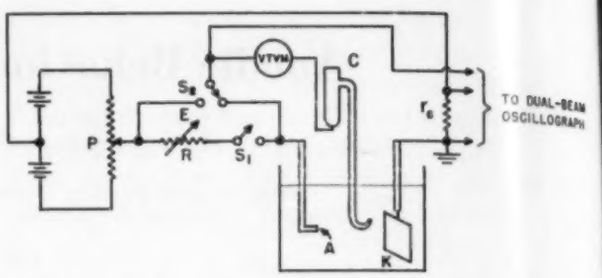

FIG. 1. Basic circuit. P, potential divider; R, 200 ohm helipot; VTVM, vacuum tube voltmeter; A, 0.021 cm² copper anode; C, 0.1*N* calomel reference electrode; K, 10 cm² platinized cathode; r_e, current resistor.

circuit resistance was controlled by a 200 ohm helipot, *R*.

Microscope and accessories.—For visual observation of the anode surface, a microscope was provided with a special mechanical stage to hold the electrolytic cell, electrodes, etc. For most work, a 16 mm (10×) objective having a numerical aperture of 0.25 and a working distance of 6 mm was used, together with a 10× eyepiece. The anode was illuminated obliquely to obtain maximum contrast. A 35 mm Praktica FX single-lens reflex camera was used to obtain photomicrographs.

Cinematographic microscope.—Cinematography of the anode surface was accomplished with a conventional 8 mm home movie camera, Bell and Howell Model 134-V. The camera lens, an f/1.9 Super Comat, was removed from the camera and mounted backward (in order to preserve the conjugate relationship for which the lens was corrected) on a short extension tube. This arrangement provided an excellent cinematographic microscope having a primary magnification of 3.4 diameters. An auxiliary lens and 45° prism were mounted in the side of the extension tube to permit simultaneous recording of the current and voltage

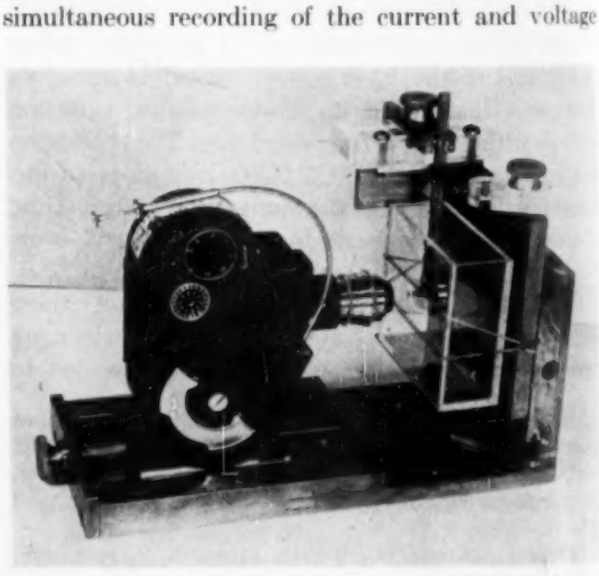

FIG. 2. Cinematographic microscope

deflections on the oscillograph screen. Fig. 2 shows the principal features of this apparatus.

Schlieren photography.—Information about the diffusion layer was obtained by using a specially constructed schlieren microscope (3). This is an optical instrument in which the intensity of light incident on the photographic film at a certain point is a linear function of the gradient of the index of refraction at the corresponding point in the object space. Even though this method has not yet been made quantitative at concentration gradients as high as those occurring in the present work, it still is very helpful in furnishing a general picture of what is occurring. Schlieren motion pictures of the diffusion layer were taken with the aid of the 8 mm camera used for microphotography.

Make Transients

General nature of transients.—If a freshly filed anode is placed in the solution and the circuit is then closed, the nature of the ensuing current vs. time curve (here designated as a "make transient") will depend on the external emf E and the external resistance R (1).

The complete circuit will be considered as consisting of two parts, the internal part and the external part. The internal part is defined as that part which extends in the cell from the anode metal to the tip of the calomel electrode. Its resistance will be denoted by r. The external part of the circuit is that part which metallically connects the anode to the cathode, plus the part from the cathode to the calomel electrode tip. Its resistance will be termed R. If i is the total cell current measured in the external circuit, the anode-calomel voltage V is given by

$$V = E - iR \qquad (I)$$

If E and R are held constant, i can still vary, but V will also vary. In the i-V plane, the above equation will be represented by a straight line, which will be called the load line, in analogy to vacuum tube terminology. (The resistance R consists mainly of the resistance of the helipot, and we shall regard as negligible the resistance of the leads, of the potential divider circuit, and of the solution between cathode and calomel, because these total approximately 1.5 ohms, or only 1% of the minimum resistance employed in the present work.)

A typical make transient for medium R (140 ohms) and high final voltage V is shown in Fig. 3*a*. At the very beginning, there is a spike (not shown) lasting about 10^{-5} or 10^{-4} sec. The current then falls rapidly from the "initial" value i_0 and becomes approximately independent of time. This region will be called the first plateau. The current actually goes

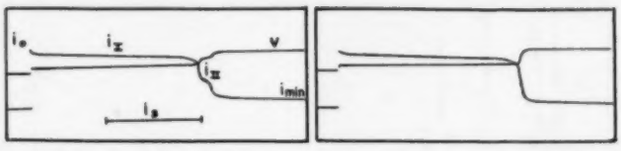

Fig. 3. Make transients. $E = +0.50$ v, $R = 140$ ohms. *a*, *Left*, freshly filed anode; *b*, *right*, electropolished anode.

through an inflection point, i_I, decreasing more or less slowly. After a rather abrupt drop to a second plateau (current i_{II}), the current drops again, then varies slowly. For the case shown in the figure, it goes through a minimum i_{min} and then rises to the steady state value i_∞. If, however, i_0 is sufficiently high, such a minimum is not observed and the current will fall continually until i_∞ is reached. The current may overshoot one or more times before settling down to the steady value, 1.7 ma. This is illustrated in the semilogarithmic plot of Fig. 4.

Electrode potential and resistance.—If an appreciable current flows, the anode-calomel voltage will, in general, differ from the reversible value, V_{rev}. The overvoltage is defined as the difference between the observed voltage (at a given current) and the reversible value. It is regarded as composed of three distinct contributions: resistance overvoltage $V_r = ir$, concentration overvoltage or polarization V_c, and "activation" overvoltage V_a (4).

The anode-calomel voltage may then be written as

$$V = V_{rev} + V_a + V_c + V_r = \epsilon + ir. \qquad (II)$$

The quantity $\epsilon = V_{rev} + V_a + V_c$ will be termed the electrode potential for present purposes. If this is constant for a certain set of circumstances, the locus of i vs. V will be a straight line with intercept ϵ and slope $1/r$. This determination is called the direct method (5) of obtaining ϵ and r. Another

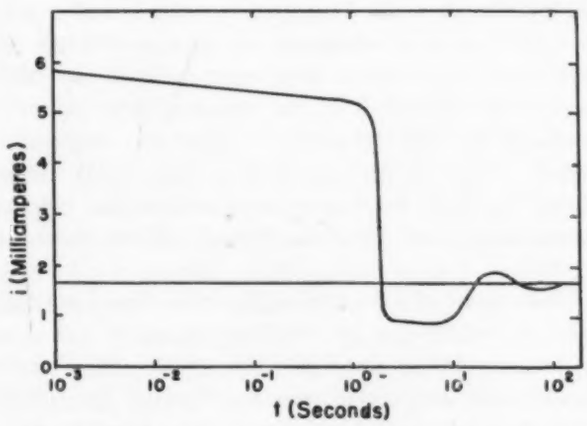

Fig. 4. Make transient for freshly filed anode. The horizontal line at 1.7 ma represents the steady-state current. $E = +0.50$ v, $R = 140$ ohms.

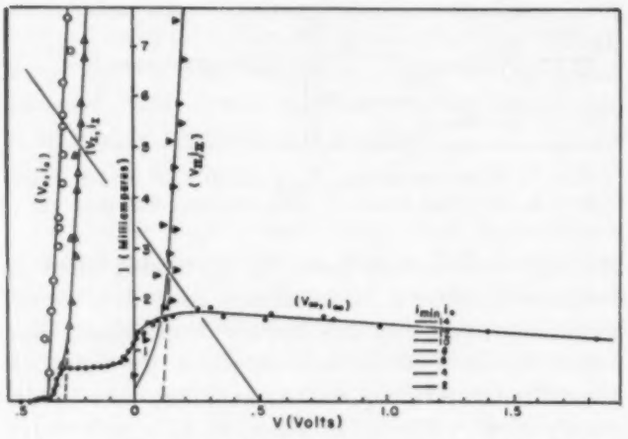

FIG. 5. Characteristic curves for the Cu | HCl (2*N*) system at 25°C with a freshly filed anode having an area of 2.1 mm².

method which may be used to check or complement this is the interruption method. This consists in breaking the circuit and observing V before and after, as well as i before, the break. Then $\epsilon = V_{off}$ and $r = (V_{on} - V_{off})/i$. Both methods were used, and they agree in all cases where they are applicable. The interruption method will not be suitable if the recording apparatus is not sufficiently fast, for a rapid decay of ϵ may escape detection. Even where this decay is observed, one must extrapolate back to $t = 0$ in order to find the value of ϵ at the time of the break. The results of Hickling and Salt (6), based on extrapolation, were criticized adversely by Frumkin (7).

For high current densities, the value of ϵ is constant in the steady state (8) and at certain critical points (for the system Cu | HCl), as will now be shown. These critical points occur when i is equal to i_0, i_I, and i_{II}, respectively. As may be seen from Fig. 5, the loci (V_0, i_0), (V_I, i_I), and (V_{II}, i_{II}), which shall be called "characteristics", become straight, mutually parallel lines above approximately 1 ma. (Similar behavior has been found for the steady state, for Hickling (8) stated that "there is a fairly general tendency for the overvoltage to approach a constant maximum value" at high current densities.) The reciprocal of the common slope of the characteristics equals the resistance, and is 12 ohms for the system (Cu | 2M HCl). Thus, the cell's internal resistance does not change appreciably until after the second plateau has been reached.

The values of ϵ determined by this direct method are $\epsilon_0 = -0.35$ v, $\epsilon_I = -0.27$ v, and $\epsilon_{II} = +0.11$ v. In other words, at high current densities these experiments show that the overvoltage (excluding that due to ohmic resistance) has one constant value for i_0, another for i_I, and another for i_{II}.

Two of the above values of ϵ were confirmed by interruption experiments, which resulted in $\epsilon_0 = -0.35$ v and $\epsilon_I = -0.27$ v. However, when the current during the second plateau and later is interrupted, the value of V after 10^{-4} sec is $\epsilon_{II} = -0.05$ v. This is reconcilable with the result of the direct method if it can be assumed that there is a rapid decay ($<10^{-4}$ sec) from $\epsilon_{II} = +0.11$ v to $\epsilon'_{II} = -0.05$ v. (The recording apparatus used in the present experiments was relatively slow, being incapable of detecting decay constants appreciably smaller than 10^{-4} sec.) The value of $\epsilon = 0.11$ v does seem to have physical significance (cf. "Break Transients").

Typical curves showing the variation of ϵ and r with time as determined by the interruption method are given in Fig. 6. Data were obtained for freshly filed anodes with $E = +0.20$ v and $R = 140$ ohms, and are plotted on the assumption that the entire voltage change at the break is due to an ir drop.

On open circuit, the potential of the copper electrode is $\epsilon_{so} = -0.44$ v (with respect to 0.1*N* calomel). Immediately after the circuit is closed, the potential jumps to $\epsilon_0 = -0.35$ v, as is evidenced by a small dot on the film. (The switch contact S_1 [Fig. 1] bounced for about 10^{-3} sec after closing, and thus provided sufficient break to observe this value of ϵ.) The potential then rises less rapidly to $\epsilon_I = -0.27$ v. It stays at this value until the end of the first plateau, when it changes abruptly to

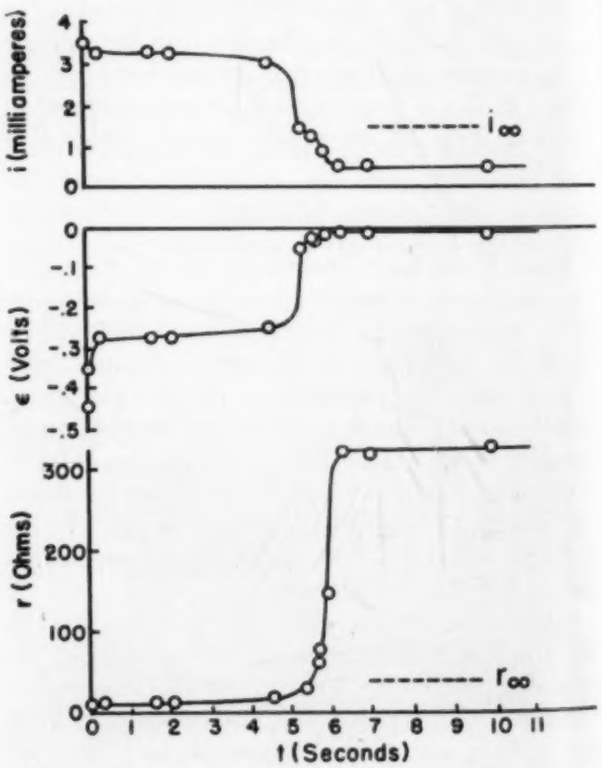

FIG. 6. Temporal behavior of ϵ and r following make. $E = +0.20$ v, $R = 140$ ohms.

$\epsilon'_{II} = -0.05$ v, the potential of the second plateau, where it remains for the rest of the transient.

The resistance r remains essentially constant at its initial value, $r_0 = 12$ ohms, until the end of the first plateau. Then, soon after the ϵ jump, it increases abruptly to a maximum value and decreases slowly toward its steady-state value r_∞, ϵ staying practically constant[5] at -0.05 v.

If one now re-examines the i vs. t curve with an eye to stating on what portions ϵ varies and on what portions r varies, the following conclusions are reached:

1. The drop in current from i_0 to i_I and the drop from i_I to i_{II} are due primarily to changes in ϵ, while the drop from i_{II} to i_{min} is due primarily to a change in r. In the case of electropolished anodes where the transition from i_I to i_{min} is relatively smooth, it is presumed that the changes in ϵ and r occur almost simultaneously.

2. Variations of the cell current subsequent to the current drop are due primarily to changes in r, for ϵ remains approximately constant at $\epsilon_{II} = 0.11$ v.

Durations of plateaus.—The duration of the first plateau is found to depend on i_0. Let t_I be the time from the make to the inflection point at the drop from i_I to i_{II}, and let $Q = \int_0^{t_I} i\,dt$. Then empirically,

$$Q \approx i_I t_I = 24\,(i_0 - 0.70)^{-0.53} \qquad \text{(III)}$$

(This is shown in Fig. 7.) If E and R be given, then i_0 and i_I can be found from the intersection of the load line with the characteristics. Then, from equation (III), t_I can be estimated. It will decrease as i_0 increases. The value 0.70 in equation (III) corresponds to the steady-state current on the lower plateau (see below).

The duration of the second plateau appears to be affected by the condition of the anode surface, being a maximum for a filed surface and a minimum for an electropolished surface. Indeed, with an electropolished anode the second plateau is sometimes entirely absent, its expected location being marked only by a slight discontinuity in the slope of the i vs. t curve (Fig. 3*b*).

Prediction of general features of a make transient.—Once the "characteristics", i.e., the straight lines associated with the critical points, have been found, it is an easy matter, knowing equation (III), to give the main features of a transient corresponding to any values of E and R.

[5] Under similar circumstances, the potential drop across the diffusion layer has been deduced to be negligible. See reference (9).

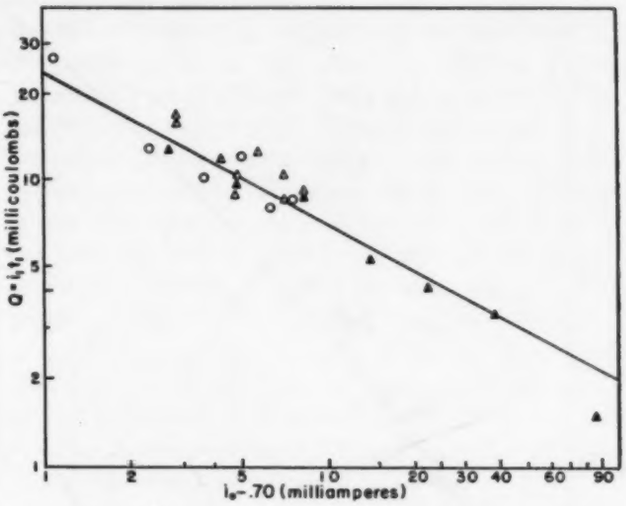

FIG. 7. Q as a function of i_0 for both freshly filed and electropolished anodes. $Q = 24\,(i_0 - 0.70)^{-0.53}$

If equations (I) and (II) are solved for i, the result is

$$i = \frac{E - \epsilon}{R + r} \qquad \text{(IV)}$$

One can substitute in the values of E and R, set $r = 12$ (the value of the solution resistance), and the values ϵ_0 and ϵ_I, to obtain i_0 and i_I. Alternatively, these can be found graphically by letting the load line intersect the characteristics corresponding to ϵ_0 and ϵ_I, respectively. The values of V are dependent on those of i by equation (I).

Once i_0 and i_I are known, t_I can be obtained from equation (III), so that the main features of the make transient up to the time that the current first drops can be given beforehand. Thus it is seen that the characteristic lines, which may be obtained quite easily, are extremely useful in prediction.

The current minimum.—In many cases the current passes through a minimum shortly after the final current drop. For currents up to 15 ma, i_{min} is found to depend mainly upon i_0, as illustrated in Fig. 8. There is also a dependence of i_{min} on the condition of the anode surface, it being smaller for electropolished anodes than for ground anodes.

Schlieren study of the anolyte.—The qualitative nature of changes occurring in the diffusion layer at the anode was determined with a schlieren microscope. The pictures shown in Fig. 9 were taken using a freshly filed anode, with $E = 0.50$ v and $R = 140$ ohms. The schlieren knife edge was adjusted to show positive and negative gradients with equal clarity, and so oriented with respect to the anode (which appears in silhouetted profile at the left of the photographs) that bright regions corresponded to a refractive index (and concentration) which was increasing toward the anode, and

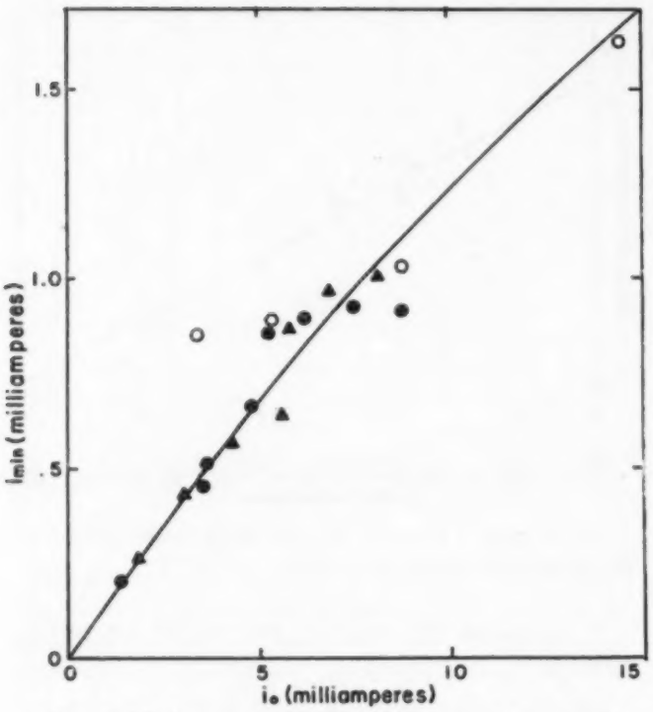

FIG. 8. Minimum current vs. initial current for a freshly filed anode.

dark regions corresponded to a refractive index (and concentration) which was decreasing toward the anode.

At $t = 0$, immediately before closing the switch, the anolyte is seen to have a uniform concentration throughout the region in which the diffusion layer is expected to develop. The bright line outlining the face of the anode is due primarily to diffraction (10), but may be enhanced somewhat by the presence of products from the acid's slow attack on the anode. After electrolysis has proceeded for 0.7 sec, a dark region is observed extending out from the anode into the solution approximately 0.15 mm (measured at the center of the anode). Since the refractive index is decreasing toward the anode in this region, it can only be a region in which the HCl concentration is decreasing toward the anode; i.e., Cl^- is being consumed at the anode-solution interface. (Some of the photographs show a brightening of the anolyte nearest the anode which lasts for about one-third the duration of the first plateau. This is as yet not explained, and is not relevant to the present discussion.) At 1.3 sec and 2.0 sec the HCl-depleted region has advanced to approximately 0.27 mm and 0.33 mm, respectively. Comparing the photographs taken at 2.0 sec (near the end of the first plateau), at 2.1 sec (on the second plateau), and at 2.2 sec (near the current minimum), it is seen that no change whatever occurs in the diffusion layer when the current drops. After 4 sec have elapsed, the HCl-depleted region has nearly reached its maximum extent of about 0.48 mm, the reduced density of this region being evidenced by the fact that it is carried upward by convection. At the same time it is observed that a bright region, corresponding to a refractive index which increases as the anode is approached, has begun to form at the face of the anode. At 6 sec the current has reached its minimum (Fig. 4), the HCl-depleted region has advanced to its maximum extent, and the material of the bright region of the anode product has begun to stream from the bottom of the anode, showing that its density is greater than that of 2*N* HCl. After 10 sec have elapsed, the current has begun to rise toward its steady-state value, the HCl-depleted layer has begun to recede, and the anode product has established a steady downward flow which tends to counteract the upward convection previously established by the HCl-depleted layer. At 300 sec the current has reached its steady-state value. The HCl-depleted region is not only appreciably reduced in extent, but is now being swept downward by the anode product.

The anode reactions.—Since, when current flows, Cl^- disappears from solution and Cl_2 is not observed to be liberated, the Cl^- must be consumed by some reaction involving the oxidation of copper. The resulting products are at least two in number, for it is observed that a layer forms on the anode and a viscous stream pours down from it after the layer has been completed.

Some evidence as to the nature of the anode reactions is furnished by the existence of the two

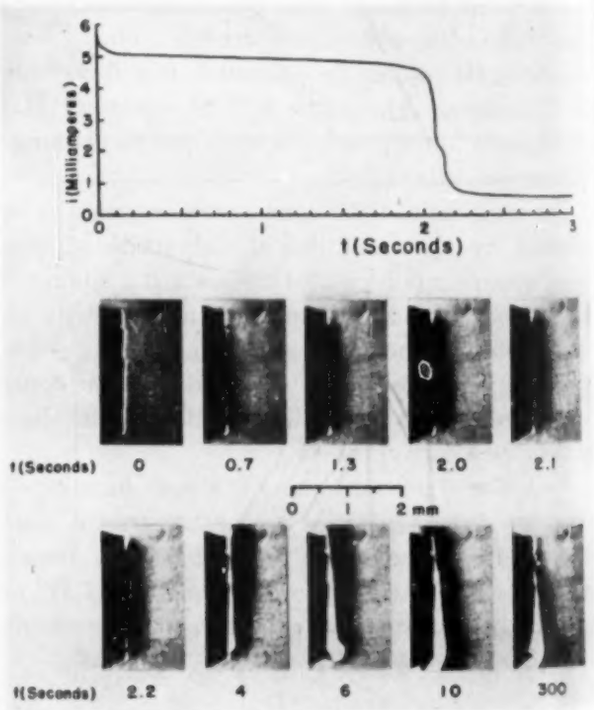

FIG. 9. Schlieren study of the anolyte following make. $E = +0.50$, $R = 140$ ohms.

electrode potentials, $\epsilon_I = -0.27$ v and $\epsilon'_{II} = -0.05$ v. The former is observed when at least part of the anode surface is exposed to the solution, while the latter potential corresponds to the surface being completely covered with the above-mentioned layer. As will be seen below, ϵ_I differs from ϵ_0 because of concentration polarization. The potential ϵ_0 is characteristic of the anode before much layer has had time to form. The anode potential ϵ_I is practically constant until the sudden transition to ϵ_{II}, or in other words is almost uninfluenced by the layer formation until the layer is about complete.

It is necessary, then, to postulate one type of reaction for the bare surface and another for the covered surface. According to Gatty and Spooner (11), "At the moment of immersion of a Cu electrode in aqueous aerated solution, the electrode is covered with a film of Cu_2O. In concentrated acid chloride solutions, (this) film is readily broken up, (and) the electrode potential will be close to that of the anodic field of bare metal. The electrode tends to establish the Cu | CuCl | Cl^- electrode potential, CuCl being the least soluble of the copper chlorides. Complex ion formation takes place between the anodically formed CuCl and the halide in solution." The picture which the authors have developed, and which is consistent with all the known facts, is as follows: (*A*) the initial reaction is between chloride ions in solution and copper metal, resulting in the formation of CuCl layer on the anode; the potential ϵ_I is then associated with the reaction

$$Cu + Cl^- \rightarrow CuCl + e^- \qquad (V)$$

(*B*) when the surface is covered, this reaction is supplanted by another, to which the potential ϵ_{II} corresponds. According to Wagner (12) "depletion of chloride ions will yield a rather well-defined electrode potential corresponding to a copper electrode in a solution saturated with CuCl in the absence of excess electrolyte, especially HCl." This reaction may be

$$Cu \rightarrow Cu^+ + e^- \qquad (VI)$$

Cuprous ions can diffuse through the CuCl layer until they meet with chloride ions, and then one may have the reaction

$$Cu^+ + Cl^- \rightarrow CuCl \qquad (VII)$$

Also, CuCl is known to react with excess Cl^- to form the soluble, colorless complexes $CuCl_2^-$ and $CuCl_3^-$ (13–16). It is assumed that the removal reaction is

$$CuCl + Cl^- \rightarrow CuCl_2^- \qquad (VIII)$$

Layer thickness.—If the anode reaction is as deduced above, then a knowledge of Q affords a convenient means for estimating the thickness of the anode layer at the time the current drops. Assuming that Faraday's laws apply, Q/zF is the number of moles of CuCl formed up to that time. Assuming further that a negligible amount of CuCl is dissolved before the current drops, the thickness of the layer is given by $\delta = QM/zFd$, where M is the gram-molecular weight of CuCl, $zF = 96{,}500$ coulombs/mole, A is the anode area, and d is the density of CuCl. Taking, for example, the value $Q = 10.5$ millicoulombs (for $i_0 = 5.6$ ma) it is found that $\delta = 1.5 \times 10^{-4}$ cm. (Clearly, the CuCl layer cannot be expected to appear in the photos of Fig. 9, for its thickness is far beyond the limit of resolution of the schlieren microscope.)

It is also possible to estimate the thickness of the layer in the steady state by breaking the circuit and observing how long it takes for the layer to be removed completely. The rate of removal after interruption is assumed to be the same as the rate of formation in the steady state, namely i_∞/zF moles/sec. The thickness of the steady-state layer will therefore be given by $\delta = i_\infty Mt/zFAd$, t is the time required for removal. With the aid of a microscope equipped with circularly polarizing film to improve image contrast, visual observation of the anode revealed that the time required for complete removal of the layer depends upon the value of V_∞ at the time of interruption, typical values of t and δ calculated from them being as follows:

V_∞ (v)	t (sec)	δ (μ)
+0.20	9.6(±0.8)	2.3(±0.2)
+0.80	14.9(±1.0)	3.3(±0.2)
+1.40	18.0(±1.6)	3.5(±0.3)

These values for δ indicate that the steady-state layer thickness is probably of the same order of magnitude as that found when the current drops from i_I to i_{min}.

Layer growth.—Moving pictures of the anode surface taken at 64 frames/sec show that the layer begins to form at many randomly distributed points as soon as electrolysis begins, and that the growth from these nuclei takes place in a sideways manner. The current drops immediately after the pores of the nearly completed layer have been so reduced in size that they are no longer resolvable on the film (i.e., diameters reduced to roughly 5 μ or less). Fig. 10 shows a series of photomicrographs of the anode face taken during the initial transient when $E = +0.70$ v and $R = 140$ ohms. Fig. 10(*a*) shows the electropolished anode immediately before electrolysis begins. Because of the oblique illumination employed, a truly specular surface would be completely dark. The bright spots which are observed are due to tiny pits left by electropolishing

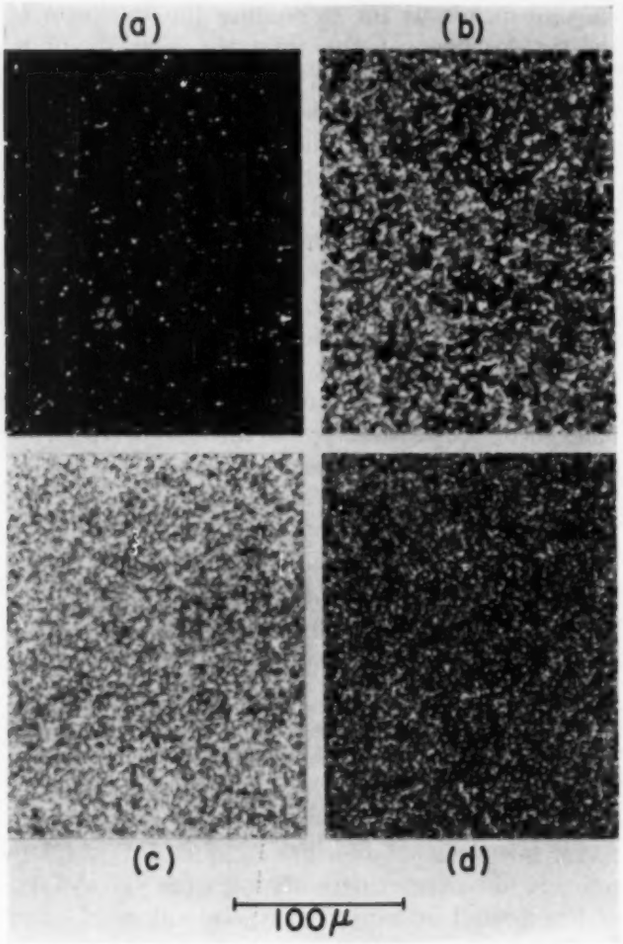

FIG. 10. Photomicrographs of the anode. (a) Before electrolysis; (b) midway on the first plateau; (c) at current minimum; and (d) steady state. $E = +0.70$ v; $R = 140$ ohms.

(17) and to a slight amount of etching which takes place while the microscope is being focused upon the immersed electrode.[6] Fig. 10(*b*), taken approximately midway on the first plateau, shows that the free surface (dark areas) is greatly reduced by the sideways growth of the layer although no appreciable change in the cell current has occurred up to this time. Approximately 5 sec after the current drops, it reaches a minimum. At this point, the completed layer appears as in Fig. 10(*c*). The current then rises until the steady state is reached (after about 5 min of electrolysis) and then the layer appears as shown in Fig. 10(*d*).

Break Transients

Dependence of potential decay on steady-state voltage.—Events subsequent to current interruption yield information on the layer removal process

[6] It was found that the undesired etching could be inhibited by making the electrode cathodic while the necessary optical adjustments were being made (cathodic current density approximately 1 ma/cm²). However, this method was not employed.

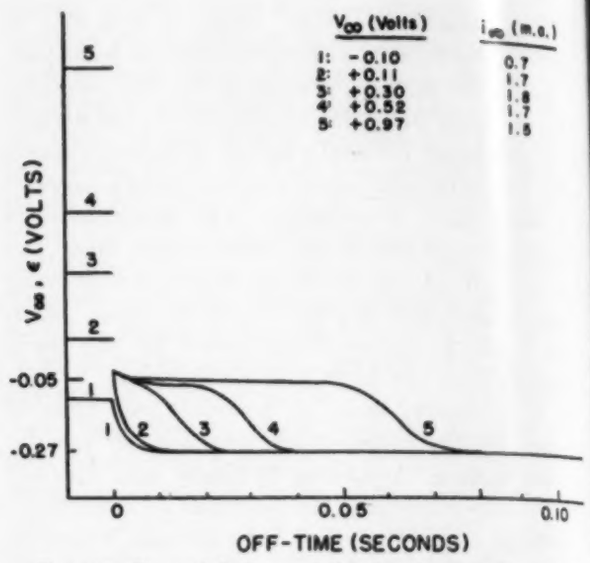

FIG. 11. Potential decay following interruption of the steady-state current, shown for various steady-state conditions.

alone, thus enabling one to separate this from that of layer formation. The curves in Fig. 11 show how the potential V varies after the break has been made, for different initial steady-state voltages V_{∞}. For values of V_{∞} greater than approximately 0 v, ϵ drops quickly to -0.05 v,[7] remains approximately constant for a brief time depending on V_{∞}, and then drops suddenly to $\epsilon_I = -0.27$ v. The potential vs. time curve has the same shape for passive iron (Fig. 12) in H_2SO_4 as it does for copper in HCl, which may indicate that similar mechanisms are operative in the two cases. The make curve for the transition from active iron to passive iron has been interpreted in terms of the formation of a layer, and now it is seen that the break curve for the passive-active transition resembles the break curve in copper, where it is known that there is a layer present. The evidence for a layer on passive iron is thus made stronger than ever, and it now remains to identify positively the reactions by which it is formed and removed.

In copper, for $V_{\infty} < -0.05$ v, the potential decay is somewhat like an exponential from V_{∞} to ϵ_I. From ϵ_I on, the potential falls slowly to $\epsilon_{00} = -0.44$ v, this process lasting many minutes (see Fig. 13). Although this method of recording does not indicate that anything special occurs at $\epsilon_0 = -0.35$ v, still one observes that stirring right after interruption does reduce the potential immediately to this value

[7] It has already been supposed that this is really composed of two drops, with $\epsilon_{II} = 0.11$ v as the intermediate value. The value -0.05 v is presumably the true electrode potential (i.e., without overvoltage) of the completed layer. The value $\epsilon_I = -0.27$ v agrees with the potential of Cu in 2*N* HCl saturated with CuCl (R. S. Cooper, private communication).

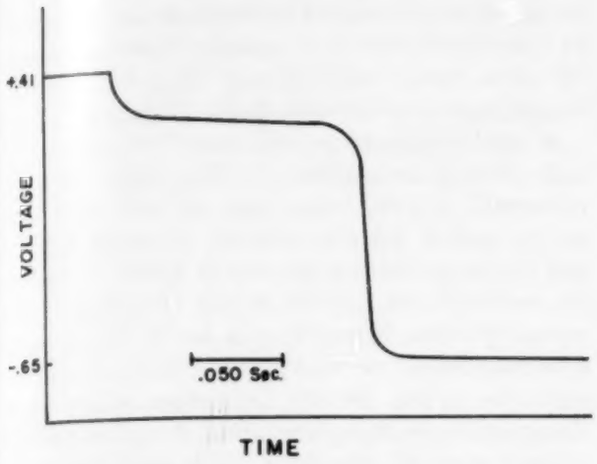

FIG. 12. Break transient for passive iron

of −0.35 v. This suggests that the difference between ϵ_0 and ϵ_I is due to concentration polarization.

The duration of the break plateau ($\epsilon = -0.05$ v) depends linearly upon V_∞. (The duration is defined arbitrarily as the time from the interruption until the midpoint $\epsilon = -0.16$ v is reached, and will be denoted by $t_{1/2}$.) Fig. 14 is a plot of the duration $t_{1/2}$ against V_∞. It is a straight line which has an intercept of +0.11 v on the V-axis. This is regarded as evidence that $\epsilon = +0.11$ v is the potential of the completed layer, as is also found from the characteristic curves. Below +0.11 v, the layer is not complete, so that there is no preparatory time necessary to make part of the surface bare.

Temporal behavior of ϵ and r.—Fig. 13 shows the temporal behavior of ϵ and r following interruption of an arbitrarily chosen steady-state condition, $V_\infty = +0.75$ v and $i_\infty = 1.6$ ma. To obtain these data, the steady-state current was interrupted for a predetermined length of time, at the end of which

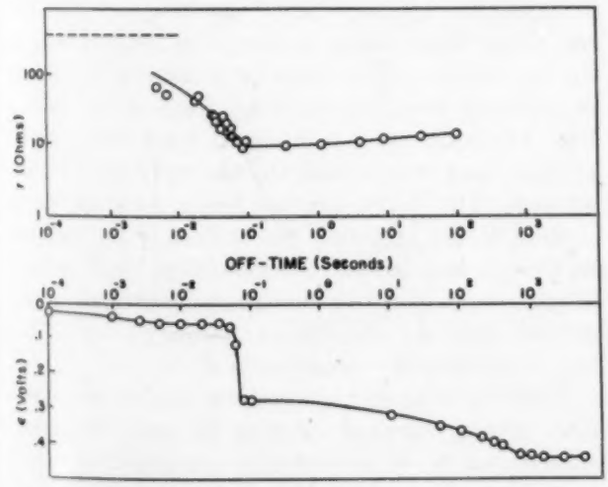

FIG. 13. Temporal behavior of ϵ and r following interruption of the steady state. $V_\infty = +0.75$, $i_\infty = 1.6$ ma.

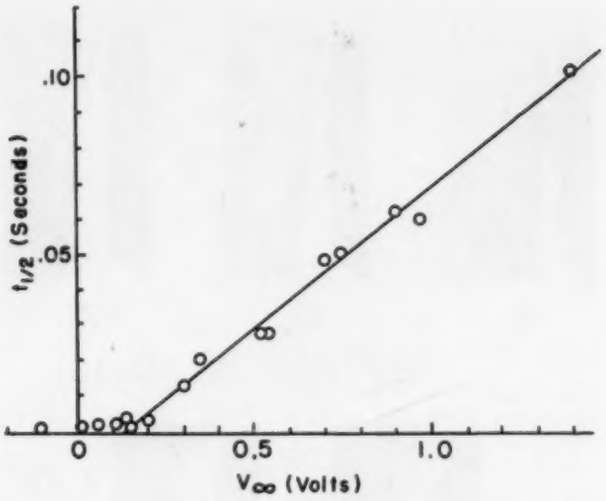

FIG. 14. $t_{\frac{1}{2}}$ vs. V_∞

the circuit was closed again. The electrode potential, ϵ, was taken to be the value of V immediately before the circuit was closed, since equation (II) becomes $V = \epsilon$ when the current is interrupted. The resistance r is determined by measuring $V_{on} = \epsilon + ir$ just before the circuit is broken, or just after it is made, and also measuring $V_{off} = \epsilon$ just after the circuit is broken, or just before it is made. Eliminating ϵ and solving for r it is seen that in either case

$$r = (V_{on} - V_{off})/i \qquad \text{(VIII)}$$

With the apparatus at hand it was not possible to obtain off-times shorter than 0.005 sec. The dashed line at $r = 400$ ohms represents the value of r at the instant of interruption (calculated on the basis that $\epsilon = \epsilon_{II} = +0.11$ v).

The data show that the abrupt drop in ϵ does not begin until the decay of r is more than 96% complete.

Schlieren study after break.—When the steady-state current is interrupted, fairly rapid changes in the anolyte seem to occur, but whether or not they correspond to the sudden drop in ϵ cannot as yet be stated with certainty. The schlieren photographs in Fig. 15 show that 10 sec after interruption the Cl^- gradient is nearly erased, while the stream of anode product continues almost unabated as the layer continues to dissolve. After 20 sec the Cl^- gradient can no longer be detected and the $CuCl_2^-$ gradient has begun to iron out, all of the layer having been removed at this time. After 40 sec the $CuCl_2^-$ is no longer streaming from the anode, and by the time 60 sec have elapsed the anolyte has almost regained the composition of the main body of solution. From Fig. 13 it can be seen that the time required for erasure of the concentration gradients is about the same as the time required for decay from $\epsilon_I = -0.27$ v to $\epsilon_0 = -0.35$ v. This is consistent with

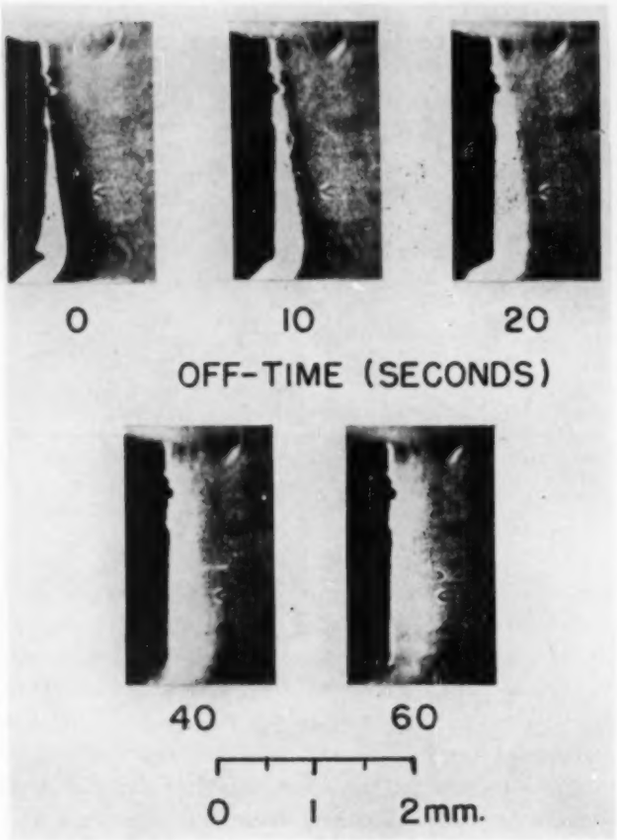

FIG. 15. Schlieren study of the anolyte following interruption of the steady state. $V_\infty = +0.25$ v, $i_\infty = 1.8$ ma.

the previous hypothesis that the difference in these two potentials is to be attributed to concentration polarization.

Discussion

The present work has demonstrated the nature of the processes associated with that portion of the make transient up to the current minimum. The early layer growth starts from randomly distributed nuclei on the anode surface and proceeds radially so that little knobs are formed. When these have grown sufficiently, they touch each other. The anode will then have a thin continuous layer upon it, and this needs (18) to be only a few molecules thick (i.e., of the order of 10^{-7} cm) in order to establish the potential characteristic of a copper electrode covered with CuCl. It was found (Fig. 8) that ϵ may increase suddenly without a corresponding change in r, indicating that the portion of the layer responsible for the increase must have negligible resistance and, consequently, be very thin. The subsequent increase in r indicates the completion of a relatively thick layer, because it exhibits a large resistance. It should be emphasized that no sharp distinction or boundary is imagined to exist between the thin ϵ-layer and the thick r-layer. Both are imagined to grow simultaneously during the course of a transient and to be completed at very nearly the same time, completion of the r-layer usually lagging, but never preceding that of the ϵ-layer.

A kinetic explanation will be achieved when one can predict quantitatively how the electrode potential ϵ and the resistance r will vary with time. At the end of the first plateau, ϵ changes rapidly, and this may indicate the rate at which the surface becomes covered (3). From the beginning of the second plateau, however, ϵ is nearly constant, so that the current changes are due to changes in the resistance r. The detailed mechanism of how these changes occur is still obscure, but it may be possible to learn more about it by suitable make and break experiments. In particular, data are needed for the variation of r with time when the steady state is interrupted for times less than 0.01 sec.

Summary

When the circuit is closed in the Cu | 2N HCl(aq) | H_2(Pt) system, the current exhibits a very brief initial spike. The anode-calomel potential may be represented at all times $>10^{-5}$ sec by $V = \epsilon + ir$, where ϵ, the electrode potential, has no noticeable dependence on i at high currents, and r, the resistance within the cell between anode and calomel, is ohmic in nature. The open circuit voltage is -0.44 v, and has four characteristic values thereafter. Immediately after the spike, $\epsilon = \epsilon_0 = -0.35$ v. The current drops from i_0 to an approximately constant value i_I (first plateau), and ϵ becomes $\epsilon_I = -0.27$ v. (This change is attributed to concentration polarization.) The charge Q which must flow before the current completes its drop to a new constant value i_{II} (second plateau) is connected with i_0 by the empirical relation $Q = 24(i_0 - 0.70)^{-0.53}$. The value of ϵ_{II} as determined by extrapolation of the (V_{II}, i_{II}) plot is $\epsilon_{II} = +0.11$ v; the value found from interruption experiments is $\epsilon'_{II} = -0.05$ v. This could be accounted for by an overvoltage term with a decay time of 10^{-5} sec or less. The value of r is constant up to the second plateau, and corresponds to the resistance of the solution. The second plateau has a duration which is shorter, the smoother the surface. It is followed by a rapid drop in i and the associated rapid increase in resistance. A slower change then occurs, and the current may go through a minimum value i_{min} before reaching the steady state i_∞.

From the moment electrolysis begins, an anode layer grows sideways, starting at many randomly spaced points. It is probably composed of CuCl, formed by the reaction $Cu + Cl^- \rightarrow CuCl + e^-$ and removed by the reaction $CuCl + Cl^- \rightarrow CuCl_2^-$. When the anode has become completely covered,

the layer is of the order of 10^{-4} cm in thickness. At this point an abrupt drop in i occurs (due to the sudden ϵ change). This is followed by a rise in resistance, which occurs when the pores are closed, and only slightly more CuCl is deposited than that necessary to cause the ϵ change. During the period when the high current was flowing a steep Cl^- gradient was established. The quick drop in i does not affect the over-all diffusion layer, and so the Cl^- continues to diffuse slowly toward the anode, building up the concentration. This will reduce the resistance of the layer, for it is more soluble in higher concentrations of Cl^-. In the steady state the layer formation reaction proceeds at the same rate as the layer removal reaction, the net reaction being $Cu + 2Cl^- \rightarrow CuCl_2^- + e^-$.

When the steady-state current is interrupted (V_∞ assumed to be greater than ϵ_{II}), V drops instantly from V_∞ to ϵ_{II} (an ir drop) then decays very rapidly to $\epsilon = -0.05$ v (an overvoltage decay) where it remains relatively constant. At the interruption r begins to decrease rapidly, presumably due to Cl^- attack on the outer part of the anode layer. When the decay of r is approximately 96% complete, the inner part of the layer apparently ruptures and ϵ drops abruptly from -0.05 v to -0.27 v (ϵ_I). After several seconds, depending on the value of V_∞ before interruption, the layer, whose thickness was of the order of 10^{-4} cm before interruption, is completely dissolved. As the concentration gradients in the anolyte gradually disappear, ϵ drops from ϵ_I to ϵ_0. Thereafter ϵ continues to drop slowly until it eventually reaches ϵ_{00}.

Acknowledgments

This work was supported at the outset by the University of Illinois Research Board and then by the Office of Ordnance Research, and the authors desire to express their deep appreciation to both organizations for their help. Professor C. Wagner and Dr. A. K. Graham gave them invaluable encouragement and aid. They also wish to thank Mr. Jack Hinde for very competent assistance with the reduction of the data, and Mr. Ralph S. Cooper for his critical reading of the manuscript.

Any discussion of this paper will appear in a Discussion Section to be published in the June 1955 issue of the Journal.

References

1. J. H. Bartlett, *Trans. Electrochem. Soc.*, **87**, 521 (1945).
2. J. H. Bartlett and L. Stephenson, *This Journal*, **99**, 504 (1952).
3. L. Stephenson, Thesis, University of Illinois (1953).
4. F. P. Bowden and J. N. Agar, *Ann. Repts. Progr. Chem.*, **1938**, 90.
5. A. L. Ferguson, *Trans. Electrochem. Soc.*, **76**, 113 (1939).
6. A. Hickling and F. W. Salt, *Trans. Faraday Soc.*, **37**, 450 (1941); **38**, 474 (1942). See also F. W. Salt, *Disc. Faraday Soc.*, **1**, 169 (1941).
7. A. Frumkin, *Acta Physicochim.*, **18**, 23 (1943).
8. A. Hickling, *Disc. Faraday Soc.*, **1**, 127 (1947).
9. G. E. Kimball and A. Glassner, *J. Chem. Phys.*, **8**, 815 (1940).
10. P. Fayolle and P. Naslin, "Photographie Instantanee et Cinematographie Ultra-rapide," p. 9, Editions de la Revue d'Optique, Paris (1950).
11. O. Gatty and E. C. R. Spooner, "The Electrode Potential Behavior of Corroding Metals in Aqueous Solutions," Chap. IV, Clarendon Press, Oxford (1938).
12. C. Wagner, Private communication.
13. St. v. Naray-Szabo and Z. Szabo, *Z. phys. Chem.*, **166**, 228 (1933).
14. S. R. Carter and F. M. Lea, *J. Chem. Soc.*, **127**, 499 (1925).
15. A. A. Noyes and M. Chow, *J. Am. Chem. Soc.*, **40**, 739 (1918).
16. G. Bodländer and O. Storbeck, *Z. anorg. Chem.*, **31**, I, 458 (1902).
17. P. A. Jacquet, *Trans. Electrochem. Soc.*, **69**, 629 (1936).
18. H. Mayer, "Physik dünner Schichten", Wissenschaftliche Verlagsgesellschaft, Stuttgart (1950).

FUTURE MEETINGS OF
The Electrochemical Society

Cincinnati, May 1, 2, 3, 4, and 5, 1955

Sessions probably will be scheduled on

Electric Insulation, Electronics, Electrothermics and Metallurgy, Industrial Electrolytics, Theoretical Electrochemistry

Headquarters at the Sheraton-Gibson Hotel

★ ★ ★

Pittsburgh, October 9, 10, 11, 12, and 13, 1955

Headquarters at the Statler Hotel

★ ★ ★

San Francisco, April 29, and 30 and May 1, 2, and 3, 1956

Headquarters at the Mark-Hopkins Hotel

★ ★ ★

Cleveland, October 8, 29, 30, and 31, and November 1, 1956

Headquarters at the Statler Hotel

★ ★ ★

Washington, D. C., May 12, 13, 14, 15, and 16, 1957

Headquarters at the Statler Hotel

★ ★ ★

Buffalo, October 6, 7, 8, 9, and 10, 1957

Papers are now being accepted for the meeting to be held in Cincinnati. Triplicate copies of each abstract (not exceeding 75 words in length) are due at the Secretary's Office, 216 West 102nd Street, New York 25, N. Y., *not later than January 15, 1955.* Complete manuscripts should be sent in triplicate to the Managing Editor of the JOURNAL at the same address.